GEOLOGICA ULTRAIECTINA

Mededelingen van het
Instituut voor Aardwetenschappen der
Rijksuniversiteit te Utrecht

No. 24

MULTIPLE BEAM GENERATION WITH A DIGITAL COMPUTER FOR ECHOSOUNDING AT LOW AND HIGH FREQUENCIES

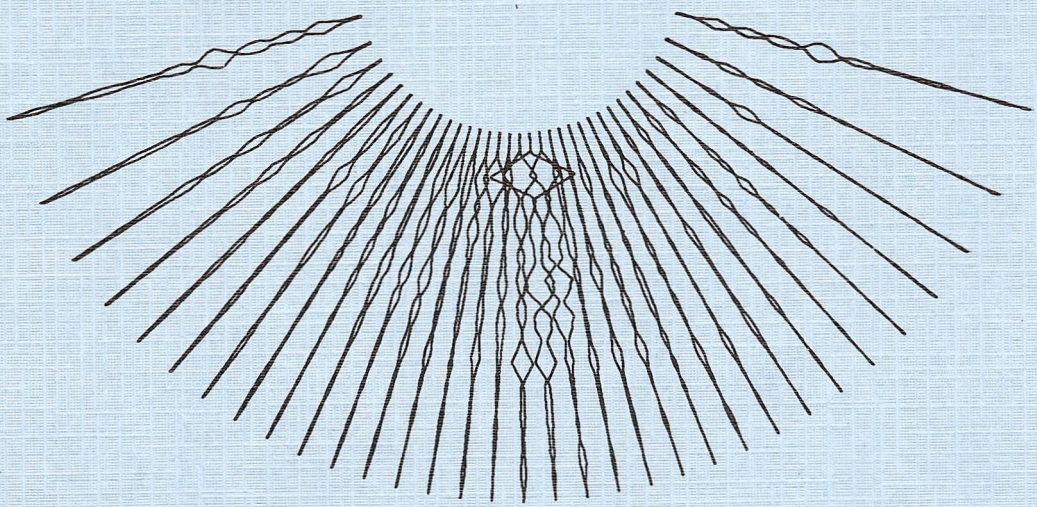

A.P. SLOOTWEG

STELLINGEN

1. Bij het ontwerp van een multi-beam echolood dient men de apertuur niet te klein te kiezen ten opzichte van de gewenste bundelbreedte, aangezien dan het hoge zijlobniveau kan leiden tot het meten van te geringe dieptes en onjuiste dieptelijnen.

Renard, V. et J.-P. Allenou, Le Seabeam, sondeur à multi-faisceaux du N/O *Jean Charcot*. Description, évaluation et premiers résultats, *Revue Hydrog. Intern.*, *56*, 35-71, 1979.

2. Het is niet terecht, dat er systematisch verschil bestaat tussen richtingen van structuren aangegeven door dieptelijnen verkregen met conventionele echoloden en van structuren aangegeven door dieptelijnen verkregen mede met een multi-beam echolood.

Phillips, J. D. and H. S. Fleming (compilers), Multi-beam sonar study of the Mid-Atlantic rift valley, 36° - 37° N, FAMOUS, *Geol. Soc. Am., Map Chart Ser., MC-19*, 1978.

3. De opvatting van Bell, dat abyssal hills, gezien het verband tussen hun afmetingen en hun aantal, een gevolg zouden zijn van evenwicht bij maximale wanorde, terwijl het relief op midoceanische ruggen daarentegen deterministisch van natuur is, kan worden tegengesproken op grond van wat bekend is over het ontstaan van abyssal hills.

Bell, I. H., Jr., Statistical features of sea-floor topography, *Deep-Sea Res.*, *22*, 883-892, 1975.

4. Op het door Collette et al. gesignaleerde probleem, dat niet empirisch te bepalen is welk van twee mechanismen (een vloeistof-dynamisch of een statisch--elastisch model) verantwoordelijk is voor de aanwezigheid en vorm van de median valley van midoceanische ruggen, kan licht geworpen worden door niet meer actieve midoceanische ruggen te onderzoeken op hun vorm en hun zwaarte-krachtanomalie. Een voorbeeld van een te onderzoeken structuur is de rug in de centrale Tasman Zee (60 miljoen jaar oud), die een ontwikkelde riftvallei vertoont.

Collette, B. J., J. Verhoef and A. F. J. de Mulder, Gravity and a model of the median valley, *J. Geophys.*, *47*, 91-98, 1980.
Hayes, D. E. and J. Ringis, Seafloor spreading in the Tasman Sea, *Nature*, *243*, 454-458, 1973.

5. De discrepantie tussen de pool van model RM2 (van Minster en Jordan) en de "best-fitting" pool voor Noord-amerika en Afrika kan verklaard worden door het gebruik van verkeerde fracture-zone richtingen.

Minster, B. J. and T. H. Jordan, Present-day plate motions, *J. Geophys. Res*, *83*, 5331-5354, 1978.
Collette, B. J. and A. P. Slootweg, Oblique spreading and fracture zones, *Nature*, *274*, p. 187, 1978.

6. Het feit, dat de richtingen van de niet-actieve gedeelten, ouder dan 9 miljoen jaar, van fracture-zones in het centrale gedeelte van de Noordelijke Atlantische Oceaan zeer weinig afwijking vertonen van een patroon van parallelcirkels om een rotatiepool, zulks in tegenstelling tot de richtingen van de niet-actieve gedeelten van dezelfde fracture-zones, geeft aan dat de afwijkingen in deze actieve gedeelten een direct gevolg zijn van het spreidingsproces, en dat ze geen belemmering vormen voor de beschrijving van het fracture-zone patroon in termen van een opeenvolging van eindige rotaties.

7. Aangezien de ontwikkeling in bolfuncties van een ronde bolkap ter grootte van de Stille Oceaan, waarop witte ruis met lage gemiddelde amplitudo gesuperponeerd is, een regelmatigheid in de kwadratische gemiddelden van de coëfficienten vertoont die overeenkomt met die, gevonden door Vening Meinesz voor de ontwikkeling van de topografie van de aarde, kan uit deze regelmatigheid geen conclusie getrokken worden omtrent het bestaan van meerdere lagen convectiestromingen.

Vening Meinesz, F. A., The results of the development of the earth's topography in spherical harmonics up to the 31st order, Provisional conclusions I and II, *Proc. of the Koninkl. Nederl. Akademie van Wetenschappen*, *B62*, 116-136, 1959.

8. Processen in de oceaan en daaropvolgende interactie met de atmosfeer zijn niet de oorzaak van de zogenaamde Suess-wiggles in het radiokoolstofgehalte van gedateerde houtmonsters.

Suess, H. E., The radiocarbon record in tree-rings of the last 8000 years, *Proc. Tenth Inter. Radiocarbon Conf.*, Bern and Heidelberg, 1979.
Druffel, E. M. and T. W. Linick, Radiocarbon in annual coral rings of Florida, *Geophys. Res. Lett.*, *5*, 913-916, 1978.

9. Afgezien dient te worden van berging van radio-actief afval in het "fossiele" gedeelte van fracture-zones aangezien deze niet tectonisch inactief zijn.

Turekian, K. K. and P. A. Rona, Eastern Atlantic fracture zones as potential disposal sites for radioactive waste, *Environmental Geology*, *2*, 59-62, 1977.
Sykes, L. R., Mechanism of earthquakes and nature of faulting on the midocean ridges, *J. Geophys. Res.*, *72*, 2131-2153, 1967.

10. Het verdient aanbeveling dat clavecimbelbouwers, die publiceren over akoestische kwaliteiten van instrumenten zich op de hoogte stellen van gangbare inzichten in de akoestiek. Tevens verdient het aanbeveling dat wetenschappers, die publiceren over de historie van de muziekinstrumentenbouw, zelf dergelijke instrumenten gebouwd hebben.

Schütze,R., Die akustischen und klanglichen Veränderungen von Rückers Cembali durch die späteren Erweiterungen im Tonumfang (Ravalement), *Colloquium,Museum Vleeshuis*, Antwerpen, 1970.
Mertin, J., Cembalo-, Clavichord- und Orgelbau aus der Gemeinsamkeit der Erzeugung historischer Tasteninstrumenten, *Beitr. zur Aufführungspraxis*, 2, Graz, 47-52, 1973.

11. Het tijdstip waarop Automatische Halve Overweg Bomen gesloten worden dient afhankelijk te worden gemaakt van de snelheid van de naderende trein.

12. Het is minder terecht dat maatschappijrelevante stellingen bij proefschriften in de wandeling als "scherts"-stellingen worden aangeduid.

Stellingen behorend bij het proefschrift: " Multiple beam generation with a digital computer for echosounding at low and high frequencies."

A. P. Slootweg

Utrecht, 23 april 1980

MULTIPLE BEAM GENERATION WITH A DIGITAL COMPUTER FOR ECHOSOUNDING AT LOW AND HIGH FREQUENCIES

PROEFSCHRIFT

TER VERKRIJGING VAN DE GRAAD VAN DOCTOR IN DE WISKUNDE EN NATUURWETENSCHAPPEN AAN DE RIJKSUNIVERSITEIT TE UTRECHT, OP GEZAG VAN DE RECTOR MAGNIFICUS PROF. DR. A. VERHOEFF, VOLGENS BESLUIT VAN HET COLLEGE VAN DECANEN IN HET OPENBAAR TE VERDEDIGEN OP WOENSDAG 23 APRIL 1980 DES NAMIDDAGS TE 2.45 UUR

DOOR

ADRI PETER SLOOTWEG

GEBOREN OP 28 OKTOBER 1944 TE AMSTERDAM

DRUKKERIJ ELINKWIJK BV – UTRECHT

PROMOTOR: PROF. DR. B.J. COLLETTE

Aan Christel

Contents

Acknowledgements

I wish to thank all persons and institutions that made possible the research reported in this dissertation.
The subject was suggested by Professor B.J. Collette who did catch somewhere the term "multi-beam sonar" when few people apart from the military had heard about it. I am very grateful for his criticism and encouragement.
Special thanks go to Dr. K.W. Rutten, who discovered for me an existing multi-beam echosounder system, and to Ir. H.A.J. Rijnja, who introduced me to the principles of sonar.

The experiment at Maasbracht was made possible by the kind permission of Rijkswaterstaat Directie Limburg, Dienstkring Maastricht Maas, to use the lock-chamber for this experiment. Mr. H.T. van der Zee made the contacts with the lock personnel and furnished drawings of the chamber. Drs. J.J. Velterop and the assistant-lockmaster Mr. H.J.M. Henckens helped to rig up the measuring system. The transducers were kindly put at my disposal by the Physisch Laboratorium RVO-TNO at The Hague.

The Netherlands Commission for Sea Research chartered H.Nl.M.S. *Tydeman* from the Royal Netherlands Navy Hydrographic Department for the spring cruise in 1979. In spite of the failure of the main propellor motor after a week's journey the experiment described was performed during the tow home. The Commanding Officer kindly allowed to deploy our airgun and streamers during this tow.
Drs. J. Verhoef and Mr. H.J.G.M. Scholten helped getting the system ready for measurement. Messrs. D. Verweij, M. Schotsman and H. van der Meer managed the mechanical and electronical hardware. Mr. J.H.M. Hoofd controlled the computer hardware and software.

Professor K. Helbig suggested various improvements in the manuscript.
I am very grateful to Dr. A. Duba for rectifying my English writings, although he had little time.
Mrs. A.M.C. van Leeuwen patiently typed the dissertation, despite the diminishing readability towards the end.
A part of the figures was taken care of by the head of the drawing department of the Instituut voor Aardwetenschappen, Mr. F. Henzen.

The research was supported by the Netherlands Organization for the Advancement of Pure Research (Z.W.O.) and by the Rijksuniversiteit te Utrecht.
It was performed at the *Vening Meinesz Laboratorium voor Geofysica en Geochemie* at Utrecht.

Samenvatting

Het feit, dat de geluidssnelheid in (zee)water zeer weinig variatie vertoont maakt het mogelijk om met behulp van de golffrontentheorie de richting, waaruit onderwatergeluid ontvangen wordt, vast te stellen. Op dezelfde manier kan men de richting kiezen waarin onderwatergeluid uitgezonden wordt.
Bovenstaande principes worden toegepast in echolodingsapparatuur voor hydrografisch gebruik, sidelooking sonar, sectorscanning sonars en imaging echosounders.
Bij hydrografische echoloden onderscheidt men narrowbeam en multibeam echoloden. Eerstgenoemde gebruiken een antenne, d.w.z. een combinatie van geluidstransducenten, om een enkele geluidsbundel met kleine openingshoek te formeren, laatstgenoemde gebruiken meerdere bundels onder verschillende hoeken.
De tot nu toe meest geavanceerde multibeam echosounders (Sonarray Subsystem en Seabeam van General Instrument) formeren simultaan bundels met verschillende richtingen met behulp van electronische schakelingen, waarbij de bundels in een vlak loodrecht op de vaarlijn liggen. Zodoende verkrijgt men langs één vaarlijn informatie in drie dimensies, vandaar de naam drie-dimensionale echoloden.
Het gebruik in deze systemen van kwetsbare onderdelen en niet-flexibele electronische bundelvorming, alsmede de hoge prijs was aanleiding om digitale bundelvorming (d.w.z. bundelvorming met een programmatisch gerealiseerd algorithme in een digitale rekenmachine) te onderzoeken.

Hiertoe werden twee experimenten gedaan:

1. Een experiment met "lage" frequentie aan boord van Hr Ms *Tydeman* in april 1979.
2. Een modelexperiment met "hoge" frequentie in de sluis in het Julianakanaal te Maasbracht in november 1977.

Het experiment aan boord van Hr Ms *Tydeman* toont aan dat een quasi-periodieke geluidsbron, zoals een airgun, onder bepaalde omstandigheden een voldoende benadering van een coherente geluidsbron kan zijn, zodat bundels gevormd kunnen worden. Bij dit experiment waren de omstandigheden zodanig, dat een frequentie van 75 Hz met voldoende amplitude ontvangen werd. Bij deze lage frequentie is het nodig de ontvangers (streamers) op aanzienlijke afstand van elkaar te slepen, terwijl de invloed van reflectie tegen het wateroppervlak niet verwaarloosd mag worden. De kenmerken van dit experiment zijn het gebruik van 3 streamers met een tussenafstand van 9 m en bundelvorming door individuele faseverschuiving en optelling.

De resultaten tonen, dat met deze opstelling een zij het niet al te nauwe bundel in verticale richting gemaakt wordt met verbeterde signaal-ruis verhouding. Een enkele zijecho kon waargenomen worden, echter met een kleine amplitude. Voldoende gegevens voor het produceren van een dieptelijnenkaart zijn niet verkregen. Dit is het gevolg van de grote openingshoek van alle bundels en de relatief grote zijlobben van de zijbundels. Bij het experiment was de relatief langzame rekenmachine een belemmering voor de on-line verwerking van de gegevens.
Theoretisch wordt beargumenteerd, dat met vijf ontvangers (streamers) en een snelle computer on-line een - zij het ruwe - contourkaart van de bodem geproduceerd kan worden, terwijl registraties met sediment-reflectoren uit verschillende richtingen mogelijk zijn naast de registratie van een nauwe, centrale bundel.

Het model-experiment in de sluis te Maasbracht toont aan, dat een rekenmachine (met bijbehorend programma) gebruikt kan worden voor het scheiden van signalen afkomstig uit verschillende richtingen en het automatisch detecteren van bodem bij aanwezigheid van storende signalen. De hoofdlijnen van dit experiment zijn een sinusvormig zendsignaal van 20 periodes lengte en een frequentie van 17.9 kHz, ontvangst op 16 en 32 kanalen en afstand-richting transformatie met een gewogen Discrete Fourier Transform (DFT). Niet essentiëel voor de verwerking doch belangrijk voor de economie van het experiment was het toepassen van apertuursynthese. Hierbij wordt niet een fysisch array van transducenten gebruikt, maar een array gesimuleerd door achtereenvolgens met een transducent op de verschillende arrayplaatsen te meten.

Uit dit experiment volgen aanbevelingen voor de bouw van een "hoog"-frequente multibeam echosounder die een zogenaamde arrayprocessor gebruikt om on-line de benodigde detectie, filtering en DFT te verzorgen. Diepte-detectie is nodig voor het maken van een dieptelijnenkaart, terwijl de gedetecteerde gegevens (diepte en bijbehorende horizontale afstand) bewaard dienen te worden voor samenvoeging achteraf. De centrale filosofie bij dit ontwerp is, dat het verwerkingsprogramma (binnen zekere grenzen) zo flexibel mogelijk is en dat on-line zonder gegevensverlies parameters gewijzigd kunnen worden. Op deze wijze kan men de mogelijkheden van de hardware, zenders, ontvangers, slinger-, stamp- en koersaanwijzers zo veelzijdig mogelijk benutten en heeft men de beschikking over mogelijkheden tussen brede bundels met grote bedekking en relatief kleine nauwkeurigheid, en smalle bundels met kleine bedekking en relatief grote nauwkeurigheid.

Na een inleidend hoofdstuk wordt in hoofdstuk 2 de betreffende theorie, welke voor beide experimenten geldt, uiteengezet.
Hoofdstuk 3 presenteert het onderzoek aan boord van Hr Ms *Tydeman* als volgt:

A. Algemene beschouwingen.
B. Experimentele resultaten.
C. Aanbevelingen voor "lage" frequentie echosounding.

Hoofdstuk 4 geeft de resultaten weer van het "hoge" frequentie onderzoek te Maasbracht:

A. Algemene beschouwingen.
B. Modelexperiment.
C. Voorstel voor een multibeam echosounder.

1. Introduction and summary

Preliminaries

The fact that the velocity of sound in (sea)water does not vary much enables us to determine through ray theory the direction from which underwater sound is received. In the same manner the direction can be chosen in which underwater sound is emitted. These principles are applied in echosounders for hydrographic use (Glenn, 1970, Burke and Robson, 1975) sidelooking sonars (Belderson, et al., 1972), sectorscanning sonar (Tucker, 1960, Ballard and van Andel, 1977, Wolff, 1976) and imaging echosounders (Metherel et al., 1969). The class of hydrographic echosounders can be divided into narrow-beam systems and multi-beam systems. The former use an antenna, i.e. an array of transducers, to generate a single beam with a small beamwidth, the latter generate several beams with different azimuths.
Up to now the most sophisticated deep-sea multibeam echosounders (Sonarray Subsystem, Glenn, 1970, and Seabeam, Renard et Allenou, 1979) generate simultaneously beams with different azimuths, utilizing electronic circuits. These beams lie in a plane perpendicular to the ship's track. In that way information in three dimensions is gathered along one track, hence the name threee-dimensional echosounders.

The use of a multi-beam echosounder

A multi-beam echosounder can be utilized for a detailed bathymetric survey of hydrographically or geographically interesting areas (see e.g. Phillips and Fleming, 1978 or Allmendinger and Riis, 1979) with high precision.
In general the end product, which would also incorporate other soundings taken in the area will be a small to medium scale contour chart. This type of contour chart can serve, together with submersible observations (Ballard and van Andel, 1977) as a basis for geomorphological research. The time needed for making a multi-beam survey is quite short compared to that needed for covering the same area with conventional (narrow-beam) echosounders (McPhee , 1977), especially with deep-ocean surveys. A contour chart of this type can only be produced after the mission, when all navigational information can be incorporated. For direct system quality control most multi-beam systems produce a contourstripchart in which no navigational data are included. This contourstripchart, plotted a few seconds after the pertinent soundings have

been taken, can be used in two other functions. Firstly, if one sails one straight track, it provides rapidly the morphology of the features encountered, e.g. the strike of large fault scarps or fracture zones with respect to the track-line. Secondly, it can be used as a navigational tool if the goal of the mission is to follow some bottom feature (e.g. a submarine canyon, Renard et Allenou, 1979), by giving information concerning the course to be steered in order to do so.
Multi-beam systems can, like deep towed sonars, cameras or GLORIA (Rusby, 1970), shed light on important scientific problems concerning plate boundary structures, tectonic fabrik and surficial features of the sea floor (OCD report, 1979).

Summary of multi-beam experiments and recommendations

Of the systems mentioned above only Seabeam is commercially available. It uses electronic hardware for the generation of beams with fixed directions. The rigidity and vulnerability of this beamforming and the high price led us to investigate digital beamforming (i.c. beamforming with a flexible software algorithm in a digital computer), using different kinds of sound sources.

To this end two experiments were conducted:

1. A "low" frequency experiment in April 1979 on board H.Nl.M.S. *Tydeman*.
2. A "high" frequency model experiment in November 1977 in a chamber of the Juliana canal lock at Maasbracht.

The experiment on board H.Nl.M.S. *Tydeman* proves that a quasi-coherent sound source, like the airgun, can under certain circumstances be a sufficient approximation of a coherent sound source, enabling the generation of beams. This experiment's circumstances were thus, that a frequency of 75 Hz was received with sufficient amplitude. At this low frequency the receivers (streamers) have to be towed at a considerable distance to each other. Furthermore the influence of reflection against the water surface can not be neglected. The features of this experiment are the use of 3 streamers with a spacing of 9 m and beamforming by individual phase-shifting and summation.

The results demonstrate that with this arrangement a not so narrow beam in vertical direction with an improved signal-to-noise ratio is generated.

A single, low amplitude side echo is observed. Sufficient data for the construction of a contourstripchart were not obtained. This was caused by the large beamwidth and the relatively high sidelobe level of the sidebeams. The relatively slow computer impeded the on-line processing of the measurements.
It is argued on theoretical grounds that with 5 receivers (streamers) and a fast computer a qualitative bottom contour chart can be produced on-line. The production of profiles with sediment reflectors from different directions is possible beside the display of a narrow central beam with a high signal-to-noise ratio.

The model experiment in the lock at Maasbracht proves that a computer (with an appropriate program) can be utilized for the separation of signals coming from different directions and for the automatic detection of the bottom reflection in the presence of disturbing signals. The principal features of this experiment are an emitted sine-wave of 20 periods' length and 17.9 kHz frequency, a receiver of 32 or 16 elements and a distance-to-direction transformation with a weighted Discrete Fourier Transform (DFT). Not essential for the mathematical procedure but important for the economy of the experiment was the use of a synthetic aterture. A physical array of transducers is simulated with one transducer by successively measuring at the different array positions. This is called a synthetic aperture.

From this experiment recommendations follow the construction of a "high" frequency multi-beam echosounder. It is recommended to use an array processor for on-line execution of detection, filtering and DFT. Depth detection is necessary for the construction of an instant contourstripchart, while the detected data (depths and horizontal range) ought to be stored for the construction of the final contour charts.
The central philosophy in this design is the flexibility of the processing program (within certain limits). Parameters can be changed by the operator without loss of data. In this way the possibilities of hardware, projectors, receivers, roll-, pitch- and course-indicators are used with versatility. Beams with large beamwidth and relatively low accuracy used to sweep a broad swath can be alternated with beams with a small beamwidth and relatively high accuracy for sweeping a narrow swath, depending on the objective of the survey.

After the exposition of the relevant theory in chapter 2, the two experiments are presented in chapter 3 for the experiment on board H.Nl.M.S. *Tydeman*, including recommendations for low-frequency echosounding, and in chapter 4 for the results of the high-freqency model experiment at Maasbracht, including a proposal for a multi-beam echosounder system.

2. General theory

The wave-equation

The theory of sound propagation as used in this thesis can be developed taking Euler's equations for compressible non-viscous liquids as a point of departure (viz Sommerfeld, 1964). In the case of an ideal gas these equations can be derived using statistical methods, but heuristic arguments (Huang, 1963) have been formulated to show their validity for compressible non-viscous liquids.

Euler's first equation reads:

$$\frac{d\vec{u}}{dt} + \frac{1}{\rho} \text{ grad } (p+p_H) = \frac{\vec{F}}{\rho} \qquad (2.1).$$

This is Euler's formulation of Newton's second law (conservation of momentum).

Here

$\vec{u}\ (\vec{r},t)$	mean liquid particle velocity,
$\rho\ (\vec{r},t)$	mass density,
$p_H(\vec{r})$	hydrostatic equilibrium pressure,
$p\ (\vec{r},t)$	local pressure excursion from equilibrium,
$\vec{F}\ (\vec{r},t)$	external force acting upon a unit volume of liquid, or volume force,
$\vec{r}$	position vector,
t	time.

Euler's second equation reads:

$$\frac{\partial \rho}{\partial t} + \text{div } \rho\vec{u} = 0 \qquad (2.2).$$

This equation is commonly called the continuity equation, it describes the conservation of mass.

Both equations can be simplified if the following conditions are met:

2a. The only volume forces considered are those maintaining hydrostatic equilibrium.
The equation describing this condition is:

$$\text{grad } p_H = \vec{F} \qquad (2.3).$$

Surface forces too are not included, thus only sound propagation is considered, not sound production.

2b. Only small variations in mean liquid particle velocity are considered So it is justified to consider only first approximations of velocity-time dependence. Or in equation form:

$$\frac{d\vec{u}}{dt} = \frac{\partial \vec{u}}{\partial t} .$$

2c. Consider only small variations in density permitting the replacement of the (time-dependent) density ρ with the (constant) mean density ρ_0 except in $\frac{\partial \rho}{\partial t}$.

Under these assumption equations (2.1) and (2.2) will transform into:

$$\frac{\partial \vec{u}}{\partial t} + \frac{1}{\rho_0} \text{grad } p = 0 \qquad (2.4)$$

and

$$\frac{\partial \rho}{\partial t} + \rho_0 \text{ div } \vec{u} = 0 \qquad (2.5).$$

Now these equations can be connected in the following way.
Under condition 2c the change in density caused by a variation in pressure is proportional to this variation:

$$\frac{d\rho}{dp} = \kappa \rho_0,$$

where

κ is the coefficient of compressibility.

This is a formulation of Hooke's law for compressible liquids, and it can be differentiated to give:

$$\frac{\partial^2 p}{\partial t^2} = \frac{1}{\kappa \rho_0} \frac{\partial^2 \rho}{\partial t^2} \qquad (2.6).$$

Returning to equation (2.4) and taking the divergence of both sides, one gets:

$$- \text{div } \rho_0 \frac{\partial \vec{u}}{\partial t} = \text{div grad } p.$$

Whereas differentiation of equations (2.5) gives

$$- \text{div } \rho_0 \frac{\partial \vec{u}}{\partial t} = \frac{\partial^2 \rho}{\partial t^2} .$$

Together with equation (2.4) it follows that:

$$- \text{div } \rho_0 \frac{\partial \vec{u}}{\partial t} = \kappa \rho_0 \frac{\partial^2 p}{\partial t^2} \qquad (2.8),$$

and the combination of (2.7) and (2.8) then yields the pressure wave equation

$$\text{div grad } p = \kappa \rho_0 \frac{\partial^2 p}{\partial t^2} .$$

It will be shown, that if

$$c = (\kappa \rho_0)^{-\frac{1}{2}},$$

c is the absolute value of the phase velocity of a sound wave, or sound velocity.
With this definition the pressure wave equation gets its well-known form (see e.g. Rayleigh, 1945):

$$\text{div grad } p = \frac{1}{c^2} \frac{\partial^2 p}{\partial t^2} \qquad (2.9).$$

The general solution of this differential equation in one dimension is due to D'Alembert who solved it in connection with the vibrations of stretched strings. This general solution,

$$F(t,x) = F_1\left(t + \frac{x}{c}\right) + F_2\left(t - \frac{x}{c}\right),$$

describes the superposed propagation of two waves in opposite directions with velocity c. D'Alembert's solution is a superposition of such waves going in different directions, and the functions F_i can be found by applying boundary conditions. By specifying an initial pressure and velocity distribution one can incorporate the effect of a sound source. The functions F_i must have continuous first and second derivatives and the resulting pressure function must be compatible with the conditions 2a-2c stated at the beginning of the chapter.

Another solution of (2.9) can be obtained through the Fourier Transform of p:

$$P(\vec{r},\omega) = \frac{1}{2\pi} \int_{-\infty}^{\infty} p(\vec{r},t) \exp(-j\omega t)\, dt,$$

where

ω is the circular frequency $2\pi f$,
j is the square root of -1.

The inverse Fourier Transform is then:

$$p(\vec{r},t) = \int_{-\infty}^{\infty} P(\vec{r},\omega) \exp(j\omega t)\, d\omega.$$

This means that $p(\vec{r},t)$ can be written as an integral of periodic functions, that are solutions of equation (2.9)

$$P(\vec{r},\omega) \exp(j\omega t) \; . \qquad (2.10)$$

Henceforth the Fourier Transform of a function in the frequency domain will be indicated by a capital letter.

If this formulation is substituted into the wave equation (2.9) the so-called reduced wave equation or Helmholtz equation results:

$$\text{div grad } P = -k^2 P \qquad (2.11),$$

where

$$k(\vec{r}) = \omega c^{-1}.$$

k is called the wave number.

In $P(\vec{r},\omega)$ the phase and the amplitude of a periodic pressure wave with circular frequency ω is represented by a complex number.

Geometrical acoustics

In order to derive the equations of geometrical acoustics let

$$P = A \exp(-j\, k_0\, W) \qquad (2.12),$$

where

$A(\vec{r},\omega)$ is the real amplitude of $P(\vec{r},\omega)$,
$W(\vec{r},\omega)$ is the phase function, or wave front equation,
$k_0 = \frac{\omega}{c_0}$,
c_0 is an arbitrary reference sound velocity which must be chosen such that, within the area to be described by the geometrical equations, c must be close to c_0.

If equation (2.12) is a solution of the Helmholtz equation then the next two equations must be satisfied:

$$\text{div grad } A + k^2 - k_0{}^2 A \text{ grad W} \cdot \text{ grad } W = 0 \qquad (2.13);$$

and

$$2 \text{ grad } A \cdot \text{ grad } W + A \text{ div grad } W = 0 \qquad (2.14),$$

where

• denotes the scalar product of two vectors.

If A varies slowly enough with $\vec{r}$ the first term in equation (2.13) can be dropped and we get the far-field approximation:

$$\text{grad } W \cdot \text{ grad } W = n^2 \qquad (2.15),$$

where

$n = \frac{k}{k_0}$, the indes of refraction.

This equation (2.15) is known as the eikonal equation of geometrical acoustics.
$W(\vec{r},\omega)$ determines the phase of $P(\vec{r},\omega)$ and surfaces where $W(\vec{r},\omega)$ = constant are called wave-fronts.

If the unit-length vector $\vec{e}_s$ is perpendicular to the wave-front W, then from equation (2.15) it follows that

$$\left| \frac{1}{n} \frac{dW}{ds} \right| = \left| \frac{\text{grad } W}{n} \right| \cdot \left| \vec{e}_s \right| = 1 ,$$

where

$|\vec{r}|$ denotes the length of vector $\vec{r}$.

Consequently two expressions follow:

$$\vec{e}_s = \frac{1}{n} \text{ grad } W \qquad (2.16),$$

and

$$\frac{dW}{ds} = n \qquad (2.17).$$

Rays in geometrical acoustics are sets of curves orthogonal to the set of wave-fronts $W(\vec{r},\omega)$.

ds is an element of the ray path and

s denotes the arclength along the ray $\vec{r}(s)$.

Then equation (2.16) gives:

$$\frac{d\vec{r}}{ds} = \frac{1}{n} \text{ grad } W \tag{2.18}.$$

When this expression is inserted into the eikonal equation (2.15) W is eliminated leaving us with

$$\frac{d}{ds} \left(n \frac{d\vec{r}}{ds} \right) = \text{grad } n \tag{2.19}.$$

This set of second order differential equations, together with the boundary conditions, generates the ray trajectories.
They are called the ray equations.

The integration of equation (2.17) along the ray provides the phase of the propagating sound wave along the ray

$$W(s) = W(s_0) + \int_{s_0}^{s} n(\vec{r}(u)) \, du \tag{2.20},$$

where

$W(s_0)$ is the phase at the starting point of the ray at s_0 .

The so-called transport equations are obtained by the insertion of equation (2.18) into equation (2.14):

$$2n \frac{dA}{ds} = - A \text{ div grad } W \tag{2.20a}.$$

This equation describes the change of the amplitude. It can be solved using the Hamilton-Jacobi theory of canonical transformations (Ahluwalia and Keller, 1977 and Goldstein, 1950).

Another way to solve this equation is obtained by the equivalent formulation of equation (2.14):

$$\text{div } (A^2 \text{ grad } W) = 0 \ .$$

Application of Gauss's theorem leads to the following integral:

$$\oint_S A^2 \text{ grad } W \cdot \vec{e}_n \, dS = 0 \qquad (2.20b),$$

where

S is a closed surface with element dS ,
$\vec{e}_n$ is a unit vector normal to S .

This equation will be used to describe the development of the amplitude $A(\vec{r},\omega)$ along a ray.

Horizontal stratification

Let us consider an infinite horizontally stratified ocean. This means that the velocity of sound and with it the index of refraction n depends only on the vertical coordinate z. This horizontal stratification is a fortunate approximation of the ocean, especially over a limited horizontal range.

For this case the ray equations (2.19) become:

$$\frac{d^2x}{ds^2} = 0 \qquad (2.21),$$

$$\frac{d^2y}{ds^2} = 0 \qquad (2.22),$$

$$\frac{d}{ds}\left[n(z)\right] = \frac{dn}{dz} \ .$$

The third ray equation can be solved (Ahluwalia and Keller, 1977) by multiplying with $n\frac{dz}{ds}$ and integrating, thus obtaining

$$\left(n \frac{dz}{ds}\right)^2 = n^2 + \text{constant} \qquad (2.23).$$

From equations (2.21) and (2.22) it follows that, if a ray starts at $(0, 0, z_0)$, this ray lies in a plane

$$x \sin \phi - y \cos \phi = 0.$$

Let $r(z)$ be the horizontal distance from its starting point along the ray

$$r^2 = x^2 + y^2.$$

Then with the help of the relation:

$$\left(\frac{dr}{ds} \right)^2 + \left(\frac{dz}{ds} \right)^2 = 1,$$

it follows with equation (2.23) that

$$n \left(\frac{dr}{ds} \right) = \text{constant} \qquad (2.24).$$

Now let $\theta(z)$ be the angle of the ray in (x, y, z) with the z-axis and let θ_0 be the initial angle. Then equation (2.24), which is Snell's law for a horizontally stratified medium, can be formulated:

$$n(z) \sin \theta(z) = n(z_0) \sin \theta_0 \qquad (2.25).$$

This law can also be derived using Fermat's principle in the plane $x \sin \phi - y \cos \phi = 0$ (Tolstoy and Clay, 1966).

Using Snell's law, equation (2.23) can be rewritten as:

$$\left[n(z) \frac{dz}{ds} \right]^2 = n^2(z) + \left[n(z_0) \sin \theta_0 \right]^2 \qquad (2.26),$$

giving for equation (2.24):

$$\frac{dr}{dz} = \pm n(z_0) \sin \theta_0 \{ n^2(z) - n^2(z_0) \sin^2 \theta_0 \}^{-\frac{1}{2}} \qquad (2.27).$$

Upon integration this yields the expression for the ray trajectory in the plane $x \sin \phi - y \cos \phi = 0$:

$$r(z) = \int_{z_0}^{z} n(z_0)\ \sin\theta_0\ \{n^2(z) - n^2(z_0)\ \sin^2\theta_0\}^{-\frac{1}{2}}\ dz \qquad (2.28).$$

In order to compute the phase along the ray let

$$W(z_0) = 0$$

and rewrite equation (2.20):

$$W(z) = \int_{z_0}^{z} n(z)\ \frac{ds}{dz}\ dz\ ;$$

which, using equations (2.26) and (2.28), results in:

$$W(z) = n(z_0)\ r\ (z)\ \sin\theta_0 + \int_{z_0}^{z} \{n^2(z) - n^2(z_0)\ \sin^2\theta_0\}^{-\frac{1}{2}}\ dz \qquad (2.29).$$

The change of $W(\vec{r},\omega)$ along a horizontal line is expressed with the help of equation (2.17):

$$\left(\frac{\partial W}{\partial r}\right)_z = n(z)\ \sin\theta(z) \qquad (2.30).$$

A ray tube or beam is a tube bounded by rays.
From equation (2.20b) is follows that the quantity

$$A^2\ \text{grad}\ W$$

is conserved within a ray tube.
This quantity is proportional to the energy of the wave (Tolstoy and Clay, 1966), so this equation describes the conservation of energy inside a ray tube.
For rays starting at (0, 0, z_0) horizontal stratification implies cilindrical symmetry in the ray pattern and in the amplitude distribution. To exploit this symmetry consider a conical shell with apex (0, 0, z_0) and with an opening angle between θ_0 and $\theta_0 + d\theta_0$ bounded by rays.
If two surfaces are defined at z_1 and z_2 perpendicular to the rays, (2.20b) gives:

$$A^2(z_1)n(z_1)r(z_1)\cos\theta(z_1)\frac{dr(z_1)}{d\theta_0} = A^2(z_2)n(z_2)r(z_2)\cos\theta(z_2)\frac{dr(z_2)}{d\theta_0} \tag{2.31}.$$

Linear velocity-depth dependence

For the calculation of rays we dissect the ocean into layers of water with a sound velocity depending linearly on depth. Continuity equations for $c(z)$, $\theta(z)$ and $A(z)$ govern the transition from one layer to another. Thus calculations for single layers with a linear velocity-depth dependence,

$$c(z) = c(z_0)\{1 + \beta(z-z_0)\} \tag{2.32},$$

can be chained into a solution for the ocean.
For a single layer the following sound propagation expressions may be obtained, taking $c_0 = c(z_0)$ as the reference velocity in equation (2.13):

$$n(z) = \{1 + \beta(z-z_0)\}^{-1} ,$$

and

$$n(z_0) = 1 .$$

Thus equation (2.27) becomes:

$$r(z) = \frac{1}{\beta}\operatorname{cotg}\theta_0 - \frac{1}{\beta}\left[\sin^{-2}\theta_0 - \{1 + \beta(z-z_0)\}^2\right]^{\frac{1}{2}} .$$

This equation can be readily written as the pair:

$$\sin\theta(z) = \{1 + \beta(z-z_0)\}\sin\theta_0 \tag{2.33},$$

$$r(z) = \beta^{-1}\sin^{-1}\theta_0\{\cos\theta_0 - \cos\theta(z)\} \tag{2.34}.$$

For this single layer the expression (2.29) can be integrated to obtain:

$$W(z) = \beta^{-1}\left[\log\{1 + \beta(z-z_0)\} + \log(1 + \cos\theta_0) - \log\{1 + \cos\theta(z)\}\right] \tag{2.35}.$$

Differentiation of equation (2.34) produces the next equation:

$$\frac{dr}{d\theta_0} = r(z) \{ \sin \theta_0 \cos \theta(z) \}^{-1} \qquad (2.35a),$$

which is used to evaluate the amplitude from equation (2.31) along a ray, giving:

$$A^2(z)\, r^2(z)\, n(z) = \text{constant} \qquad (2.36).$$

This expression shows that for cylindrical waves in water with a sound velocity depending linearly on depth the amplitude is inversely proportional to the horizontal distance but for the influence of the square root of the index of refraction.

All formula's derived in the previous section hold only if $\sin \theta(z)$ does not equal 1, which indicates a reversal of the ray with respect to the z-direction, a so-called turning point. As we want to measure the ocean bottom, we are not interested in turning rays. Also, as can be seen from equation (2.35a), when $\theta(z)$ approaches 90 degrees, small deviations of θ_0 result in large deviations of $r(z)$, meaning essentially that the rays used in measuring the ocean bottom should not approach a turning point, because of the loss of lateral precision.
For this reason we will consider in the following section only cases where $\theta(z) - \theta_0$ is small, and we will compute accordingly second order approximations. From equation (2.33) it follows that this condition is fulfilled either for

$$\beta(z-z_0) \ll 1 ,$$

or for $\sin \theta_0$ small.

Second order approximations

First, from equations (2.33) we obtain:

$$\sin \{\theta(z) - \theta_0\} = \beta(z-z_0) \tan \theta_0 + \tfrac{1}{2}\beta^2 (z-z_0)^2 \tan^3 \theta_0 .$$

This approximation is used for substitution into equation (2.34), giving:

$$r(z) = (z-z_0) \tan \theta_0 + \tfrac{1}{2}\beta (z-z_0)^2 \tan \theta_0 \cos^{-2} \theta_0 \qquad (2.37).$$

This equation can also be obtained by developing (2.34) in a Taylor's series in the neighborhood of $z = z_0$.

By the same procedure it follows from equation (2.35) that

$$W(z) = (z-z_0) \cos^{-1} \theta_0 + \tfrac{1}{2}\beta(z-z_0)^2 \cos^{-3} \theta_0 \{\sin^2 \theta_0 - \cos^2 \theta_0\} \quad (2.38).$$

Equation (2.37) can be inserted into equation (2.36):

$$A(z) \{(z-z_0) + \tfrac{1}{2}\beta(z-z_0)^2 (1 + \cos^{-2} \theta_0)\} = \text{constant} \quad (2.39),$$

taking the first order approximation of the square root of $n(z)$.
Travel time along the ray can be computed using:

$$\frac{ds}{dt} = c(z) \ ;$$

applying equation (2.17) and integrating yields:

$$t(z) - t(z_0) = c_0^{-1} W(z) \ .$$

Combining this with equation (2.38) we obtain:

$$t(z) - t(z_0) = c_0^{-1} (z-z_0) \cos^{-1} \theta_0 + \tfrac{1}{2}\beta c_0^{-1} (z-z_0)^2 \cos^{-3} \theta_0 \times$$

$$\times (\sin^2 \theta_0 - \cos^2 \theta_0) \quad (2.40).$$

This equation in combination with equation (2.29) yields the time-dependence of the amplitude A along the ray:

$$A(z,\omega) \{t(z) - t(z_0) + \frac{3}{2}\beta(z-z_0)^2 c_0^{-1} \cos \theta_0^{-1}\} = \text{constant} \quad (2.41).$$

Two remarks should be made:

1. Equations (2.31), (2.36), (2.39) and (2.41) do not hold for $z \to z_0$, because the amplitude becomes infinite. So a point source at (0, 0, z_0) can not exist. However, any wavefront surface away from z_0 serves as a source of energy, and thus as a reference for the calculation of $A(z,\omega)$.

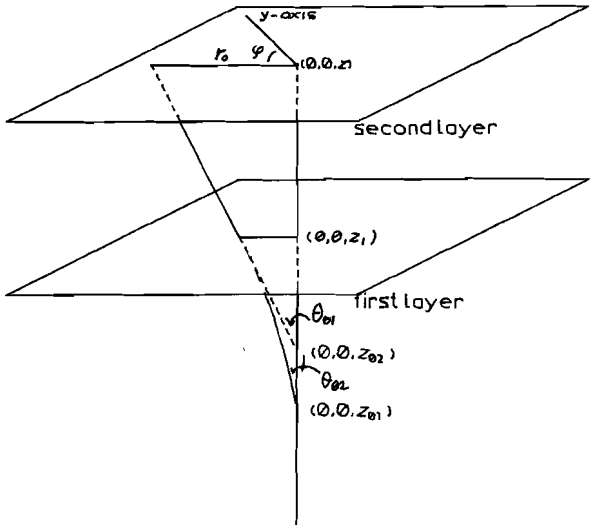

Figure 2.1 Rays through two layers of water.

2. If there are two layers of water with different velocity gradients β_1 and β_2 and if one considers the continuity of the ray $\vec{r}(z)$ starting in $(0, 0, z_{01})$ with an initial angle θ_{01}, it can be shown that, by solving the continuity equations:

$$(z_1 - z_{01}) \tan \theta_{01} + \tfrac{1}{2}\beta_1 (z_1 - z_{01})^2 \tan \theta_{01} \cos^{-2} \theta_{01} =$$

$$= (z_1 - z_{02}) \tan \theta_{02} + \tfrac{1}{2}\beta_2 (z_1 - z_{02})^2 \tan \theta_{02} \cos^{-2} \theta_{02} ,$$

and

$$\tan \theta_{01} + \beta_1 (z_1 - z_{01}) \tan \theta_{01} \cos^{-2} \theta_{01} = \tan \theta_{02} +$$

$$+ \beta_2 (z_1 - z_{02}) \tan \theta_{02} \cos^{-2} \theta_{02} ,$$

it is possible to calculate a point $(0, 0, z_{02})$ and an initial angle θ_{02} where the ray in the second medium (after crossing the boundary) can be brought to come from if the first medium did not exist (see figure 2.1).

The signal amplitude can be redefined to a suitable reference wavefront.
It can also be shown from ray geometry that all rays starting in the first layer at $(0, 0, z_{01})$, with θ_0 within a neighborhood of θ_{01}, seem to come in the second layer from $(0, 0, z_{02})$, with an initial angle within a neighborhood of θ_{02}.
This process can be repeated for several layers.

Phase and amplitude in a horizontal plane

Let us consider rays starting (or seeming to start) at $(0, 0, z_0)$, and ending at $(r_0 \sin\phi, r_0 \cos\phi, z)$ (fig 2.1).
Then from equations (2.33) and (2.34) it follows that the initial angle (or apparent initial angle) can be computed with:

$$\theta_0 = \arctan \left[2\beta r_0 \{2(z-z_0) + \beta(z-z_0)^2 + \beta r_0^2\}^{-1} \right],$$

from which, when terms with β^2 are dropped, it follows:

$$\sin\theta_0 = r_0 \left[\{(z-z_0)^2 + r_0^2\} \{1 + \beta(z-z_0)\} \right]^{-\frac{1}{2}} \qquad (2.41).$$

From equation (2.30) it follows that:

$$\left(\frac{d^2W}{dr^2}\right)_z = r_0^{-1} \sin\theta_0 \cos\theta_0 \cos\theta(z) .$$

Now a Taylor expansion to the second degree can be made to compute the phase distribution as a function of r in a neighborhood of r_0, keeping z fixed.
With the help of these equations and (2.30) it follows:

$$W(r) = W(r_0) + (r-r_0)\, n(z) \sin\theta(z) + \tfrac{1}{2} \cos\theta_0 \cos\theta(r_0) \times$$

$$\times \left[\{r_0^2 + (z-z_0)^2\} \{1 + \beta(z-z_0)\} \right]^{-\frac{1}{2}} (r-r_0)^2 .$$

In this equation the second term becomes negligible if

$$(r-r_0) \ll \left[\{1 + \beta(z-z_0)\} \{r_0^2 + (z-z_0)^2\} \right]^{\frac{1}{2}} .$$

In the previous section we already stated that

$$\beta(z-z_0) \ll 1 \qquad (2.41a),$$

so that

$$(r-r_0) \ll \{r_0^2 + (z-z_0)^2\}^{\frac{1}{2}} \qquad (2.41b)$$

is necessary for a first-order approximation of the phase distribution.

If more than one layer is involved the condition (2.41a) should be taken as a sum over all layers:

$$\sum_i \mid \beta_i \ (z_i - z_{i-1}) \mid \ll 1 \qquad (2.41c),$$

where z_i is the coordinate of the boundary between layer i-1 and layer i. From Matthews (1939) it can be computed that this sum does not exceed 0.05 in most parts of the ocean to a depth of 5000 m.
Condition (2.41b) limits the neighborhood for which the wavefront may be approximated by a plane wavefront in the Fraunhofer approximation. The extent of the neighborhood depends on the allowable phase difference and thereby on the signal wavelength.

Thus it is established that if we have a sound source at $(0, 0, z_0)$ with a signal strength A_1 at unit distance, the resulting pressure in a neighborhood of $(r_0 \sin \phi, r_0 \cos \phi, z)$ can be described by:

$$P(\vec{r},\omega) = A_1(\omega) \frac{r_1}{r_0} \exp\{-j\, k_0\, n(z)\, (r-r_0) \sin \theta(r_0)\} ,$$

where r_1 is the horizontal distance at which the amplitude A_1 is reached, noting that:

$$\lim_{r_1 \to 0} \frac{r_1}{r_0} = (z-z_0)^{-1} .$$

If we define a complex quantity describing amplitude and phase:

$$A^*(r_0,\omega) = A_1(\omega) \frac{r_1}{r_0} \exp\{-j\, k(z) r_0\},$$

for P the following expression results:

$$P(\vec{r},\omega) = A^{*}(r\ ,\omega)\ \exp\ \{-j\ k(z)r\} \qquad (2.42)$$

for r in a neighborhood of r_0.
This expression is equivalent to the Fraunhofer far-field formulation (Horton, 1969).

The principle of reciprocity

Several reciprocal theorems are used in the field of underwater acoustics. They are all elaborations of a principle of reciprocity proved by Rayleigh for certain circumstances (Rayleigh, 1945), although some have been formulated before Rayleigh's proof. Rayleigh's principle is used expediently for the calibration of standard hydrophones (Albers, 1965). Helmholtz' reciprocal theorem, showed by Rayleigh (1945) to be a special case of Rayleigh's principle of reciprocity, states that, when an excitation at point A results in a velocity-potential in point B, the same velocity-potential would be observed at point A had point B been the source of the excitation, if certain conditions are met. A result of this theorem is that when a transmitting transducer has a certain directional characteristic, depending on the spectral content of the emitted signal, the same characteristic is exhibited when the transducer is used for the reception of signals with the same spectral content. Another result of the principle shows, that if a ray connects two points, sound may be propagated from either point to the other along this ray. The phase and amplitude at either end point are interchanged when the direction of propagation is reversed.

The infinite receiver-processor

To proceed les us define a coordinate system (figure 2.2) in which a sound source is located at (x_i, y_i, z_i). Let r_i be the ray connecting (x_i, y_i, z_i) with $(0, 0, 0)$, let α_i be the angle of r_i with the x-axis and let β_i be the angle of r_i with the y-axis, both in $(0, 0, 0)$.
If θ_i is the angle of the ray r_i with the z-axis in $(0, 0, 0)$ then:

$$\cos \alpha_i = x_i \, (x_i^2 + y_i^2)^{-\frac{1}{2}} \sin \theta_i \ ,$$

$$\cos \beta_i = y_i \, (x_i^2 + y_i^2)^{-\frac{1}{2}} \sin \theta_i \ .$$

If $\beta(\alpha^1, \beta^1, \omega) \cos \alpha^1 \, d \cos \beta^1$ is the total signal strength received at $(0, 0, 0)$ from sources with

$$\alpha^1 \leqslant \alpha_i < \alpha^1 + \sin^{-1} \alpha^1 \, \mathrm{dcos} \, \alpha^1 \ ,$$

$$\beta^1 \leqslant \beta_i < \beta^1 + \sin^{-1} \beta^1 \, \mathrm{dcos} \, \beta^1 \ ,$$

then the signal strength received at $(x, y, 0)$ can be written, applying equation (2.42), as:

$$P(x, y, \omega) = \int_{-1}^{+1} \int_{-1}^{+1} B(\alpha^1, \beta^1, \omega) \exp \{-j k_0 \times$$

$$\times (x \cos \alpha^1 + y \cos \beta^1)\} \, \mathrm{dcos} \, \alpha^1 \, \mathrm{dcos} \, \beta^1 \ .$$

where $(x, y, 0)$ lies within a neighborhood of $(0, 0, 0)$.

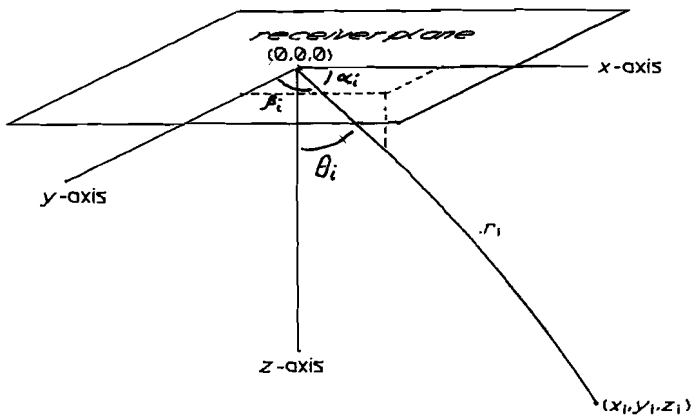

Figure 2.2 Receiver plane geometry.

Let us for a moment assume that equation (2.43) holds for the whole plane $z = 0$.

If an infinite continuous receiver is defined in this plane, that receives at each point $(x, y, 0)$ the signal $P(x, y, \omega)$, with a processor that applies a phase shift equal to

$$k_0 (x \cos \alpha + y \cos \beta) \tag{2.44a},$$

where α and β define an arbitrary direction, to this signal before it integrates the signals to obtain one output, this output would be:

$$C(\alpha, \beta, \omega) = \int_{-\infty}^{\infty} \int_{-\infty}^{\infty} P(x, y, \omega) \exp \{j k_0 (x \cos \alpha + y \cos \beta)\} \, dx dy.$$

If we introduce equation (2.43) into this integral and interchange the order of integration, we obtain upon integration, taking the Cauchy principal value:

$$C(\alpha, \beta, \omega) = \lim_{M \to \infty} \lim_{N \to \infty} \int_{-1}^{1} \int_{-1}^{1} B(\alpha, \beta, \omega) \{k_0 (\cos \alpha^1 - \cos \alpha)\}^{-1} \times$$

$$\times \sin \{k_0 \, M(\cos \alpha^1 - \cos \alpha)\} \{k_0 (\cos \beta^1 - \cos \beta)\}^{-1} \times$$

$$\times \sin \{k_0 \, N(\cos \beta^1 - \cos \beta)\} \, d\cos \alpha^1 \, d\cos \beta^1 \, .$$

Dirichlet's sieve formula then leads to the solution:

$$C(\alpha, \beta, \omega) = 4\pi^2 k_0^{-2} \, B(\alpha, \beta, \omega) \tag{2.44}.$$

The output of the processor applying the phase shift (2.44a) is seen to be proportional to the signal strength originating from sources i with:

$$\alpha \leqslant \alpha_i \leqslant \alpha + \sin^{-1} \alpha \, d\cos \alpha$$

and

$$\beta \leqslant \beta_i \leqslant \beta + \sin^{-1} \beta \, d\cos \beta \, .$$

If now a substitution of co-ordinates is made as follows:

$$\ell = \cos \alpha \ ,$$
$$m = \cos \beta \ ,$$
$$u = \lambda_0^{-1} x \ ,$$
$$v = \lambda_0^{-1} y \ ,$$

where λ_0 is the local wavelength $\frac{2\pi}{k_0}$ (depending on ω),

it can be seen that

$$P(u, v) = \int_{-\infty}^{\infty} \int_{-\infty}^{\infty} B(\ell, m) \exp \{-2\pi j(\ell u + m v)\} \, d\ell \, dm \qquad (2.45),$$

and

$$B(\ell, m) = \int_{-\infty}^{\infty} \int_{-\infty}^{\infty} P(u, v) \exp \{2\pi j(\ell u + m v)\} \, du \, dv \qquad (2.46).$$

Here P and B are still dependent on ω, which is omitted for convenience.
In other words:
If $B(\ell, m)$ is considered as a function of ℓ and m with

$$B(\ell, m) = 0 \quad \text{for} \quad \{|\ell| > 1 \quad \text{or} \quad |m| > 1\} \ ,$$

then P and B form a Fourier pair of functions.
Technically this is a two-dimensional transformation from the aperture distance (in wavelength) domain to the direction cosine domain. Thus by Fourier transforming the measured pressure-distribution on an infinite plane surface we can obtain exactly the angular incoming pressure distribution, which is still defined in the frequency domain.
In the following section this transform property will be used to elucidate the properties of array receivers.
Using a generalized function, we can also write equation (2.44) as:

$$C(\ell, m) = \int_{-\infty}^{\infty} \int_{-\infty}^{\infty} B(\ell^1, m^1) \, {}^2\delta \, (\ell - \ell^1, m - m^1) \, d\ell^1 \, dm^1 \qquad (2.47),$$

where ${}^2\delta(\ell, m)$ is the two-dimensional Dirac delta function.

Here the delta function $^2\delta\ (\ell-\ell^1, m-m^1)$ can be interpreted as the receiver directional or "beam" pattern for the "look" direction (ℓ, m). Accordingly the measured angular pressure distribution $C(\ell, m)$ is generated by the convolution of the incoming signal strength with the receiver directional pattern.

The non-ideal receiver

In general we do not have an infinite receiver, nor do we have continuous space-sampling. This can be dealt with in the following manner. Define a weighting function $W(u, v)$, which may incorporate the finiteness of the receiver and/or the space-sampling properties. Employing this weighting function we can determine an estimate $C(\ell, m)$ of the incoming angular pressure distribution $B(\ell, m)$ with the equation:

$$C(\ell, m) = \int_{-\infty}^{\infty} \int_{-\infty}^{\infty} W(u, v)\ P(u, v)\ \exp\{2\pi j(\ell u + mv)\}\ du\ dv \qquad (2.48).$$

This estimate will be called the angular spectrum of the incoming pressure distribution. For a fixed direction (ℓ, m) this quantity will be called the beam signal for that direction. It incorporates beam amplitude and beam phase.
The computation of $C(\ell, m)$ is called beamforming or beam steering.

It is seen from the convolution rule that

$$C(\ell, m) = \int_{-\infty}^{\infty} \int_{-\infty}^{\infty} F(\ell-\ell^1, m-m^1)\ B(\ell^1, m^1)\ d\ell^1\ dm^1 \qquad (2.49),$$

where

$$F(\ell, m) = \int_{-\infty}^{\infty} \int_{-\infty}^{\infty} W(u, v)\ \exp\{2\pi j(\ell u + mv)\}\ du\ dv \qquad (2.50).$$

Thus analogously to equation (2.47) $F(\ell-\ell^1, m-m^1)$ can be called the receiver pattern for the "look" direction (ℓ, m), and this pattern is the inverse Fourier transform of the weighting function $W(u, v)$.
This property gives a tool to evaluate implications of receiver design in terms of the receiver pattern, and, conversely, to determine a weighting function when pattern specifications are given.

If the weighting function can be factored into two functions with separated variables:

$$W(u, v) = W_1(u) \cdot W_2(v) \qquad (2.51).$$

Then the pattern may also be separated:

$$F(\ell, m) = F_1(\ell) \cdot F_2(m) \ ,$$

where

$$F_1(\ell) = \int_{-\infty}^{\infty} W_1(u) \exp(2\pi j \ \ell u) \, du \ ,$$

and

$$F_2(m) = \int_{-\infty}^{\infty} W_2(v) \exp(2\pi j \ mv) \, dv \ .$$

The following remark can be made about these patterns.
They are defined between $-\infty$ and $+\infty$, however they have only significance for the directions where $B(\ell^1, m^1)$ is not equal to zero, as can be seen from equation (2.49). So the pattern specification needs only be given for $|\ell^1| \leqslant 1$ and $|m^1| \leqslant 1$.
Also from equation (2.49) it can be deduced that the receiver sensitivity depends on the differences between the "look" direction of the receiver and the direction out of which the contribution to the angular spectrum comes, i.e. $(\ell-\ell^1, m-m^1)$.
However, because ℓ is the cosine of the angle α, the angular pattern is deformed when the "look" direction changes (see figs 2.3 and 2.4).

Influence of element directivity

In the previous sections it has been assumed that the receiver elements $(du \ dv)$ have an omnidirectional sensitivity characteristic. If $F^1(\ell^1, m^1)$ is the receiver element pattern (all elements identical) then $B(\ell^1, m^1)$ is multiplied by $F^1(\ell^1, m^1)$ before the receiver phase shift is applied.

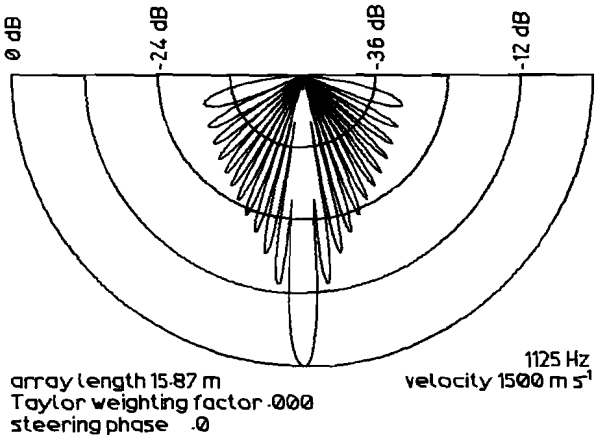

Figure 2.3 One-dimensional beam pattern for $\ell = 0$.

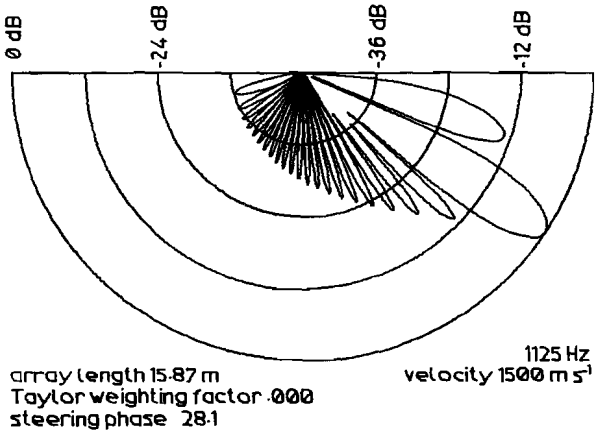

Figure 2.4 One-dimensional beam pattern for $\ell = 0.83$.

Thus the resultant measured output will be:

$$C(\ell, m) = \int_{-\infty}^{\infty} \int_{-\infty}^{\infty} F(\ell-\ell^1, m-m^1)\ F^1(\ell^1, m^1)\ B(\ell^1, m^1)\ d\ell^1\ dm^1 \qquad (2.52),$$

and the resulting pattern is obtained by multiplying the pattern associated with the omnidirectional assumption with the pattern of a single element:

$$F(\ell-\ell^1, m-m^1)\ F^1(\ell^1, m^1)\ .$$

This resulting pattern is clearly different for different "look" directions (ℓ, m) .

The finite receiver

In this section we deduce the influence of the finiteness of the receiver.

Let the weighting function be:

$$W(u, v) = \Pi\left(\frac{u}{\hat{u}}\right) \Pi\left(\frac{v}{\hat{v}}\right) ,$$

where

$$\Pi(x) = \begin{cases} 1 & \text{for } |x| < \frac{1}{2} \\ 0 & \text{for } |x| > \frac{1}{2} \end{cases}$$

(see Bracewell, 1978) .
This weighting function describes the effect of limiting the receiver to a rectangle with sides $\hat{u}\ \lambda_0$ and $\hat{v}\ \lambda_0$.
In this case W is separable, so we can consider a weighting function in one dimension:

$$W = \Pi\left(\frac{u}{\hat{u}}\right) .$$

The length $\hat{u}\ \lambda_0$ is called the aperture of the receiver in this direction.

Fourier transformation provides the pattern

$$F = \hat{u}\ \ \mathrm{sinc}\ (\hat{u}\ell) \qquad (2.53),$$

where

$$\text{sinc}\ (x) = \begin{cases} 1 & \text{for } x = 0, \\ \dfrac{\sin \pi x}{\pi x} & \text{for } x \neq 0 \ . \end{cases}$$

As is seen in figure (2.3) the delta function with infinitely small beamwidth of the infinite receiver is replaced by the sinc - function.
This can be interpreted by stating that with a finite aperture we do not measure the exact angular pressure distribution, but a weighted average of the angular pressure distribution.

Beamwidth

The half-power beamwidth $\hat{\ell}$ is defined as follows:

$$\text{If } \ell \in (-\tfrac{1}{2}\hat{\ell}, \tfrac{1}{2}\hat{\ell}) \text{ then } |F(\ell)| \geq 2^{-\frac{1}{2}} F(0) \ .$$

From equation (2.50) one calculates for a rectangular aperture:

$$\hat{\ell}\hat{u} = 2 \operatorname{sinc}^{-1}(0.7071) = 0.885 \qquad (2.54).$$

For large valves of $\hat{u}$ and "look" angles near 90^0 the following approximation can be made

$$\Delta\alpha \approx 51\ \hat{u}^{-1} \text{ degrees} \qquad (2.55),$$

where $\Delta\alpha$ is the half-power beamwidth in degrees

Theoretical considerations show that equation (2.54) does not give the best attainable beamwidth-aperture product.
One of the Fourier uncertainty relations (Papoulis, 1962) shows that the following inequality exists:

$$\hat{\ell}\ \hat{u} \geq 0.5 \ ,$$

the equal sign indicating the theoretically best obtainable beamwidth.

This means that the uniformly weighted continuous receiver that has the pattern of equation (2.53) is not the optimum receiver with respect to half-power beamwidth.

Space-sampling and array properties

Let us proceed by the introduction of a set of discrete receiving elements i placed at (u_i, v_i). The effect is described by the generalized function:

$$W(u, v) = \sum_i {}^2\delta(u-u_i, v-v_i) \qquad (2.56).$$

This function has the Fourier transform

$$F(\ell, m) = \sum_i \exp(2\pi j\, \ell u_i) \exp(2\pi j\, m v_i) \qquad (2.57).$$

Thus the resulting receiver pattern is given by a superposition of periodic functions in two dimensions. Again, if the function W is separable into a product according to equation (2.51) then F can also be separated. This condition is met when the receiver elements are placed on the intersections of a not necessarily regularly spaced rectangular grid.
If we consider for convenience a weighting function in one dimension:

$$W(u) = \sum_i \delta(u-u_i) ,$$

where $\delta(u)$ is the one-dimensional Dirac delta function, then it follows that

$$F(\ell) = \sum_i \exp(2\pi j\, \ell u_i) .$$

If the spacing of the I elements in one direction is uniform and the distance between adjacent elements is $\hat{u}_1\ \lambda_0$ then the receiver pattern can be written as a geometric progression:

$$F(\ell) = \sum_{i=0}^{I-1} \exp(2\pi j i\, \ell\hat{u}_1) = \frac{1 - \exp(2\pi j\, \ell\hat{u}_1 I)}{1 - \exp(2\pi j\, \ell\hat{u}_1)} \qquad (2.58).$$

The discrete Fourier Transform

Now the expression (2.48) can be elaborated for the transformed receiver output of a rectangular array of $I \times K$ uniformly spaced elements placed at $(u_i, v_k, 0)$:

$$C(\ell, m) = \int_{-\infty}^{\infty} \int_{-\infty}^{\infty} \sum_{i=0}^{I-1} \sum_{k=0}^{K-1} {}^{2}\delta(u-u_i, v-v_k)\, P(u, v)\, \exp\{2\pi j \times$$

$$\times (\ell u + m v)\}\, du\, dv \ .$$

Since the delta function is separable, we obtain, upon integration,

$$C(\ell, m) = \sum_{i=0}^{I-1} \sum_{k=0}^{K-1} P(u_i, v_k)\, \exp\{2\pi j\, (\ell u_i + m v_k)\} \ ,$$

and if the elements are regularly spaced in both directions:

$$C(\ell, m) = \sum_{i=0}^{I-1} \sum_{k=0}^{K-1} P(i\bar{u}_1, k\bar{v}_1)\, \exp\{2\pi j\, (i\ell\hat{u}_1 + km\,\hat{v}_1)\} \qquad (2.60),$$

where

$\hat{u}_1$ is the spacing of the elements in the u co-ordinate,
$\hat{v}_1$ is the spacing of the elements in the v co-ordinate.

The last equation clearly shows that $I \times K$ estimates of the angular pressure distribution can be obtained by a two-dimensional inverse Discrete Fourier Transform (DFT) for values of ℓ and m given by:

$$\ell_{i^1} = i^1 \hat{\ell}_1 \ , \quad i^1 = 0 \ldots I-1 \ ,$$
$$m_{k^1} = k^1 \hat{m}_1 \ , \quad k^1 = 0 \ldots K-1 \ ,$$

where

$$\hat{u}_1 \hat{\ell}_1 = I^{-1} \qquad (2.61),$$
$$\hat{v}_1 \hat{m}_1 = K^{-1} \qquad (2.62).$$

The outputs of this DFT are the discrete beams of the receiver.

The sampling theorem (Bracewell, 1978) implies that, if $W(u, v)\ P(u, v)$ is a band-limited function, then its transform $C(\ell, m)$ is sampled critically when the intervals are taken as $\ell_1 = \frac{1}{\hat{u}}$ and $m_1 = \frac{1}{\hat{v}}$, where $\hat{u}$ and $\hat{v}$ are the apertures of the array in wavelengths.
Now when we take the aperture as:

$$\hat{u} = I\hat{u}_1$$

and

$$\hat{v} = K\hat{v}_1 \quad ,$$

equations (2.61) and (2.62) show that the DFT just results in critical sampling. Thus one cannot obtain more than $I \times K$ mutually independent samples of the angular pressure distribution when using an array $I \times K$ elements.

The properties of this array can be studied through the pattern (2.58).
The modulus of this pattern is :

$$|F(\ell)| = \left|\frac{\sin(\pi \ell\ \hat{u}_1 I)}{\sin(\pi \ell\ \hat{u}_1)}\right| \qquad (2.63).$$

For this element distribution the half-power beamwidth to aperture relation is dependent on I thus:

I	2	4	8	16
$\hat{\ell}\ \hat{u}$	1.000	0.901	0.892	0.887

So for large I the case of a continuous receiver is approached.

Major lobe suppression

The equation (2.63), well-known in optics as the grating response, shows a periodic character with period $(\hat{u}_1)^{-1}$ (see e.g. figure 2.5).

This means, that a signal will be measured in beams belonging to different directions, corresponding to non-zero order maximums, the secondary major lobes. This can be avoided by choosing $\hat{u}_1$ in such a way that the first order major lobe occurs for $|\ell| \geq 2$.
This means that in the interval $-1 < \ell < 1$ only one major lobe occurs for all "look" directions.
This condition is met for

$$\hat{u}_1 \leq 0.5 \qquad (2.64).$$

If for some reason, e.g. because elements are physically too large, more then one major lobe occurs in the region $-1 < \ell < 1$ then it may be suppressed by using a non-uniform element spacing (see Anton and Rockmore, 1976 and Wang, 1975) in one dimension or even a random distribution in the receiver plane (Willey, 1962). Of course one can not use the DFT in these cases to compute beams.

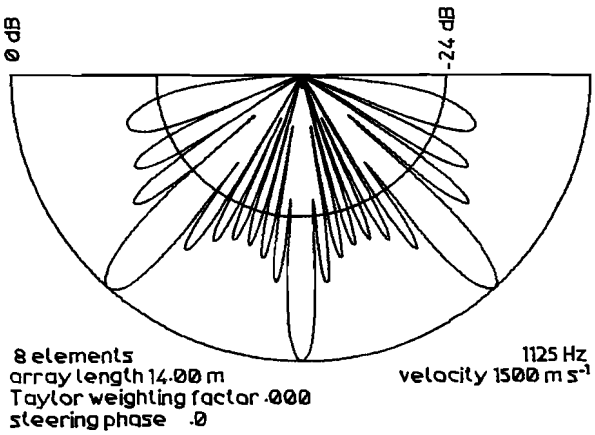

Figure 2.5 Beam pattern showing secondary major lobes.

Side lobe suppression

It can be seen from equation (2.63) or figure (2.3) that, except for directions for which $|F(\ell)| = 0$, the pressure distribution of all directions contributes to the measured amplitude of a given beam. This so-called sidelobe effect can be responsible for the loss of a weak signal in a beam when strong signals are present in other beams. It is equivalent with the smearing effect in the spectral estimator.
The process by which sidelobes are controlled is commonly called shading. It is the same as the application of a window in time-frequency operations (see Harris, 1978).

For a linear array, phased in direction $\ell = 0$ with a uniform spacing of $\hat{u}_1 = 0.5$ Dolph (1946) showed that Chebyshev polynomials can be used to generate a weighting function with a transform having sidelobes equal to or less than a predetermined value. However, when the sidelobes are thus suppressed, the beamwidth is increased. Dolphs method has been adapted by Riblet (1947) and Pritchard (1953) to include different array spacings and directions other than $\ell = 0$. Taylor (1955) gave an expansion in a power series of cosines that is most effectiye for the nearest sidelobes.
If one weights with this series truncated after the first cosine term, this is called simple Taylor weighting, or cosine-on-a-pedestal weighting. The well-known Hamming and Hanning windows are examples of simple Taylor weighting.

The definition of the simple Taylor weighting function is :

$$W(i\,\hat{u}_1) = 1 - 2F_1 \cos\{2\pi(I+1)^{-1}(i+1)\} \qquad (2.65),$$

whence a beam pattern results defined as follows:

$$F(\ell) = (1-a^I)(1-a)^{-1} + 2F_1\{a+a^I - h(1+a^{I+1})\}(1-2h\,a+a^2)^{-1},$$

where

$$a = \exp(2\pi j\,\ell\,\hat{u}_1),$$
$$h = \cos\{2\pi(I+1)^{-1}\}.$$

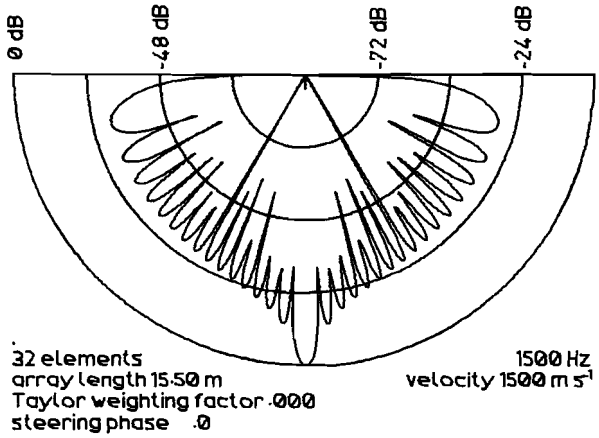

Figure 2.6 Beam pattern of an unshaded array.

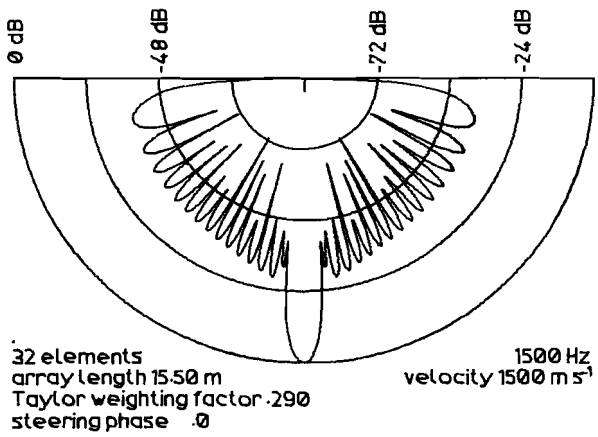

Figure 2.7 Beam pattern of an array shaded with a simple Taylor function with $F_1 = 0.29$.

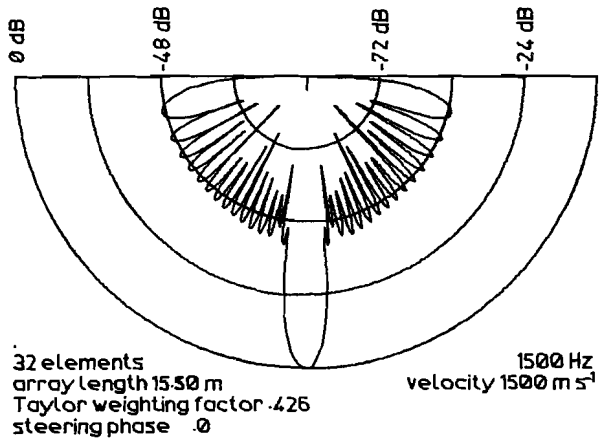

Figure 2.8 Beam pattern of an array shaded with a Hamming window.

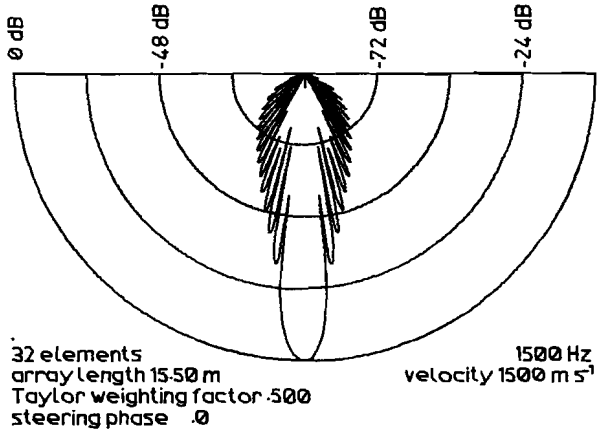

Figure 2.9 Beam pattern of an array shaded with a Hanning window.

For large I the pattern can be calculated and the following properties listed (see McCord, 1978) for different windows :

window	F_1	$\hat{\ell}'/\hat{\ell}$	s.l.(dB)	M.L.(dB)	figure
rectangular	0	1	- 13.3	0	(2.6)
without a name	0.29	1.262	- 28.5	- 0.68	(2.7)
Hamming	0.426	1.503	- 42.8	- 1.34	(2.8)
Hanning	0.500	1.650	- 31.7	- 1.76	(2.9)

where

$\hat{\ell}$ is beamwidth without shading,

$\hat{\ell}'$ is beamwidth with the indicated shading,

s.l. is maximum sidelobe level in dB with respect to the main lobe,

M.L. is matched filter loss (see the end of this chapter).

Signal bandwidth considerations

Since all expressions derived from equation (2.11) onward are formulated in the frequency domain, all phase-shifts are dependent on wavelength and thus on frequency. This means that these expressions can be transformed to the time domain quite simply when the incoming signals have a narrow well-defined bandwidth.
In this case the equation

$$c(\ell, m, t) = \int_{-\infty}^{\infty} C(\ell, m, \omega)\, \delta(\omega-\omega_0)\, \exp(j\omega t)\, d\omega \qquad (2.66)$$

describes the reception of narrow-band signals with the band centered at ω_0. The output signal is, upon integration:

$$c(\ell, m, t) = C(\ell, m, \omega_0)\, \exp(j\omega_0 t) \qquad (2.67)$$

But for broadband signals we have to rewrite the equations (2.43) to (2.50).

If $B(\alpha^1, \beta^1, \omega)\, d\cos\alpha^1\, d\cos\beta^1\, d\omega$ is the total signal strength as in equation (2.43), it follows from equation (2.11) that B is defined on a frequency interval $(\omega, \omega + d\omega)$. Then we can compute

$$b(\ell, m, t) = \int_{-\infty}^{\infty} B(\ell, m, \omega) \exp(j\omega t)\, d\omega$$

as the total waveshape coming from directions $(\ell, \ell + d\ell; m, m + dm)$. Now we want to compute the transform of $P(x, y, \omega)$ in the time domain. This results in

$$p(x, y, t) = \int_{-\infty}^{\infty} \int_{-\infty}^{\infty} b(\ell, m, t - c_0^{-1}(\ell x + m y))\, d\ell\, dm ,$$

where

c_0 is the sound velocity at the receiver.

This equation describes the reception of time-shifted waveforms from all directions.
Beam-steering in the broadband case is equivalent with time-shifting.
The relation :

$$c(\ell, m, t) = \int_{-\infty}^{\infty} \int_{-\infty}^{\infty} f(\ell - \ell^1, m - m^1)\, b(\ell^1, m^1, t)\, d\ell^1\, dm^1 ,$$

which is the Fourier Transform of equation (2.49), is the estimate of the incoming waveform in the time domain, and describes beamforming in the time domain.
The filter $f(\ell, m)$ has become dependent on the spectral content of $b(\ell, m)$ in the following way:

$$f(\ell, m) = \int_{-\infty}^{\infty} \left(\frac{\omega_0}{\omega}\right)^2 F\left(\frac{\omega_0}{\omega}\ell, \frac{\omega_0}{\omega} m\right) B(\ell, m, \omega)\, d\omega ,$$

where

$$F(\ell, m) = \int_{-\infty}^{\infty} \int_{-\infty}^{\infty} W\left(\frac{x\omega_0}{2\pi}, \frac{y\omega_0}{2\pi}\right) \exp\left\{2\pi j \left(\ell \frac{x\omega_0}{2\pi} + m \frac{y\omega_0}{2\pi}\right)\right\} d\frac{x\omega_0}{2\pi}\, d\frac{y\omega_0}{2\pi}$$

and ω_0 is a reference circular frequency at which the filter $F(\ell, m)$ has been specified.
In the following we will consider only narrow-band signals that obey equation (2.67).

The analytic signal

Equation (2.60) shows that the input needed for directional analysis consists of a complex signal providing amplitude and phase information. The physical underwater world yields only real signals. Here the analytic signal (Bracewell, 1978 and Horton, 1969) can be used. The analytic signal known from detection theory can be described by:

$$a(t) = f(t) - i\, f_H(t) \qquad (2.68),$$

where

$f_H(t)$ is the Hilbert transform of $f(t)$.

Now if $f(t)$ is quasi-coherent we can formulate

$$a(t) = |a| \exp(j\bar{\omega}t) \qquad (2.69),$$

where

$|a|$ is called the envelope, slowly changing with time
$\bar{\omega}$ is the mean circular frequency.

Theoretical considerations (Rayleigh, 1945) and measurements in different contexts (Jones et al., 1964 and Medwin et al., 1979) show that phase-shifts can occur depending on the properties (see Officer, 1958) of the boundary layer, when acoustic rays are reflected or scattered by the ocean bottom. Choy and Richards (1975) give a description of the situation when rays are not minimum travel-time.
They demonstrate that such phase-shifts can be eliminated using the Hilbert transform (which is equivalent with a phase-shift of 90 degrees in the analytic signal). Newman (1976) suggests that the envelope of the analytic

signal is a good estimate of the instantaneous energy present in the signal at time t, independent of phase-shifts. The time when the envelope reaches its maximum is unaffected by these phase-shifts.
The Hilbert transform can be used to generate a broadband analytic signal as input for the beamformer described by equation (2.60).

Quadrature detection

When using pulsed monochromatic signals the analytic signal can be obtained by another process (Wolff, 1976), known from radar theory (Skolnik, 1970) as quadrature detection. This detection combines narrow-band filtering with the generation of the analytic signal. In this process the input time series $p(t)$ is convolved with two reference signals as follows:

$$f(t) = p(t) * w(t) \cos \omega_0 t \qquad (2.70),$$

$$f_H(t) = -p(t) * w(t) \sin \omega_0 t \qquad (2.71),$$

where

- $w(t)$ is a time-dependent weighting function controlling the spectral shape of the filter,
- ω_0 is the pass-band center frequency,
- $*$ signifies convolution.

The pair $(w(t) \cos \omega_0 t, w(t) \sin \omega_0 t)$ is the complex inverse Fourier Transform of a band-pass filter that is easily implemented digitally.
Here $f(t)$ is called the in-phase component and $f_H(t)$ is called the quadrature component.
In this way the complex input for the beamformer (2.60) can be obtained. The pair $(f(t), f_H(t))$ is equivalent with $P(u, v, \omega_0)$, for quasi-coherent signals, if $p(t)$ is the pressure input signal at (u, v).

Doppler frequency shift

Ocean bottom surveys are performed from moving platforms so the influence of source and receiver motion should be evaluated.

A general case of a transmitter emitting a continuous wave signal and a receiver, both moving in different directions along the surface of an ocean with a horizontal stratification, a bilinear sound velocity-depth relation and a constant depth has been described recently (Kays et al., 1979). From this case it follows that, when source and receiver move with the same speed in the same direction over a deep ocean, classical treatment can be followed, if one allows for refraction. The Doppler effect can be expressed through the change of the phase of the received signal with time :

$$\frac{dW}{dt} = \left(\frac{\partial W}{\partial r} \right)_z \frac{dr}{dt} \quad ,$$

where

$$\frac{dr}{dt} = -v \cos \phi \quad ,$$

v is the platform's speed with respect to the medium carrying the signal, ϕ the angle between the platform's heading and the projection of the ray on a horizontal plane.

With equation (2.30) we show that

$$\frac{dW}{dt} = -n(z) \sin \theta(z) \; v \cos \phi \quad .$$

The relation between phase rate and Doppler frequency shift can be calculated from equations (2.10) and (2.12).
Accordingly:

$$\Delta \omega = -k_0 \frac{dW}{dt} \qquad (2.72) \quad ,$$

where $\Delta \omega$ is the Doppler frequency shift.
This equation inserted into the previous one gives then the classical Doppler shift equation :

$$\frac{\Delta\omega}{\omega_0} = c^{-1} \; (z) \; v \cos \alpha \quad ,$$

where α is the Doppler cone angle, between the incoming ray and the velocity vector of the platform.

For the situation that the moving platform emits a signal with frequency ω_0 in a direction α along a ray $\vec{r}$, and that this signal is reflected and received again by the platform, the Doppler shift is approximated to first order by :

$$\frac{\Delta\omega}{\omega_0} = 2\ c^{-1}\ (z)\ v \cos\ \alpha \qquad (2.73).$$

From this equation one calculates that for a platform speed of 15 knots (7.7 m s^{-1}) the relative Doppler frequency shift ranges from -0.01 to +0.01, for a Doppler cone angle of 180^0 and 0^0, respectively. In order not to loose Doppler-shifted echoes the receiver band-width shoud exceed $4\ c^{-1}\ (z)\ v\ \omega_0$ rad s^{-1} .

Noise

In principle noise is that part of a signal that does not contain information we want to extract. This definition goes much further than other definitions (e.g. Bedenbender et al., 1970), who concentrate in the case of noise in seismic signals on ambient noise and tow noise. For array processing it is convenient to divide noise into two categories (see Berkhout, 1979) :

1. spatially coherent noise ,
2. spatially incoherent noise .

Category 1 noise includes antenna sidelobe effects, propellor noise and reverberations. Antenna sidelobe effects and reverberations must be reckoned with in the design of the echo processor and in the interpretation of the results. So-called optimum signal processing (Bryn, 1962) makes use of frequency domain filtering after beamforming, whereas "conventional" detection does not. However, for quasi-monochromatic echoes, conventional echo detection as used in the described experiments is optimal (Schultheiss, 1977).

Category 2 noise includes internal noise (tow noise, electrical noise, digitising noise) of the array elements and ambient sea noise. If an array

is composed of I elements, for the internal noise we can make the following statement. As the internal noise of each element is uncorrelated with that of other elements, the signal to noise ratio (see the next section) of the array is improved by a factor I with respect to the signal to noise ratio of one element. Ambient sea noise, generated by sea life, by wind or distant shipping (see Bannister, 1979), or even by the medium itself (Albers, 1965), can be supposed to be spherically or circularly isotropic. For spherically and circularly isotropic noise Lewis and Schultheiss (1971) showed that for a linear uniformly weighted array with I elements the improvement of the signal to noise ratio (called array again) can be approximated by:

$$G_s(\omega) = 2(I-1)\hat{u}_1 \quad \text{for spherically isotropic noise} \tag{2.74}$$

and

$$G_s(\omega) = \pi(I-1)\hat{u}_1 (1-\ell^2)^{\frac{1}{2}} \quad \text{for circularly isotropic noise} \tag{2.75},$$

where ℓ is the "look" direction of the beam former, in the circular case the array lies in the plane of the noise.
It can be seem that the improvement is roughly proportional to the number of elements.

The matched filter

If a time sequence consists of noise and signal we can at a certain time t_0 define a quantity called signal-to-noise ratio as follows:

$$\sigma = \frac{|a(t_0)|^2}{\langle |v(t)|^2 \rangle} \quad ,$$

where

$|a(t_0)|$ is the envelope of a signal at time t_0,
$\langle |v(t)|^2 \rangle$ is the expected value of the amplitude-squared of the zero mean random quantity $v(t)$, noise.

If the spectral density $\Phi(\omega)$ of the noise and the Fourier transform $A(\omega)$ of the signal are known, then σ may be maximized by filtering the time

sequence with the linear filter, defined in the frequency domain (Nahi, 1969) by:

$$H(\omega) = \alpha \exp(-j\omega t_0)\, A(-\omega)\, \Phi^{-1}(\omega)$$

where α is an arbitrary constant.

If the random noise is white, then $\Phi(\omega) \equiv 1$ and the filter H is determined uniquely by the signal wave form. This filter is called the matched filter. It is equivalent with a convolution in the time domain of the input sequence with the time-reversed complex conjugate of the expected signal. Quadrature detection (equations 2.70 and 2.71) is an implementation of a matched filter if the expected signal is a harmonic wave with frequency ω_0 and envelope $w(t)$.
However, if $w(t)$ differs from the expected signal envelope, the maximum attainable signal-to-noise ratio for that filter is less than that of the matched filter. The quantity specifying the level difference is called matched filter loss.

The matched filter is also applied to signals in the aperture distance domain. In equation (2.46) the input signal P is convolved with the distance-reversed complex conjugate of the expected signal indicated in equation (2.45). As long as the weighting function $W(u, v)$ has a constant value, the equation (2.50) defines a matched filter for plane wave reception. The same is true for equation (2.57). Equally, if array shading is applied, the signal-to-noise performance of the beam former is degraded. As above the level difference is called matched filter loss. In the preceding section figures were given for the matched filter loss of several windows.

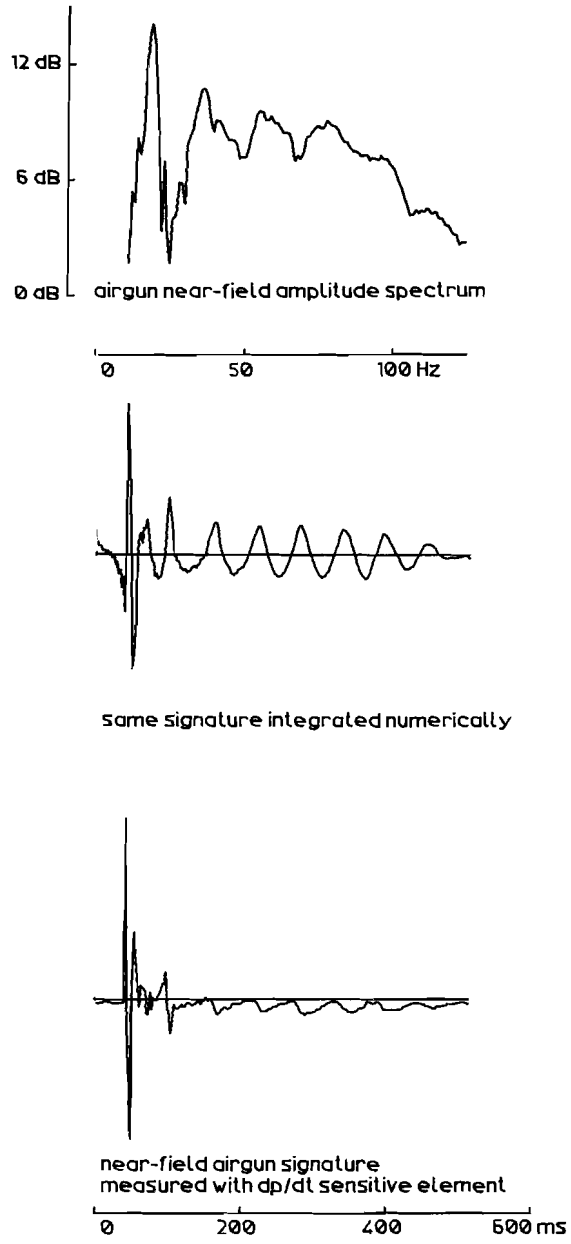

Figure 3.1 Airgun signature and spectrum. The lowermost signature was digitized from an oscilloscope photograph taken on board M. V. Aegis *on 13 May 1968 .*

3. Multiple beams at low frequency

A. General considerations

Airgun

The airgun (Ewing and Zaunere, 1964) is a pneumatic sound source that successfully replaced explosives as a high-amplitude broadband signal source in seismic reflection profiling. At the time of the "shot" it releases a portion of compressed air into the water. The fact that this bubble oscillates some time before surfacing or coming to rest influences greatly the spectral content of the airgun signal.
Ideally (Rutten, 1969) the airgun has a spectrum with broadened lines of equal amplitude, but the non-linear property of water for high-amplitude sound waves and interference with the reflection of the signal against the water surface distort this spectrum (see figure 3.1). Ziolkowski (1970) showed that the fundamental period (or bubble pule period) calculated for a theoretical model given by him is in agreement with experimental values within the measurement error. Apart from the bubble pulse period the development of the output pressure wave can be calculated from this model.

Receiver

Seismic profiling is performed with a hydrophone array towed behind the survey vessel as a receiver (Bedenbender et al., 1970). This array, called streamer or eel, consists of a hose of synthetic material filled with a suitable liquid with suspended hydrophones, connected in series and/or parallel. Hydrophones are omnidirectional pressure-sensitive transducers. For multichannel surveys streamers are divided into sections and the output of each section may be processed separately. The directional sensitivity of a streamer is dependent on the configuration of hydrophones and on the frequency of the incoming signal (Knott and Nowak, 1969).

Ghost

Since streamers are towed at some distance below the water surface the

directional sensitivity of a hydrophone array is influenced by the reflection of sound waves against this surface. This influence can be included in the receiver pattern by adding to each hydrophone a virtual hydrophone above the water surface so that the entire array is mirrored with respect to the water surface. The signal on the virtual hydrophone is dependent on the surface reflection coefficient and the phase shift this signal experiences at the water-air boundary.

If the sound velocity is constant between the water surface and the lowest hydrophone we can expand equation (2.56) into three dimensions, adding the surface reflection:

$$W(u, v, w) = \sum_{i=1}^{I} \{ {}^3\delta(u-u_i, v-v_i, w-w_i) - R\ {}^3\delta(u-u_i, v-v_i, w+w_i) \} \tag{3.1}$$

where

${}^3\delta(u, v, w)$ is the three-dimensional Dirac delta function,

$w = \lambda_0^{-1} z$,

(u_i, v_i, w_i) are coordinates of i-th hydrophone with respect to the water surface,

I is the number of hydrophones,

$-R$ reflection coefficient of the water surface, the negative sign being caused by the π rad phase shift (see discussion further on).

This weighting function gives the following pattern:

$$F(\ell, m) = \sum_{i=1}^{I} \exp(2\pi j\, \ell u_i) \exp(2\pi j\, m v_i) \{ \exp(2\pi j\, q w_i) + - R \exp(-2\pi j\, q w_i) \} \tag{3.2}$$

where $q = \cos\theta$.

q is not an independent variable, because $\ell^2 + m^2 + q^2 = 1$.

This general formula can be simplified if one assumes that all hydrophones have the same distance $w\lambda_0$ to a flat water surface. The pattern F can be factored as follows:

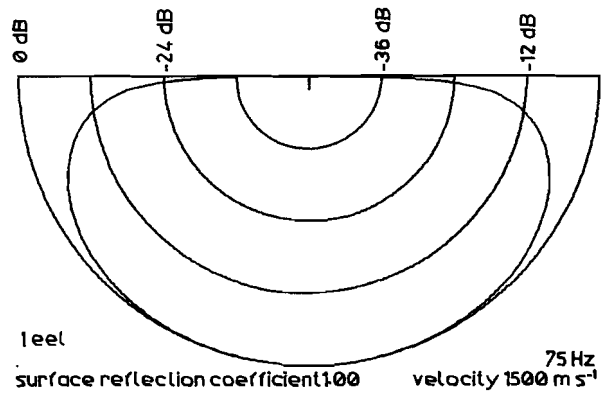

Figure 3.2 Pattern of single streamer at 5 m depth.

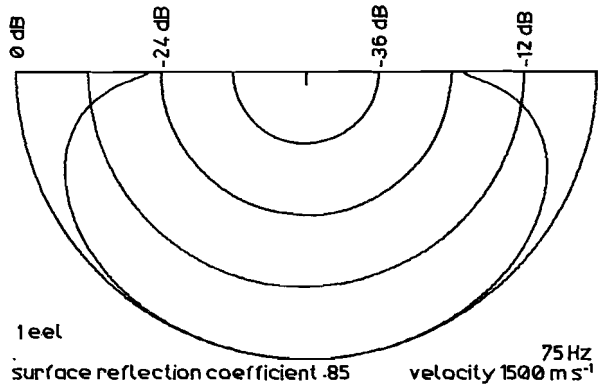

Figure 3.3 Pattern of single streamer at 5 m depth.

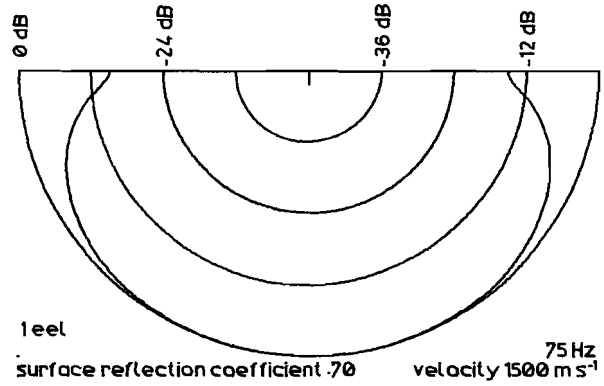

Figure 3.4 Pattern of single streamer at 5 m depth.

$$F(\ell, m) = F_1(\ell, m)\, F_2(q) ,$$

where

$$F_1(\ell, m) = \sum_{i=1}^{I} \exp(2\pi j\, \ell u_i) \exp(2\pi j\, m v_i) \qquad (3.3),$$

$$F_2(q) = \exp(2\pi j\, qw) - R \exp(-2\pi j\, qw) \qquad (3.4).$$

$F_1(\ell, m)$ is the pattern of the hydrophones suspended in an unbounded ocean and $F_2(q)$ describes the influence of the so-called ghost effect of the water surface.
Here $F_2(q)$ plays the role of the single element directivity pattern $F^1(\ell^1, m^1)$ in equation (2.52), but $F_2(q)$ is symmetrical with respect to rotation about the z-axis, whereas $F^1(\ell^1, m^1)$ generally is not.
The properties of $F_2(q)$ are studied through the absolute value,

$$|F_2(\theta)|^2 = 1 + R^2 - 2R \cos\{4\pi\, z\lambda_0^{-1} \cos\theta\} \qquad (3.5).$$

It can be seen easily that if $\theta \to 90^0$, the value of $|F_2(\theta)|$ will approach $(1-R)$, which means that near-horizontal rays will always be attenuated. Also it can be seen that for $\theta = 0^0$ maximum amplification occurs at $z = 0.25\ \lambda_0$ (Hubbard, 1965). Figures (3.2) through (3.4) show that for $z = 0.25\ \lambda_0$, $|F_2(\theta)|$ does not change appreciably when R varies between 0.7 and 1. This is especially true for directions with $\theta < 60^\circ$.

Transformation

Suppose K identical straight streamers with I hydrophones each are towed in parallel at a constant and equal depth.
Tow direction is along the u-axis (see fig. 3.7)
The beam amplitude given by equation (2.52) can then be calculated making the following two substitutions.

1. $F^1(\ell^1, m^1) = F_2(q^1)\, F_3(\ell^1)$, (3.6) ,

where

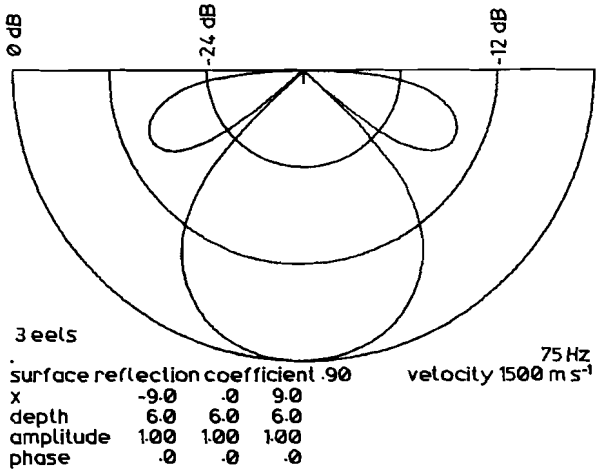

Figure 3.5 Three-streamer central beam pattern in a plane perpendicular to the streamers; no shading.

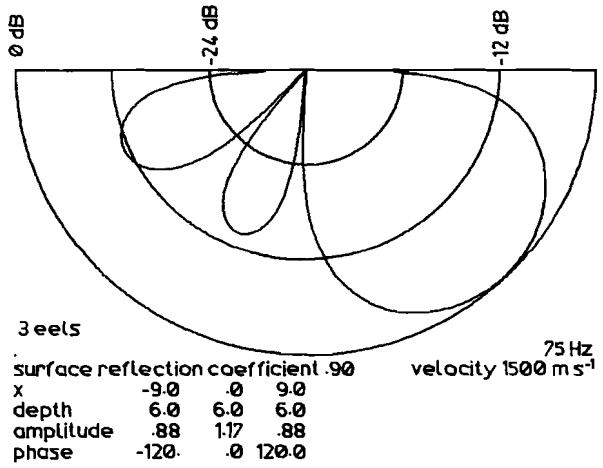

Figure 3.6 Three-streamer side beam pattern in a plane perpendicular to the streamers; with shading.

$F_2(q^1)$ is the ghost factor from equation (3.4) and

$$F_3(\ell^1) = \sum_{i=1}^{I} W_i^1 \exp(2\pi j\, \ell^1 u_i^1)$$

with:

W_i^1 is the weight of the i-th hydrophone,

u_i^1 is the u co-ordinate of the i-th hydrophone with respect to the first hydrophone in the streamer,

$F_3(\ell^1)$ is the streamer factor.

2. $$F(\ell, m) = \sum_{k=1}^{K} W_k \exp(2\pi j\, \ell u_k) \exp(2\pi j\, m v_k) ,$$

where

(u_k, v_k) are the co-ordinates of the first hydrophone of the k-th streamer

W_k the weight of the k-th streamer in the beam former.

The assumption is made that each streamer has one output consisting of the weighted sum of all hydrophone signals. This is equivalent with constant beam steering in the "look" direction $\ell = 0$. Therefore the streamer factor is included in $F^1(\ell^1, m^1)$.
If these substitutions are made for $F(\ell, m)$ and $F^1(\ell^1, m^1)$ we may, according to chapter 2, form K independent beams by performing a DFT on the weighted streamer outputs.

So far nothing has been said about frequency. In the experimental section it is shown, that a useful frequency in the reflected airgun signal under the circumstances described there is 75 Hz. This implies a spacing of 10 m between streamers to satisfy the secondary maximum criterion (2.64). So the number of streamers towed in parallel can not be large, and instead of using equation (2.60) implemented as a Fast Fourier Transform (FFT; see chapter 4) we can phase-shift and sum straightforwardly according to equation (2.60). The slight increase in computation time depending on the efficiency of the FFT (Cooley and Tukey, 1965) is mitigated by the possibility to adjust the

the individual streamer weights and phase shifts for each beam separately. Hardly any signal is expected from directions with near-grazing angles of incidence, i.e. from directions contributing to the sidelobes of the vertical beam. Thus it is justified to use equal weights in the vertical beam to get a narrow beam width (illustrated in figure 3.5) at the expense of high sidelobes. The side-lokking beams, however, need strong shading to eliminate the normal reflection (figure 3.6).

Automatic depth-tracking

In order to keep computing time and memory storage to a minimum, it is useful to employ a depth-tracker in each beam. This tracker should define the first echo on each beam and accordingly set the measurement window to include all backscattering echoes. However, such a tracker is dependent upon a favourable signal-to-noise ratio and it might easily lose the bottom echo, or lock onto reverberations. The next section shows that, if one uses an unsophisticated echo-detector no echoes are detected in 12% of the shots and 30% of the detections may be false.

Total reflection

A remark has to be made about total reflection.
Rayleigh (1945) states on theoretical grounds, that as the sound velocities in air and water have a ratio of 4.3 approximately the reflection of sound against a flat water surface is never total. However the smallness of the ratio between the densities of air and water, which is about 1.30×10^{-3}, means that the reflection coefficient for plane waves does not deviate more from minus 1 than 1×10^{-4}. This circumstance accounts for the phase jump of π rad. Of course, the unevenness of the water surface influences the reflection coefficient. From measurements made by Wijmans (1974) to investigate the spatial coherence of sound reflected by an uneven water surface it can be seen that the phase shift still is π rad when the standard deviation of the water surface is 0.4 m and the wind velocity is 14 m s^{-1}, especially at grazing angles of incidence. A conclusion about the absolute value of the reflection coefficient can not be drawn from Wijmans' paper. As already mentioned this value does not influence the ghost factor much if the angle of incidence is less than 60^0 and the receiver is put at a depth of 0.25 λ_0.

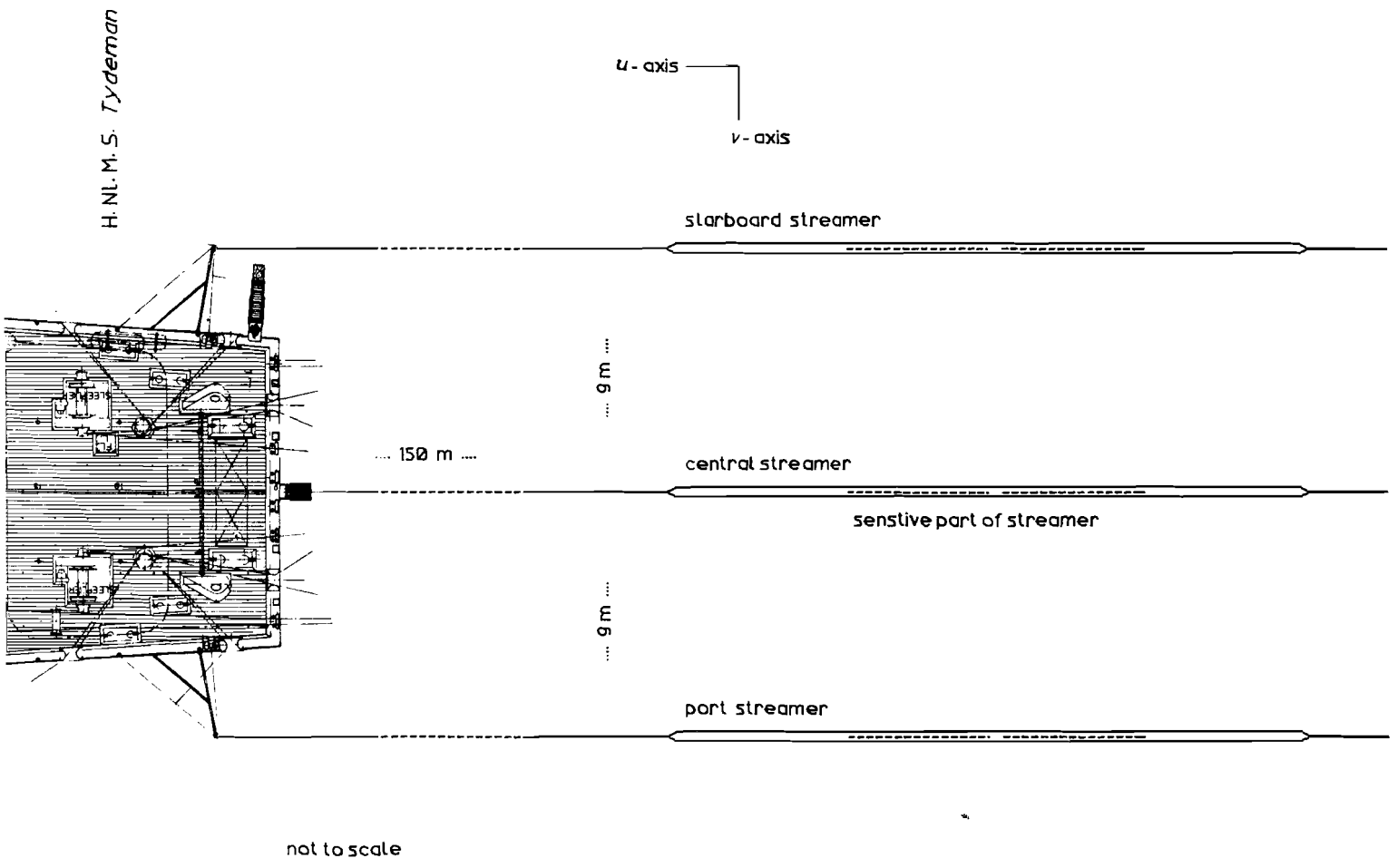

Figure 3.7 Arrangement of streamers during the experiment.

B. Experimental results

Introduction

To investigate the possibility of utilizing available (and relatively cheap) seismic profiling equipment for bathymetric measurements with improved lateral resolution and multiple beam generation, an experiment was conducted on board the Dutch oceanographic vessel H.Nl.M.S. *Tydeman* on 2 and 3 April, 1979 during a voyage of the Vening Meinesz Laboratorium.
The normal profiling equipment consists of a Bolt PAR air gun model 600B with a 20 cubic inch (328 cm^3) firing chamber operated at 120 atm (Giles, 1968) and a streamer, built by the technical staff of the laboratory, employing 32 Teledyne T-1 hydrophones over a length of 28.5 m. After filtering the received signal is recorded on a variable density paper recorder. To perform this experiment two additional streamers were towed from the vessel's starboard and port bathythermograph boom (see figure 3.7). A digital computer (Hewlett-Packard 21 mx) digitized the three streamer signals and stored them on magnetic tape cartridges. The cartridges, containing 19 shots each, were analyzed in the laboratory to yield the result presented in this chapter.

The site of the experiment

As shown in the trackchart with the schematic seismic profile (figure 3.8), the experiment was executed over the northern continental rise and slope of the Bay of Biscay. Actually the investigation was divided into two sections S and T on account of a cable failure. Section S was conducted over the continental rise between Trevelyan escarpment and Meriadzek Terrace (Smith and Van Riessen, 1973). The bathymetry of the S-area is shown in figure (3.9). Section T was performed across the higher part of the slope above the Terrace. The detailed bathymetry is illustrated in figure (3.10). On these figures the location of the first shot of each cartridge on the ship's track is also indicated with the number of the file on the cartridge. An important difference between section S and section T is that section S has a lower signal level as a result of the greater depth.

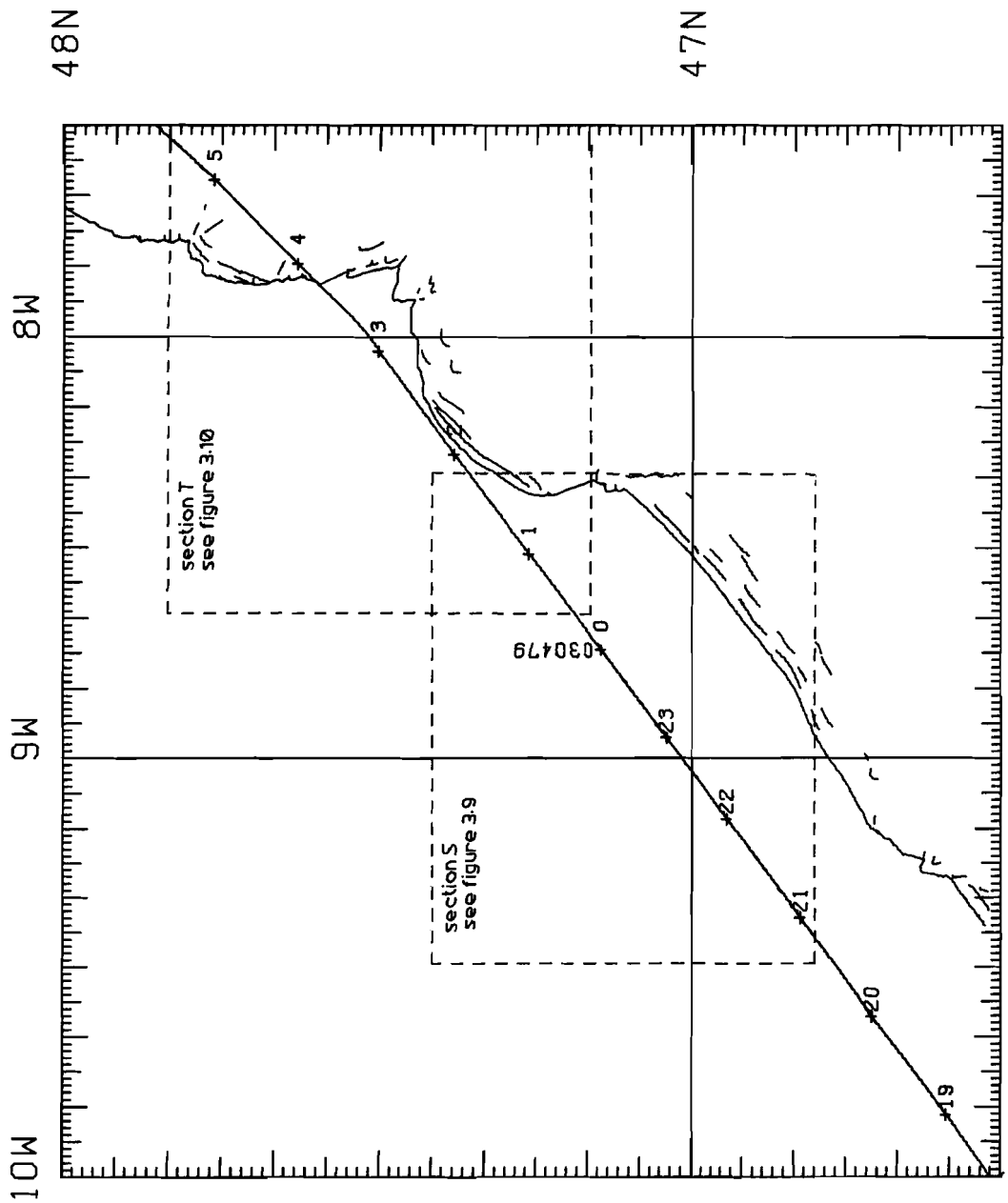

Figure 3.8 Track chart showing the site of the low-frequency experiment. Indicated are the schematic profile of the subsurface and areas S and T.

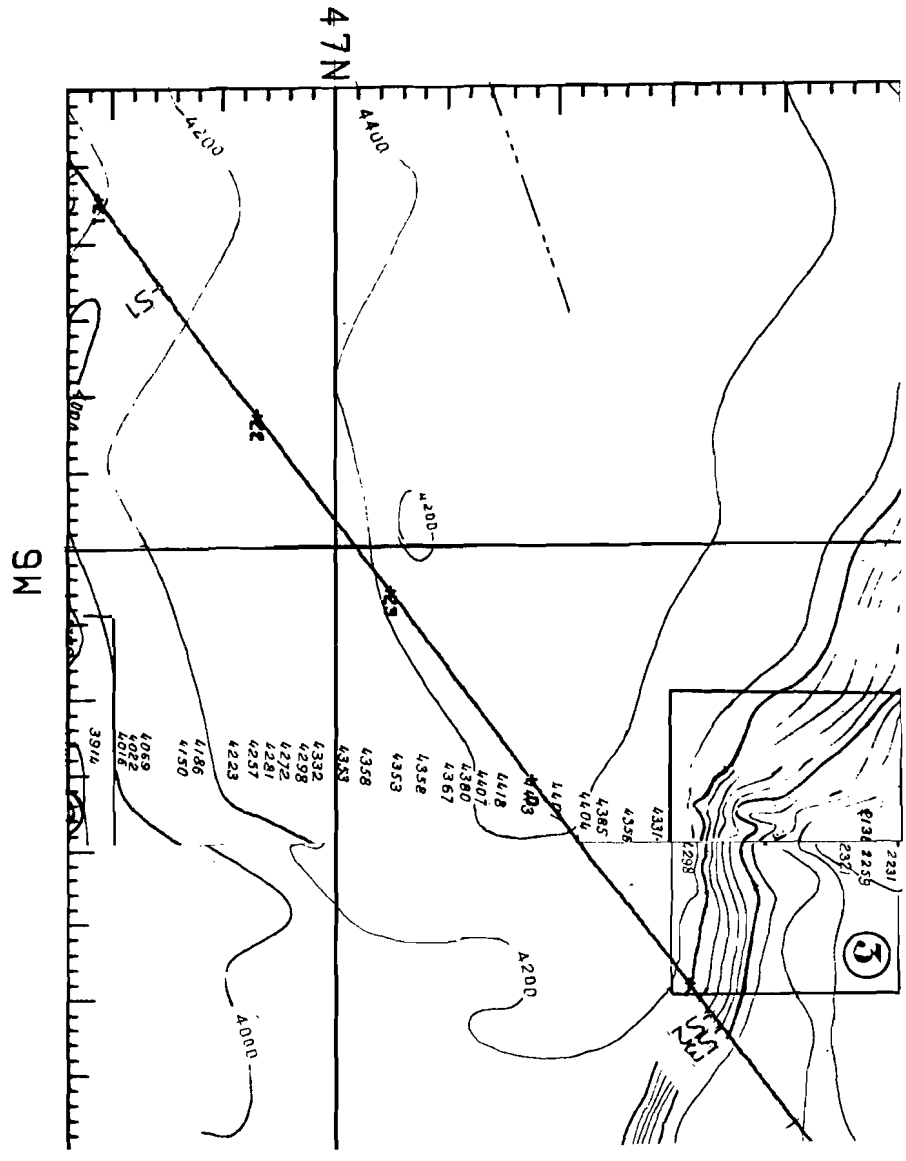

Figure 3.9 Detailed bathymetry of section S (from Carte Bathymétrique provisoire, C.N.E.X.O., 1975). Indicated are the first shots of each file.

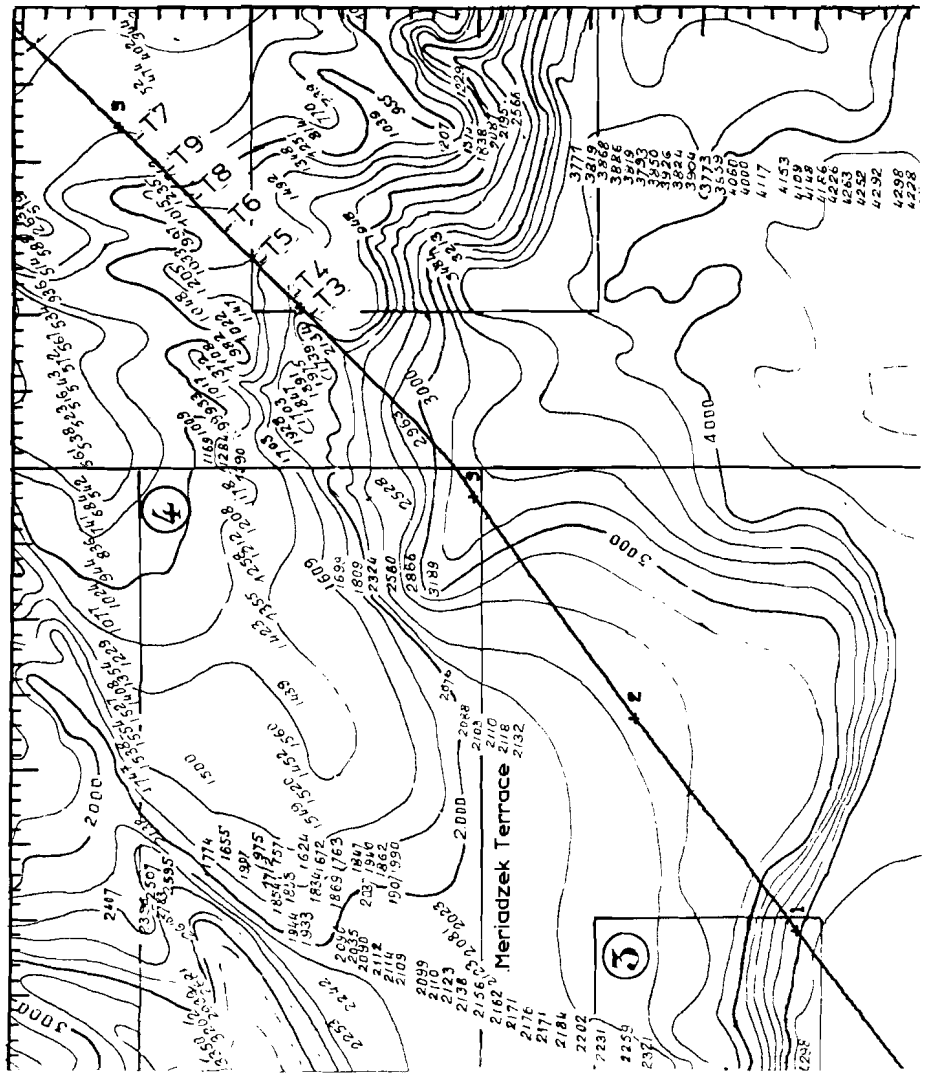

Figure 3.10 Detailed bathymetry of section T (from Carte Bathymétrique provisoire, C.N.E.X.O., 1975). Indicated are the first shots of each file.

Experimental arrangement

A block diagram of the hardware layout is shown in figure (3.11). The streamers were standard streamers with built-in preamplifiers. The sensitivity contour diagram of a standard streamer in the (ℓ, m) plane is shown in figure (3.12). They were towed 150 m behind the ship at a depth of 6 m. The preamplifiers of both outer streamers had high-pass filter characteristics: a cut-off frequency of 10 Hz and a 12 dB octave^{-1} roll-off. The central streamer preamplifier had broad-band characteristics. An anti-alias filter was employed in each signal line with a cut-off frequency of 300 Hz and a 6 dB octave^{-1} roll-off. The 15 bit analog-to-digital (A/D) converter was paced externally by a signal source with a frequency of 1200 Hz, the signal lines were multiplexed and converted consecutively. Since the airgun synchronization signal was multiplexed as a fourth signal line, this resulted in a sample frequency for each streamer input of 300 Hz. Likewise the streamer inputs were delayed with respect to each other by 0.833 ms. All three streamer signals had a low-frequency disturbance, expecially the central streamer signal. During section T this central streamer had to be attenuated 21 dB to prevent it from exceeding the range of the A/D converter.

On-line software

The 21 mx computer used has a Real-Time Executive (RTE)-M3 operating system with 32k of system memory and 48k of partition memory. The data capture programs (5, including the supervisor) are all system resident, and work in time sharing. Partition memory is available for user programs and intermediate data storage.
The analog-to-digital imput program puts in blocks of 4 × 128 samples using direct memory access. When the block is ready it is moved immediately to the supervisor buffer and a new block is started without loss of datapoints. To start a measurement cycle the supervisor scans the airgun synchronization channel (i.e. the fourth row of the input block) to detect the shot. If no shot is detected the supervisor suspends itself until a new block arrives. If a shot is detected the supervisor interrupts the input program and instructs it to start a new block at a preset time after the detected shot moment. Each new data block, as soon as received by the supervisor, is written into empty partition memory, until sufficient blocks are stored.

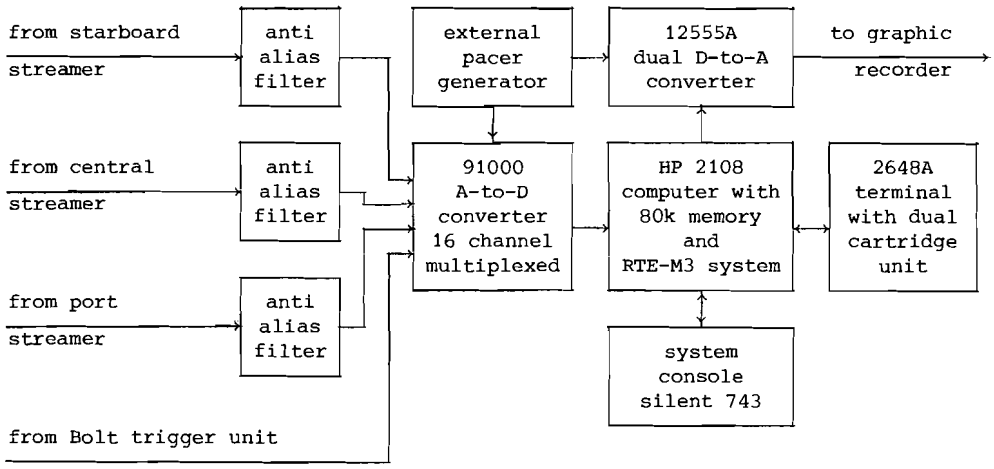

Figure 3.11 Block diagram of electronics and computer hardware layout.

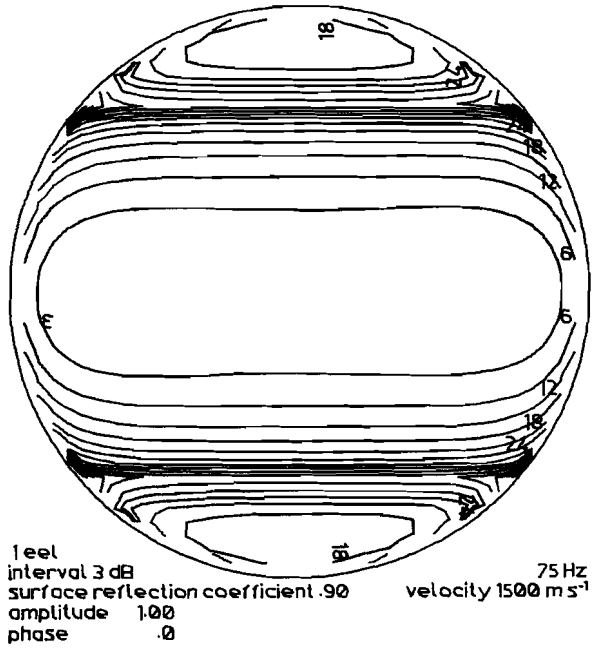

Figure 3.12 Directional sensitivity contour diagram in the (ℓ, m)-plane for a standard streamer ; tow direction is upward.

Then the supervisor signals to a user program and returns to the shot detection routine. The possibility exists to store into another part of empty partition memory the block containing the direct arrival of the airgun signal and the succeeding block. This memory is managed by a special file managing program. The user program used in this experiment just collected the data blocks of two consecutive shots and caused the file manager to put them on a cartridge file for off-line processing. In the program system it is possible to dump on-line processed data in an output buffer of which the successive elements are converted to an analog voltage synchronized with the input sampling. In this way one may record signals on a graphic recorder.

Off-line software

The output of the experiment consists of magnetic cartridges each containing 19 × 3 signals (traces) of length 768 samples. All traces were filtered first with a FFT-based Butterworth high-pass filter having a cutt-off frequency of 50 Hz and a steepness of 48 dB octave^{-1} to remove the low-frequency disturbances. An inspection of the filtered signal revealed the presence of a sufficiently strong signal with a central frequency of 75 Hz. This was not unexpected because oscilloscope photographs taken on board of M.V. *Mercurius* in December 1978 also show the presence of signals with this frequency in the reflected signal.

After the filter a quadrature detection was done according to equations (2.70) and (2.71) with $\omega_0 = 2\pi . 75$ rad s^{-1}. The function $w(t)$ was defined as follows:

$$w(t) = \begin{cases} 0 & \text{for} \quad \omega_0 t \leq -2\pi , \\ 0.5 - 0.5 \cos 2\omega_0 t & \text{for} \quad -2\pi \leq \omega_0 t \leq 0 , \\ 1 & \text{for} \quad 0 \leq \omega_0 t \leq 4\pi , \\ 0.5 + 0.5 \cos 2\omega_0 t & \text{for} \quad 4\pi \leq \omega_0 t \leq 6\pi , \\ 0 & \text{for} \quad 6\pi \leq \omega_0 t . \end{cases} \tag{3.6a}$$

The detector has thus a length of four wavelengths and each end was tapered with a cosine taper over one wavelength. The amplitude spectrum of this detector is shown in figure (3.13). The detector has a bandwidth of 29 Hz, which is necessary because the signal frequency shows some variation.

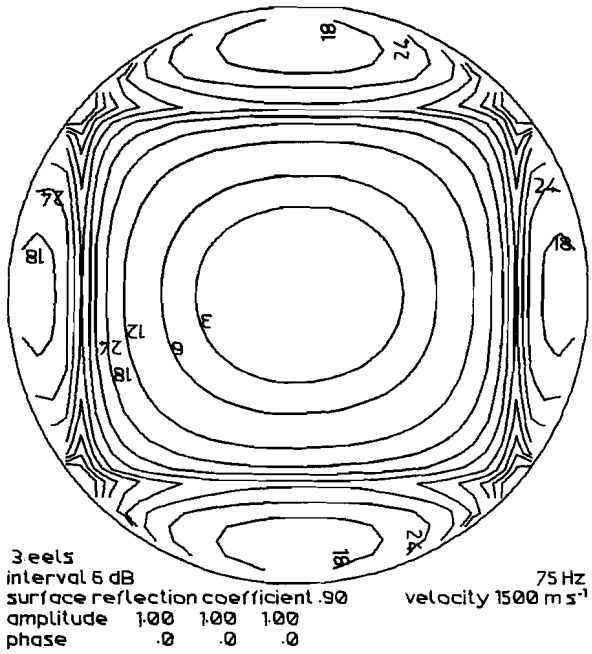

Figure 3.14 Sensitivity contour diagram for the central beam of a three streamer system.

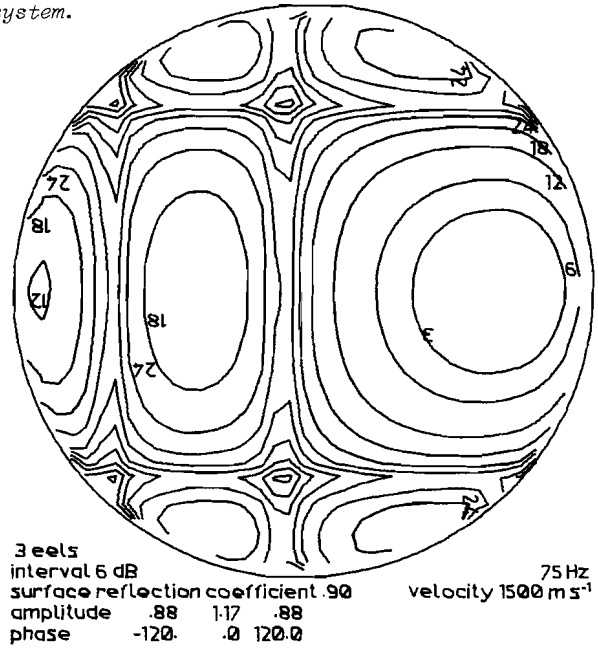

Figure 3.15 Sensitivity contour diagram for a side beam.

The in-phase and quadrature outputs f_k and f_{Hk} were then used for phase-shifting and summing according to the following equation:

$$c_n(t) = \sum_{k=1}^{3} W_{nk} \{f_k(t) + j\, f_{Hk}(t)\} \exp(2\pi j\, \phi_{nk} / 360^\circ) ,$$

with the following constants:

		port beam	central beam	starboard beam
starboard streamer		1	2	3
shading	W_{1k}	0.88	1.0	0.88
phaseshift	ϕ_{1k}	-120°	0°	120°
central streamer				
shading	W_{2k}	1.17	1.0	1.17
phaseshift	ϕ_{2k}	0°	0°	0°
port streamer				
shading	W_{3k}	0.88	1.0	0.88
phaseshift	ϕ_{3k}	120°	0°	-120°

The phaseshifts given in the table were modified by the software to eliminate the previously mentioned time-shift produced by the A/D converter. This set of shadings is the best compromise between beamspread factor and sidelobe suppression with a streamer spacing of 9 m, as can be seen in figures (3.5) and (3.6). The sensitivity contour diagram in the (ℓ, m) plane for the central beam is shown in figure (3.14). Tow direction is upward. The diagram for a side beam is likewise given in figure (3.15).

Beam representation

Now two ways are open for the representation of the beam calculation.

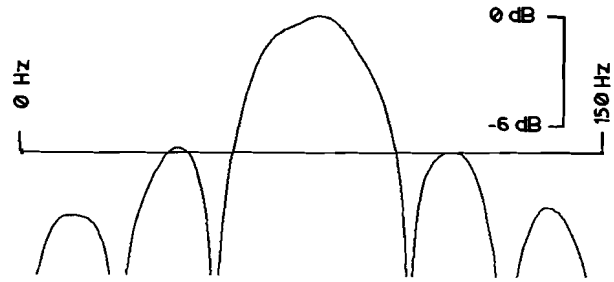

Figure 3.13 Amplitude spectrum of quadrature detector.

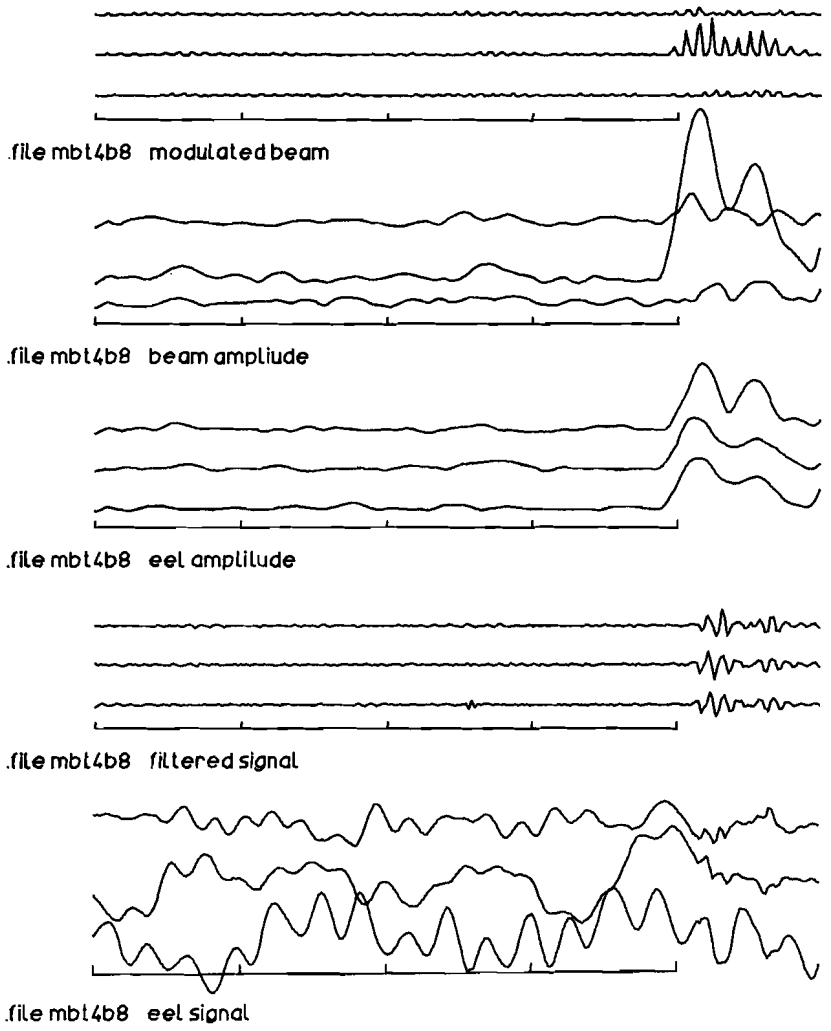

Figure 3.16 Illustration of the output of different processing steps.

The first method utilizes the beam amplitude, defined here as:

$$\bar{c}_n(t) = M^{-1} \sum_{m=0}^{M-1} |c_n(t + m\Delta t)| \qquad (3.7) ,$$

where

Δt is the sample interval,

M is determined by the mean expected signal length.

The beam amplitude is an estimate of the beam signal envelope, and consequently the instant when the beam amplitude reaches a maximum defines the arrival time of the reflected signal in this beam. The beam amplitude can be used for digital measurement of arrival times, but it is not very well suited for analog representation of beam signals, because of the low-frequency character of the envelope.

The other method is an inversion of equations (2.70) and (2.71) as follows:

$$c^*_n(t) = \text{Re}\{c_i(t)\} \cos \omega_0 t + \text{Im}\{c_i(t)\} \sin \omega_0 t \qquad (3.8) .$$

In this manner a synthetic signal is composed, consisting of a carrier with frequency ω_0 modulated with the envelope of the beam signal. This signal is more suited for analog representation, especially if it is suitably clipped and rectified. However the arrival time is not indicated by the onset of the signal but by the maximum of the amplitude. The consecutive steps of software processing are illustrated in figure (3.16).

Streamer calibration

In order to get valid conditions for a beamforming process it is necessary that either the sensitivities of the different streamers are equal, or there is a procedure to measure these sensitivities and to account for them in the processing software. The measurement of these sensitivities may be done in fair weather sailing across a flat plain by checking the echo amplitudes.

In the experiment described here no time was available to accomplish this check so another way was chosen. All digitally recorded tracks were examined as follows.

After quadrature detection the streamer amplitude was calculated with the equation :

$$\bar{p}_k(t) = M^{-1} \sum_{m=0}^{M-1} \left| f_k\,(t + m\Delta t) + j\, f_{kH}\,(t + m\Delta t) \right| \qquad (3.9)\ ,$$

analogous to equation (3.7), with $M = 4$.
Then for each streamer the maximum amplitude per shot p_{kM} was found and a threshold defined according to

$$\bar{p}_{kT} = 0.2\ \bar{p}_{kM}\ .$$

All amplitudes below this threshold were considered to be noise with an isotropic character. The relative streamer sensitivities were then found by calculating the mean noise per streamer per shot and normalizing on the starboard streamer.
The measurement results are listed in the following table :

	central/starboard streamer	port/starboard streamer
section S	1.30 ± 0.08	} 0.60 ± 0.07
section T	0.118 ± 0.007	

The difference between section S and section T is explained by the attenuator of 21 dB as aforementioned. From these results the proper prescalings for each streamer were calculated and used in the subsequent beam calculations.

Measurement results

A display of the processed tracks is presented in figures (3.17) through (3.19) in chronological order from bottom to top. File T7 is omitted because

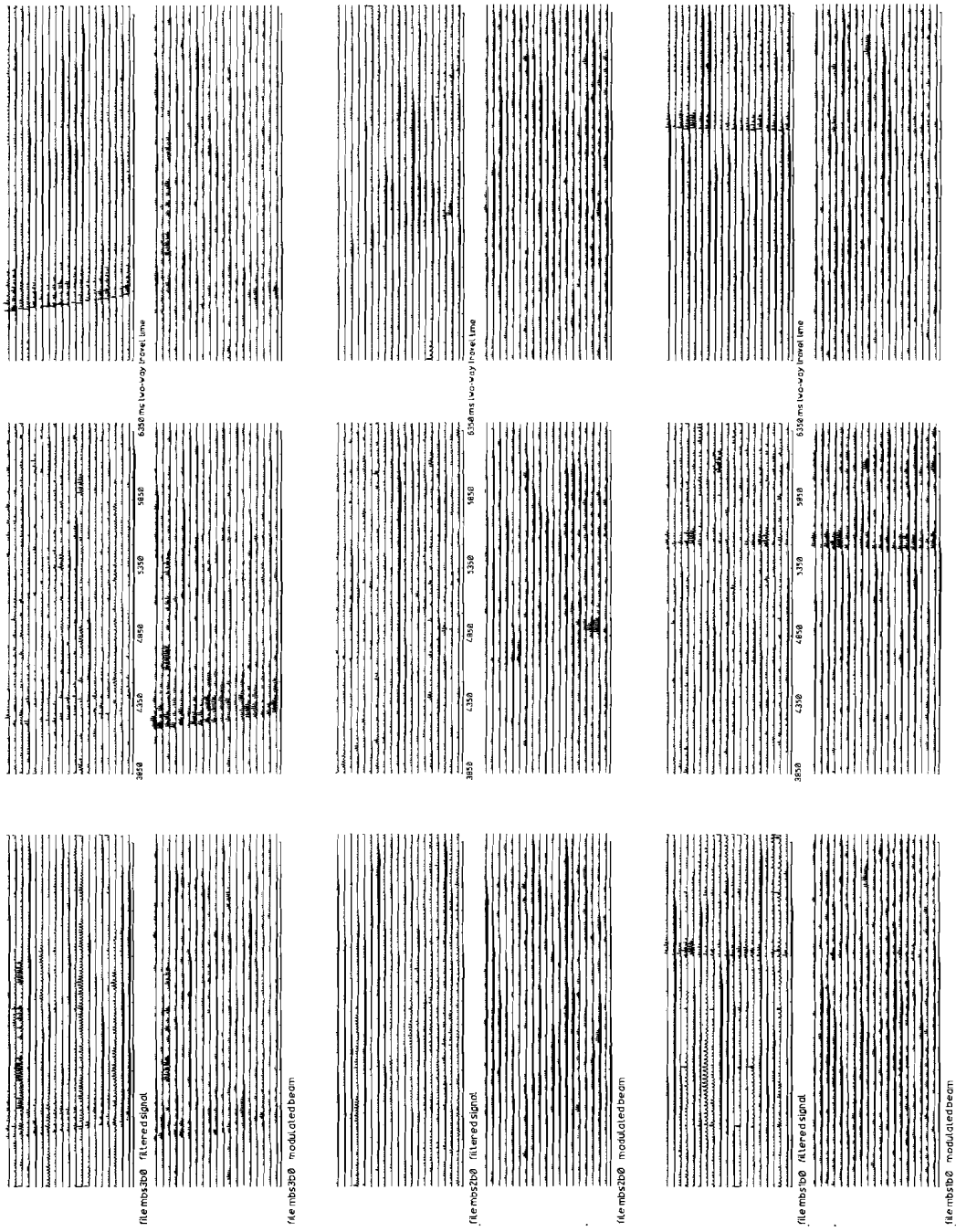

Figure 3.17 Section S processed output: filtered streamer and modulated beam.

Figure 3.18 Section T; first 3 processed files: filtered streamer and modulated beam.

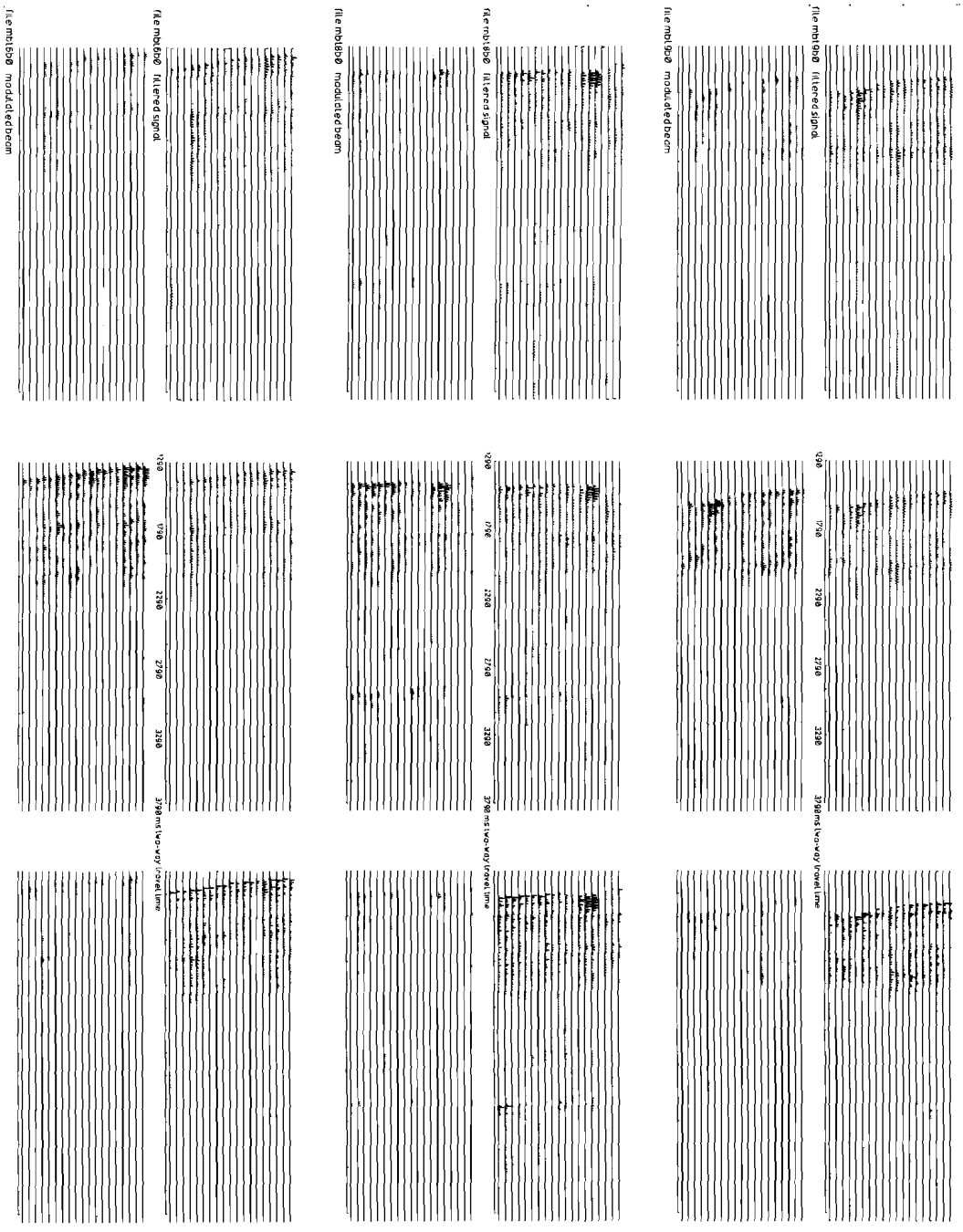

Figure 3.19 Section T; last 3 processed files: filtered signal and modulated beam.

Table 3.1

file	G.M.T.	depth (a)	depth (b)	detected shots (c)	detected shots (d)	bottom echo signal-to-noise ratio: before beamforming	bottom echo signal-to-noise ratio: after beamforming	bottom echo sidelobe ratio: portbeam	bottom echo sidelobe ratio: starboard beam	cross-track slope angle
S1	2124	4140	4133	14	10	14.6 12	29 15	0.26 12	0.33 10	0.8°
S2	0108	3520	3588	14	3	4.6 7	19 13	0.38 8	0.32 10	- 5°
S3	0112	3180	3185	13	6	11.2 10	22 13	0.28 11	0.36 9	- 5°
T3	0357	1800	1836	19	19	52 17	148 22	0.28 11	0.22 13	+ 8°
T4	0403	1640	1512	18	14	27 14	57 18	0.21 14	0.35 9	- 4°
T5	0414	1380	1220	19	13	6.7 8	12.5 11	0.19 14	0.27 11	- 4°
T6	0425	1100	1026	18	15	17 12	26 14	0.24 12	0.31 10	- 2°
T8	0435	1240	1090	17	11	24 14	36 16	0.27 11	0.28 11	- 6°
T9	0445	800	1148	18	12	25 14	38 16	0.22 13	0.28 11	+ 9°
		m	m			(ratio) dB	(ratio) dB	(ratio) dB	(ratio) dB	

the bottom reflection lay outside the range of the program, for which the depth must exceed 960 m.
In these figures the 19 shots of each file are represented twice. The upper block of each file shows the filtered streamer signals with the starboard signal to the right and the central streamer signal in the central block. The lower block of each file shows the modulated beam signals, also with the starboard beam to the right and the central beam in the middle. All signals shown in the figures (3.17) through (3.19) are rectified so that only the positive half of the signal is displayed.

In addition table (3.1) gives some statistical characteristics of each file. Listed under depth are (a) the depth from figures (3.9) and (3.10), (b) the mean depth of all successfully detected bottom echoes in the file. The last phrase requires some explanation. A rather unsophisticated subroutine was used to detect the first echo in each track. For each the amplitude was calculated according to equation (3.9) and a threshold $\overline{p}_{kT}$ was set. If all three streamer amplitudes exceeded their respective thresholds an echo was considered to be present, and the first maximum in $\overline{p}_k(t)$ then gives the time of the bottom echo. For each file the number of shots where such an echo was found is listed under (c). Each echo was inspected and compared with the graphic recording to check its validity. The number of successfully detected bottom-echoes is listed under (d). Only tracks with a successfully detected bottom-echo were used for the other statistical quantities. Of the 171 shots 150 contained a detected echo, and 103 a successfully detected bottom-echo.

The bottom echo signal-to-noise ratio is calculated after high-pass filtering and quadrature detection, thus in a narrow frequency band. The table shows that an improvement of this ratio occurs through beamforming. The results corroborate Lewis and Schultheiss' theory (see equations 2.74 and 2.75) that an improvement can be expected proportional to the number of streamers minus one. The bottom-echo sidelobe ratio also shows the expected behaviour (figure 3.6) if allowance is made for the fact that here the noise level was not taken into account. The differences between port beam ratio and starboard beem ratio show no correlation with the cross-track slope. Thus, from these ratios no conclusion can be drawn about the general slope of the region. This can be seen from the side beam pattern, which shows a large variation for

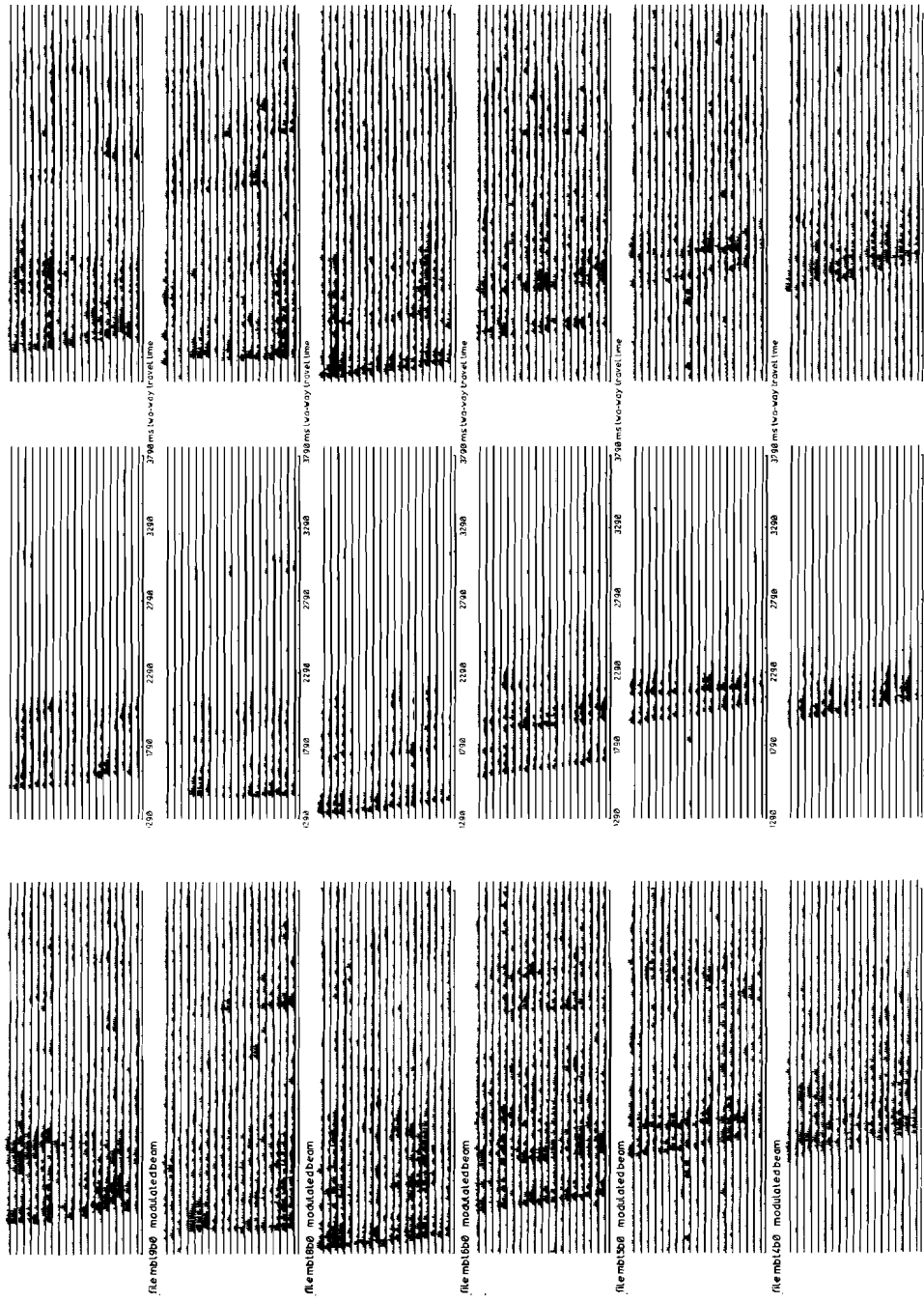

Figure 3.20 Section T; modulated beam signals of which side beams are boosted.

look angles between $+10^{\circ}$ and -10°. If one inspects bottom echo side lobe ratios of single shots, this behaviour is confirmed by a variance in ratios belonging to consecutive shots. The reason this effect may well be found in the irregular depth of the streamers due to bad weather during the experiment.

Side echoes

Figure (3.20) shows modulated beams for the files T3 through T9. In order to search for side echoes the side beams are boosted 14 dB with respect to the central beam. In these files the side beam sidelobe response to the bottom echo is well above the noise level. In file T8 a multiple reflection can be observed at 3000 ms two-way travel time. The reflection from 3240 till 3290 ms two-way travel time in file T5 has the right depth to be a multiple reflection but it has the wrong slope, so nothing definite can be said about it. In file T4 the bottom depth is such that multiple reflections lie outside the block. An echo can be seen in the port beam of this file from 3040 till 3290 ms. This echo, that has a slope in the tow direction opposite to that of the main echo, is not observed in the central beam. Its level is about 3 dB less than that of the sidelobe or side effect of the main echo in the port beam, and about 17 dB below the level of the main echo in the central beam. Between the main echo and the multiple reflection in file T8 another reflector is seen at 2600 ms, equally strong in all three beams. This reflector can also be interpreted as a side echo.

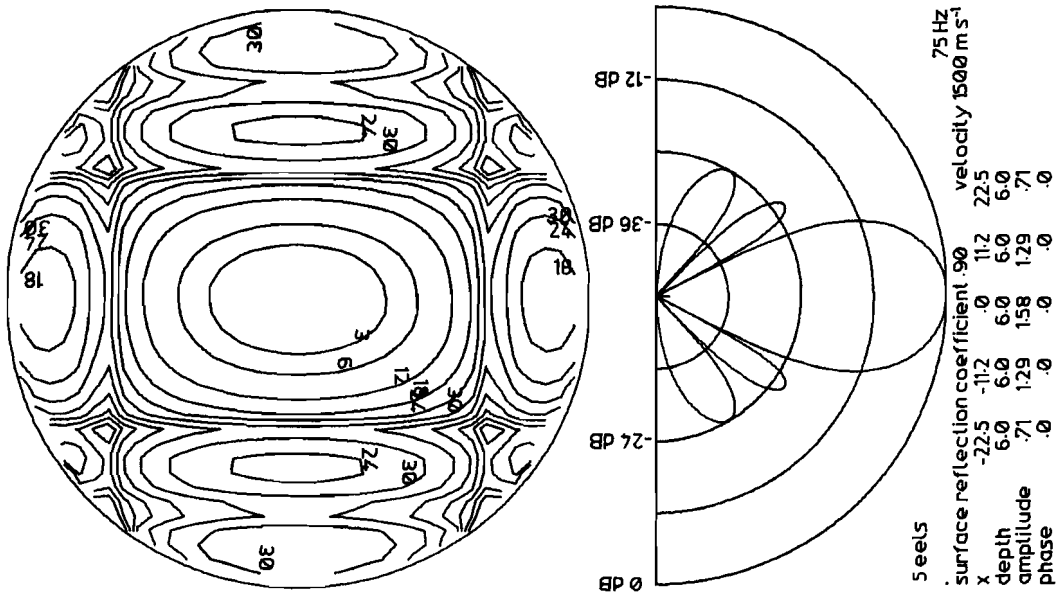

Figure 3.21 Athwartship beam pattern(right)and sensitivity contour diagram(left) of the central beam of a 5 streamer system with the indicated shading.

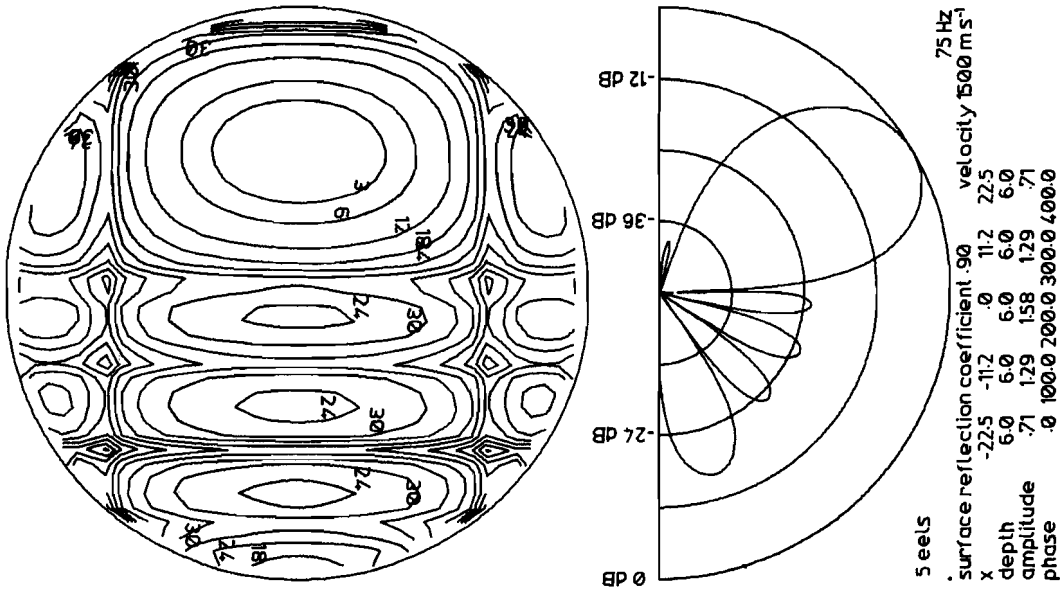

Figure 3.22 Athwartship beam pattern(right) and sensitivity contour diagram(left) for a side beam of a 5-streamer system with the indicated shadings and phase shifts.

C. Conclusions and recommendations

3 and 5 streamer systems

As indicated by the experimental evidence of the previous section a 3 streamer system may be used for improvement of the signal-to-noise ratio in the central beam up to a factor 2, and for elimination of far-out side-echoes by adjustment of the directional characteristics of the system (according to figure 3.14). Side beams can be used to find strong side echoes, but no automatic detection of side-echoes is possible, partly because of the lack of resolution of this system. The only way to detect echoes is to use correlation by human eye. Furthermore, the 3 streamer system is not suited for the measurement of the cross-track slope of the bottom for small and intermediate slope angle.

The system may be improved by narrowing the beamwidth. According to equation (2.54) this can be done by enlarging the aperture. In order to avoid non-zero order maximums, more streamers have to be used. To obtain a beamwidth of 20° at the frequency of 75 Hz an aperture of 45 m must be used. A central beam with such a beamwidth will receive all normal echoes from bottoms having a slope up to 10°. The directional pattern of the central beam in a plane perpendicular to the streamers in a 5 streamer system is shown in figure (3.21), together with its sensitivity contour diagram in the (ℓ, m)-plane.
Next to this central beam two side-beams are formed with a crossover level of 6 dB. With the shadings and phaseshifts indicated in figure (3.22) these beams have a maximum sensitivity in the direction of 30° and a maximum sidelobe level of -20 dB. Figure (3.22) also shows their directional pattern and sensitivity contour diagram.
The beams are formed using simple Taylor weighting with a cosine factor of 0.29. With these beams, which have a 6 dB improvement of the signal-to-noise ratio and a -20 dB sidelobe level, it must be possible to detect strong side-echoes automatically, to do depth-tracking and to detect weak side-echoes visually. If sufficient strong side-echoes are detected automatically, their slant range can be converted into an off-track depth reading. This reading can then be used to construct a qualitative contour chart displaying the strike of major geological features. Refraction caused by a layered ocean

can be neglected because of the 20° beamwidth.

Timing

The off-line processing of the *Tydeman* cartridges on the same 21 mx system was not very fast, partly because there was no need to speed up the software at the cost of flexibility of the process, and partly because of hardware limitations. The following times were obtained by measurement:

filter one streamer signal	7 s ,
quadrature detection, beamforming for one beam per streamer	5 s ,
beam amplitude or modulated beam; per beam	5 s .

whence

total time per shot for a 3 streamer × 3 beam system $3 \times (7 + 3 \times 5 + 5) =$	81 s ,
total time per shot for a 5 streamer × 3 beam system $5 \times 7 + 3 \times (5 \times 5 + 5) =$	125 s .

These times can be improved in three ways.
First the quadrature detection, which was defined as a convolution (equations 2.70 and 2.71) can be formulated in the frequency domain and combined with the 50 Hz filter. The beamforming must then also take place in the frequency domain. The condition enabling this procedure is that enough memory space is available. An estimate of the time needed for one shot is, assuming that beamforming can be done within 3 sec per beam,

in the 3 × 3 case :	$3 \times (7 + 3 + 5)$	45 s ,
in the 5 × 3 case :	$5 \times 3.5 + 3 \times (3.5 + 3 + 5) =$	52 s .

The next improvement could be the use of a computer with a faster memory and/or floating point hardware. More than 6 times improvement is gained by using a HP F-series computer with a scientific instruction set (HP, 1978). 1.7 times improvement is gained by using high performance memory in this

F-series computer (HP, 1978). In this way the times cited above can be reduced to:

in the	3 × 3	case :	less than	4.4 s ,
in the	5 × 3	case :	less than	5.1 s ,

The third way to reduce calculation time is to use a microprogram for the Fast Fourier Transform. As floating point calculations do not take much longer than memory accesses, a micro-program can be used to minimize these accesses.

The memory necessary includes 2048 16-bit words for each streamer input and for each beam output, in total 16k words for the 5 × 3 case. This memory must be immediately accessible to the transforming program. The aforementioned measures can bring the calculation time to within 10 s thereby enabling the on-line transformation of 5 streamer inputs into 3 beams at a shot rate of 0.1 s^{-1}.

Recommendations

A system is proposed having the following features:

5 streamers towed with a total spread of 45 m at a depth of 6 m.
3 beams formed with simple Taylor weighting.
The central beam has a width of 20° and a sidelobe level of -20 dB.
The side beams are directed at 30° and have the same sidelobe level.
Beamforming parameters reside within the transforming program; they can be redefined by the operator for special purposes.
A 21 mx F-series computer with sufficient high-performance memory.
An automatic depth-tracking program
Automatic detection of strong side-echoes } with digital output
Display of weaker side-echoes, not automatically detectable by the system.
If side-echoes are detected in both side beams the system has a coverage comparable to the depth.
A contour chart output can then be generated.

4. Multiple beams at high frequency

A. General considerations

High-frequency sound sources

A transducer used to produce sound in water is called an underwater sound projector, in short, projector. If one needs a quasi-coherent output with a predetermined waveform at high frequency, one generally uses a projector converting electrical energy into acoustic energy.
The principle of such projectors can be electromagnetic, electrostatic, magnetostrictive or piezoelectric. The first two principles are of historical interest only. Nowadays, most transducers for echosounding equipment use magnetostrictive projectors (Ulrich, 1976, Renard et Allenou, 1979) and piezoelectric ceramic (v.d. Burgt, 1968, and Mazzola et al., 1979) devices.
As stated in chapter 2 we may use the formula for beamforming at the receiver as well as for beamforming at the projector.
Transducers utilized for beamforming by means of an array should be smaller than half the wavelength of the projected signal, according to equation (2.64) to inhibit the insonification of unwanted areas by non-zero order maximums in the array pattern.

The maximum output of a transducer is limited by the condition, that the instantaneous absolute pressure must exceed the vapour pressure of water. If the absolute pressure gets lower, cavitation can occur at the water interface of the transducer, causing a decrease in efficiency of the conversion into acoustical energy. For a continuous wave signal excited near the water surface, the output radiation flux density that may be projected without cavitation loss equals $3.\ 10^{-5}$ W m^{-2}. Cavitation is not instantaneous, so short acoustic pulses may have a higher flux density than a continuous wave signal (Albers, 1965). The flux density is proportional to the pressure amplitude squared, so if the hydrostatic pressure is doubled, the permissible output flux density is quadrupled.

The consequence of cavitation is that a large radiation surface is needed when large projector power is used. To meet this and the requirement for omnidirectionality either the number of array elements must be high, or the

frequency has to be lowered to allow for large projectors.

Piezoelectric and magnetostrictive transducers usually have a complex admittance with a large conductance component near the mechanical resonance frequency. The efficiency of energy conversion is maximal when the signal frequency lies within a narrow band around the mechanical resonance frequency. This narrow band can be widened considerably if the electrical driving circuit is tuned to the mechanical resonance frequency of the transducer (Hueter and Bolt, 1955). Nevertheless, the actually projected acoustic signal may be distorted by the narrow bandwidth. This distortion is known as ringing. It can be diminished by the use of an acoustic feedback system (Mazzola et al., 1979).

High-frequency receivers

Projecting transducers that convert electrical signals can also be used as hydrophones. The sensitivity of such hydrophones is maximal at the mechanical resonance frequency. However, small individual variations in the mechanical and electrical parameters of the hydrophone may result in considerable variations of the sensitivity and phaseshift characteristics of the hydrophone. Most piezoelectric transducers exhibit a constant sensitivity in a region well below the mechanical resonance frequency. This is especially true if the hydrophone is not tuned electrically and connected to a high-impedance amplifier input (Rijnja, 1971). In the region mentioned the phase difference between the pressure wave and the electrical output signal is then negligible. Thus it is common practice to use hydrophones with a relatively high mechanical resonance frequency for phase-critical applications. This implies the use of two sets of transducers: one for transmission and one for reception.

Receiver mounting

To minimize the reception of sound from near-horizontal directions and to minimize the coupling between adjacent hydrophones, the receiver elements may be embedded in a suitable material in such a way, that the sensitive surface of the receiver is mounted flush with the material surface.

If the surface of this material outside the receiver elements is flat and the receiver elements are small compared with the signal wavelength, we may use Rayleigh's (1945) reflection formula:

$$R = (\rho_1 \cot\theta - \rho \cot\theta_1)\ (\rho_1 \cot\theta + \rho \cot\theta_1)^{-1} \qquad (4.1)$$

where

R reflection coefficient,
ρ density of water,
ρ_1 density of reflective material,
θ angle of incidence

and

$$\theta_1 = \arcsin(n \sin\theta)$$

with n is the index of refraction between water and the reflective material. From equation (3.4) the element pattern may be calculated, letting w go to 0:

$$|F^1(q)| = 2\left\{1 + \frac{\rho}{\rho_1}(nq)^{-1}\ (1-n^2+n^2q^2)^{\frac{1}{2}}\right\}^{-1} \qquad (4.2),$$

where $q = \cos\theta$.

This formula shows that $|F^1(q)| \to 0$ for $q \to 0$.
Sound waves with grazing angles of incidence are thus extinguished.
Figure (4.1) shows the pattern of a receiver element embedded in rubber bonded cork, a material with a refractive index of 0.31 and a density ratio of 1.0 with water. This pattern does not deviate more than 1 dB from a cosine pattern for $\theta < 60^\circ$. The low sound velocity makes rubber bonded cork well suited for this application.

Using the Fast Fourier Transform

The Discrete Fourier Transform is defined as follows (Bracewell, 1978):

$$X_k = \sum_{i=0}^{I-1} x_i \exp(2\pi j\, i\, k\, I^{-1}) \quad k = 0 \ldots K-1 \qquad (4.3).$$

Cooley and Tukey (1965) published a method to reduce the number of computations involved in the evaluation of this formula, thereby enabling widespread use of it (under the name of Fast Fourier Transform, FFT) in digital computers, and even in analog computers (Wolff, 1976).
Many implementations of this FFT exist (G-AE subcommittee, 1967). Most operate on series with a length that is a power of two only. Generally, these are the fastest ones. Other FFT programs accept series with other restricted lengths, or with an arbitrary length. If these programs transform a series with a power-of-two length, they can be as fast as those mentioned above. However, if they operate on series with an arbitrary length they have a computation time at least twice as long as the time needed for the transformation of a series with a length that is the next higher power of two (Van der Steen, 1978). If one uses the FFT for beamforming in a time-critical situation one should choose for an array with a power-of-two length. The exact relationship between computation time and array element number depends on the computer timing. With the present-day computer hardware it seems that not the number of complex multiplications (Cooley and Tukey, 1965) determines the computation time, but the number of memory accesses. At least, measurement on a HP 21 mx M-type computer indicates that this realtionship between time t and number of elements n is (for a Cooley-Tukey based complex FFT):

$$t = 3.13\, n^{1.132} \text{ ms} \quad \text{for} \quad n \geqslant 4,$$

rather than

$$t \approx n \log n.$$

B. High-frequency model experiment

Introduction

In 1977 a way was sought to generate a realistic set of signals suitable for the study of the problems connected with beamforming in a digital computer. Af first a solid state model was tried consisting of a sheet of methyl metacrylate into which an ocean boundary was to be cut. Longitudinal waves would be used to measure this boundary. The model parameters (wavelength, attenuation of sound) and the occurence of surface waves caused this model to be impracticable for the purpose stated. A solution was then sought in a wet model with water as the acoustic medium. The depth required to simulate an ocean-like situation led us at first to gravel pits along the river Lek, but the difficulty to fix a measuring system over the water without influencing the underwater acoustic field made us decide to choose one of the deepest locks in the Netherlands for signal collection. The measurements were made on 12 November 1977 in the third chamber of the triplet lock (see figure 4.2) in the Juliana canal at Maasbracht (Topographic map sheet 58C 18928×35035).

The lock chamber

The lock has a water level difference of 12.25 m and a maximum depth of 17.15 m. The maximum depth expressed in wavelengths of the signal frequency (17.86 kHz) is 209, giving a maximum signal phase deviation from the linear case (see equation 2.42) of 0.2 rad within a circle with a radius of 8 wavelengths, if refraction is neglected. Under these circumstances the lock chamber is a reasonable model for multiple beam experiments.

Figure (4.4) gives a cross-section along the axis of the chamber. Indicated are the receiver array center points of the measuring series A through E and the level of reference at 31.53^{+} (31.53 m above the Normal Amsterdam Level), that will be given a depth of 0 m. The concrete chamber floor had been cleaned some months before the measurements. The floor exhibits several steps and a sill of which the part that emerges at low level can be seen in figure (4.3). The width of the chamber (figure 4.5) is 16 m. This is rather narrow and it may cause unwanted horizontal reflections. However, this

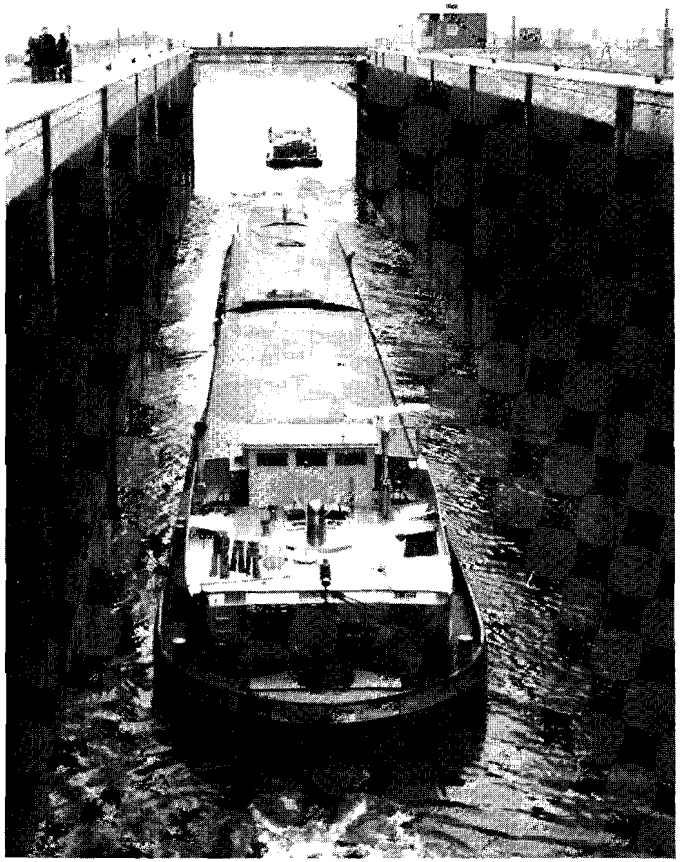

Figure 4.2 The chamber of the lock at Maasbracht

Figure 4.3 Detail of the chamber showing the sill

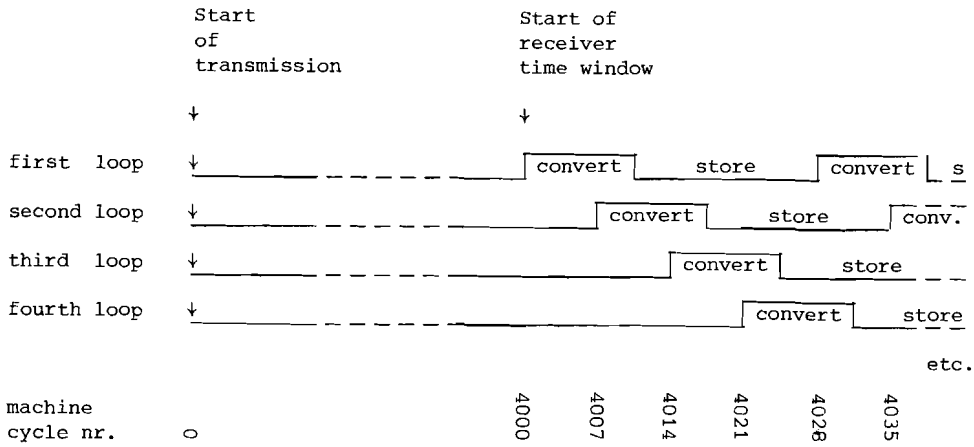

Figure 4.9 Timing diagram of received signals.

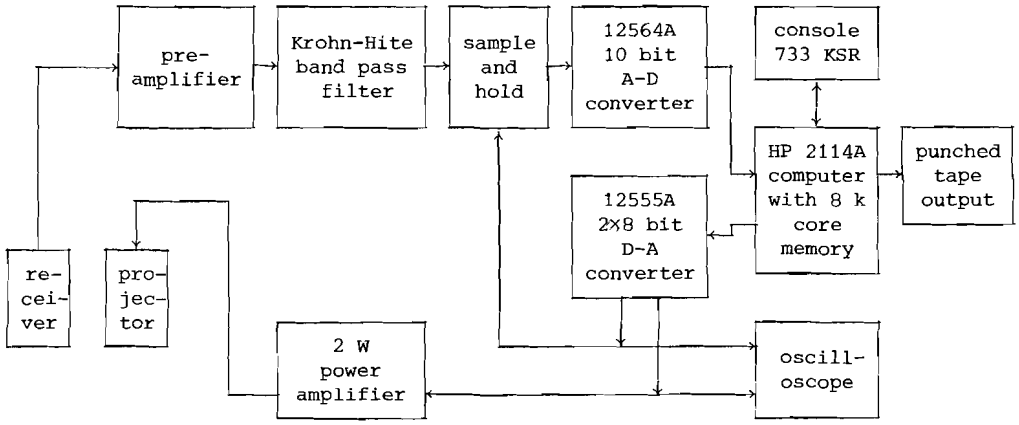

Figure 4.8 Block diagram of electronics and computer hardware used at Maasbracht.

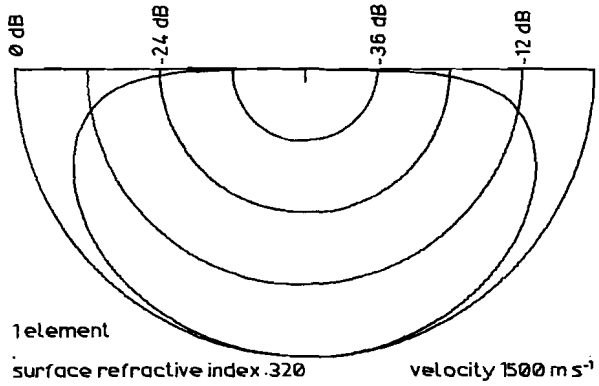

Figure 4.1 One-dimensional pattern of a transducer bedded in rubber bonded cork.

limited width greatly facilitated the installation of the measuring system.

The measuring system

Five pieces of 5 m steel-wire were connected in a double Y-fashion. As indicated in figure (4.5), the four remaining ends were fastened to four bollards on the embankment and drawn taut by means of rigging screws. On the wire parallel to the embankment two pulleys were mounted, each bearing one transducer: the projector and the receiver, both suspended in the water (see figure 4.6). Each pulley was movable individually by means of a 5 mm nylon rope operated from the embankment. For each measurement the transmitter was kept fixed and the receiver was moved along the wire to occupy the different channel positions spaced 4.2. cm (ideally 4.22 cm) apart. This displacement was controlled by measuring the displacement of the nylon rope, of which both end points had been tied together, on the embankment. In this way linear transducer arrays with apertures of 130.8 cm (for 32 elements) and 63.3 cm (for 16 elements) were simulated with the axis parallel to the embankment of the lock chamber. Results from beamforming with signals from this array should conform with the longitudinal cross-section of the chamber (figure 4.4).

The projector was suspended bare, with its sensitive surface of 16 cm^2 facing downward. The receiver was fitted with a 19 cm diameter flat reflector made from rubber bonded cork. The surface of the reflector, in which the receiver was mounted flush, also faced downward. Both transducers were ceramic transducers type ZP 18, manufactured by the Physisch Laboratorium TNO in The Hague. They have a capacitance of 6100 pF and a diameter of 4.5 cm. Used as a receiver, their sensitivity is -96 dB re 1 V Pa^{-1}. Used as a projector, they have an output level of 44 dB re 1 Pa A^{-1} at the resonant frequency of 20 kHz. Operating in the tuned mode, they have a -3 dB frequency band from 19 to 27 kHz. The sum of the motional resistance and the internal loss resistance is 290 Ω.

The electrical system

A block diagram of the electrical system is shown in figure (4.8). The system is illustrated in figure (4.7). The transmitted signal was generated digitally

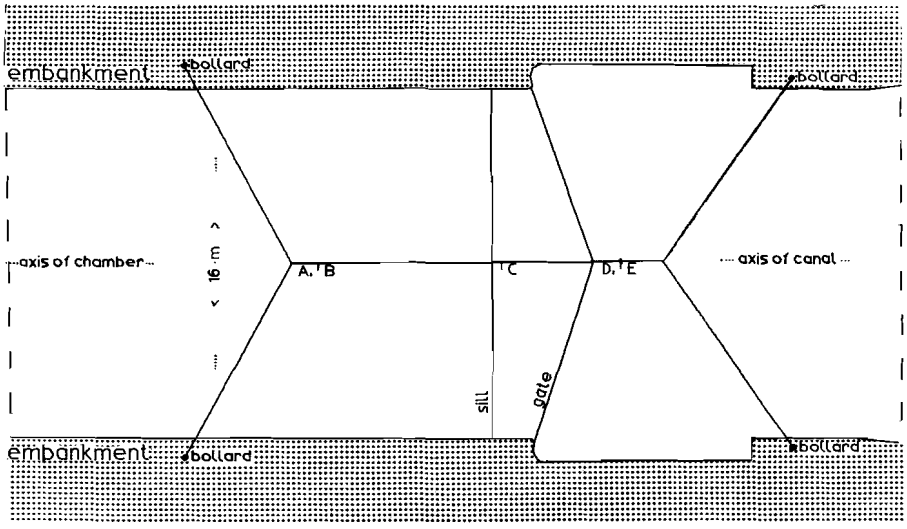

Figure 4.5 Plan of the lock chamber, showing the measuring system and the sill.

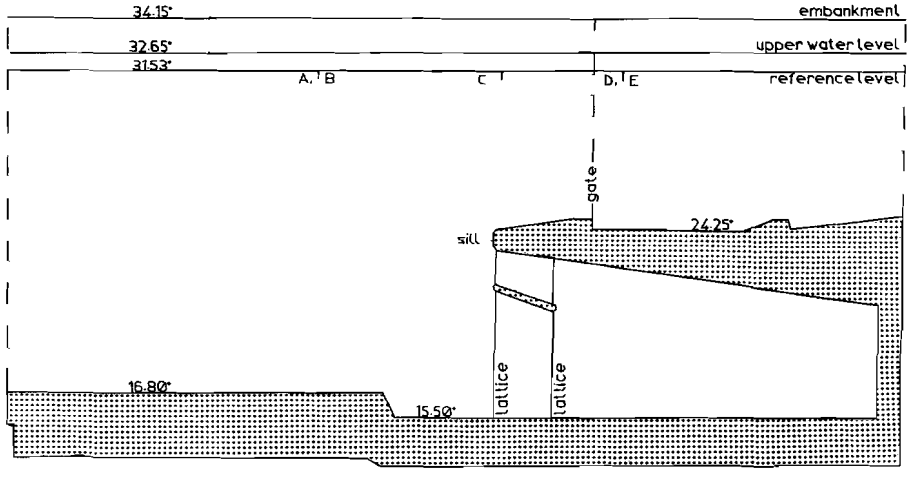

Figure 4.4 Cross-section along the longitudinal axis of the lock chamber.

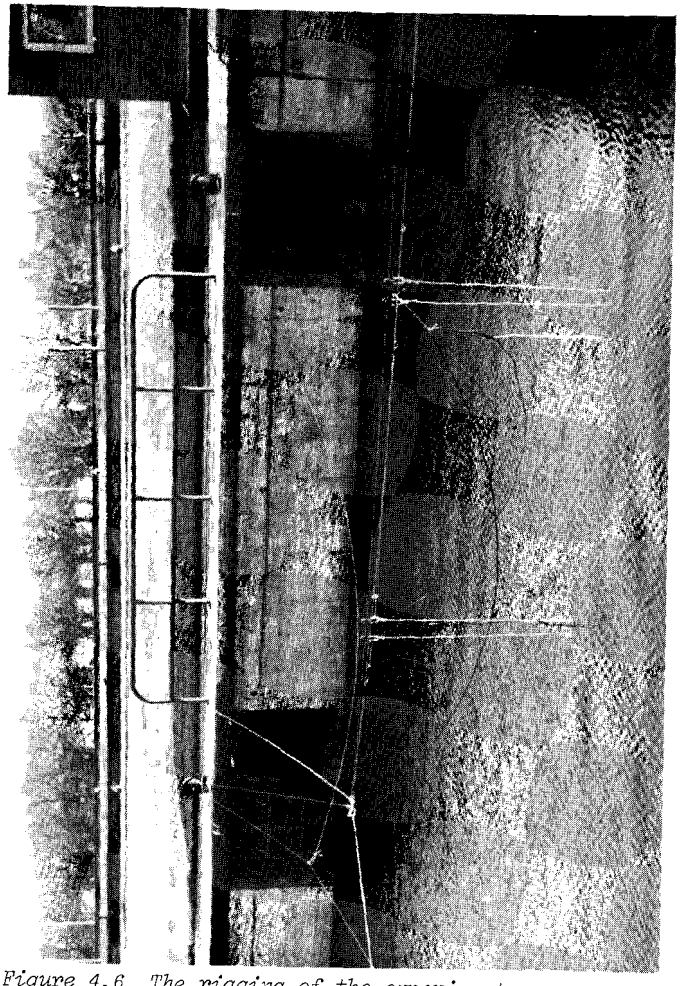

Figure 4.6 The rigging of the experiment.

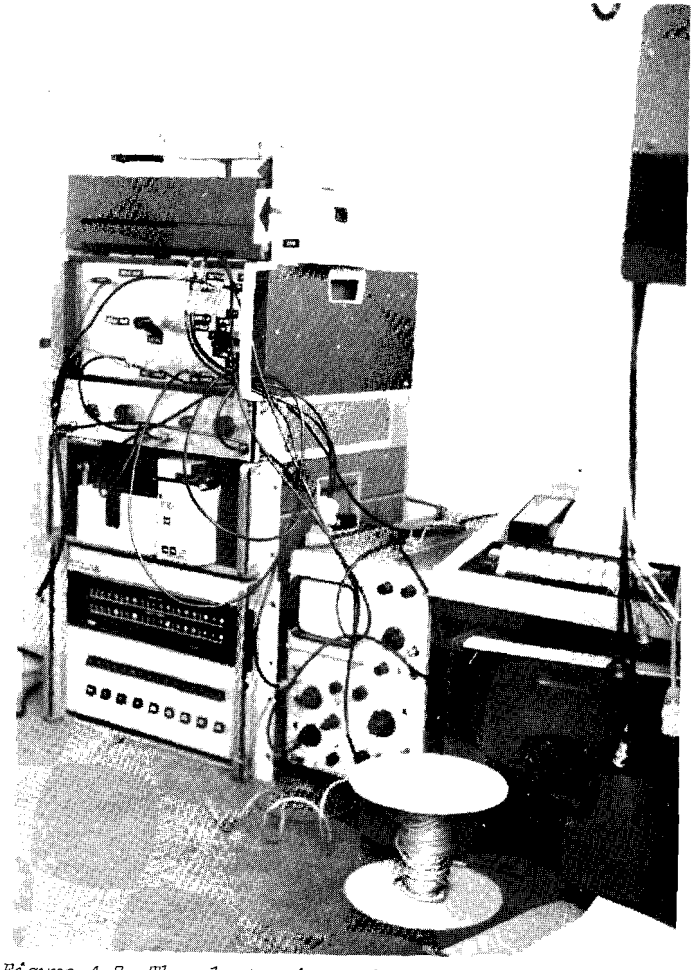

Figure 4.7 The electronics and the computer hardware.

in the computer, converted into a voltage by the digital-to-analog converter and fed through a variable attenuator into the 2W power amplifier. The amplifier was coupled with the projector through a series inductance of 10 mH, thus electrically tuning the projector circuit to the frequency of 20 kHz.
The received signal was amplified by a preamplifier with high input impedance (22 MΩ). The amplification was set at 33.5 dB in series A and B and 27 dB in series C, D and E. The signal was then put through a band pass filter with a passband from 15 to 25 kHz and a steepness of 24 dB octave^{-1} with a Butterworth signature. The filtered signal was sampled by a sample-and-hold circuit at times determined by the computer program and converted into a number.

The oscilloscope was used for monitoring the transmitted, received and filtered signals in the analog phase. Upon completion of the measurement of one channel the oscilloscope was used to display the digitized signal, which was converted back again for this purpose. After passing visual inspection, the signal was punched on paper tape while the receiver was moved to a new position and allowed to settle.

Measurement software

The Hewlett-Packard 2114A computer performed the following tasks:

(1) Generate the projector signal and set the reception time window.
(2) Wait till sampling time has come, start analog-to-digital conversion, put in converted value.
(3) Repeat (2) until the end of the time window.
(4) Repeat (1) through (3) for the next loop (see figure 4.9).
(5) After completion of the last loop, restart with first loop for optional stacking.
(6) Display recorded signal on oscilloscope.
(7) Store recorded signal on punched tape and restart.

The projector signal, a twenty wavelengths sine pulse, was stored in memory, interlaced with output instructions. In this way a conversion rate of 166.7 kHz could be attained for the projector output signal. The timing of this

conversion as well as that of the receiver pacing was based on the central processor clock that, measured with a crystal timebase generator, had a frequency of 499760 ± 13 Hz. One processor cycle lasted about 2 μs. Figure (4.9) gives a timing diagram for the input signal collection. The need for several loops was caused by the difference between the sample interval (7 cycles or about 14 μs) and the time for conversion and storage of the value (minimum 27 cycles or about 54 μs). Each loop converted maximal 500 values consecutively. After the completion of a loop and before a new loop started a pause of about 50 ms was inserted to allow for the extinction of the previous signal. After the completion of the last loop the program could start the first loop anew, adding the newly received values to the values present in memory (stacking) to reduce noise.

Measurement series

In this way 5 series of measurements were made, designated series (or file) A, B, C, D and E.
Files A and B were recorded with the receiver centre point at the same location over the deepest part of the chamber (see figure 4.4), file A with the gate closed and file B with the gate open. File C was recorded with the receiver centre point over the sill. Files D and E were recorded with the receiver centre point between the open gate doors, file D with a 20-fold stack and file E without stacking. A list of parameters pertaining to these files is given below

file	projector-receiver distance	array aperture	depth of transducers below reference level	number of channels	time between transmission and time window	time window length	number of stacks	upper lock gate
A	169	130.8	-6	32	10	28	10	closed
B	79	130.8	-6	32	8	28	10	open
C	84	130.8	0	32	8	28	10	open
D	108	130.8	-2	32	8	18	20	open
E	108	63.3	-2	16	8	18	1	open
	cm	cm	cm		ms	ms		

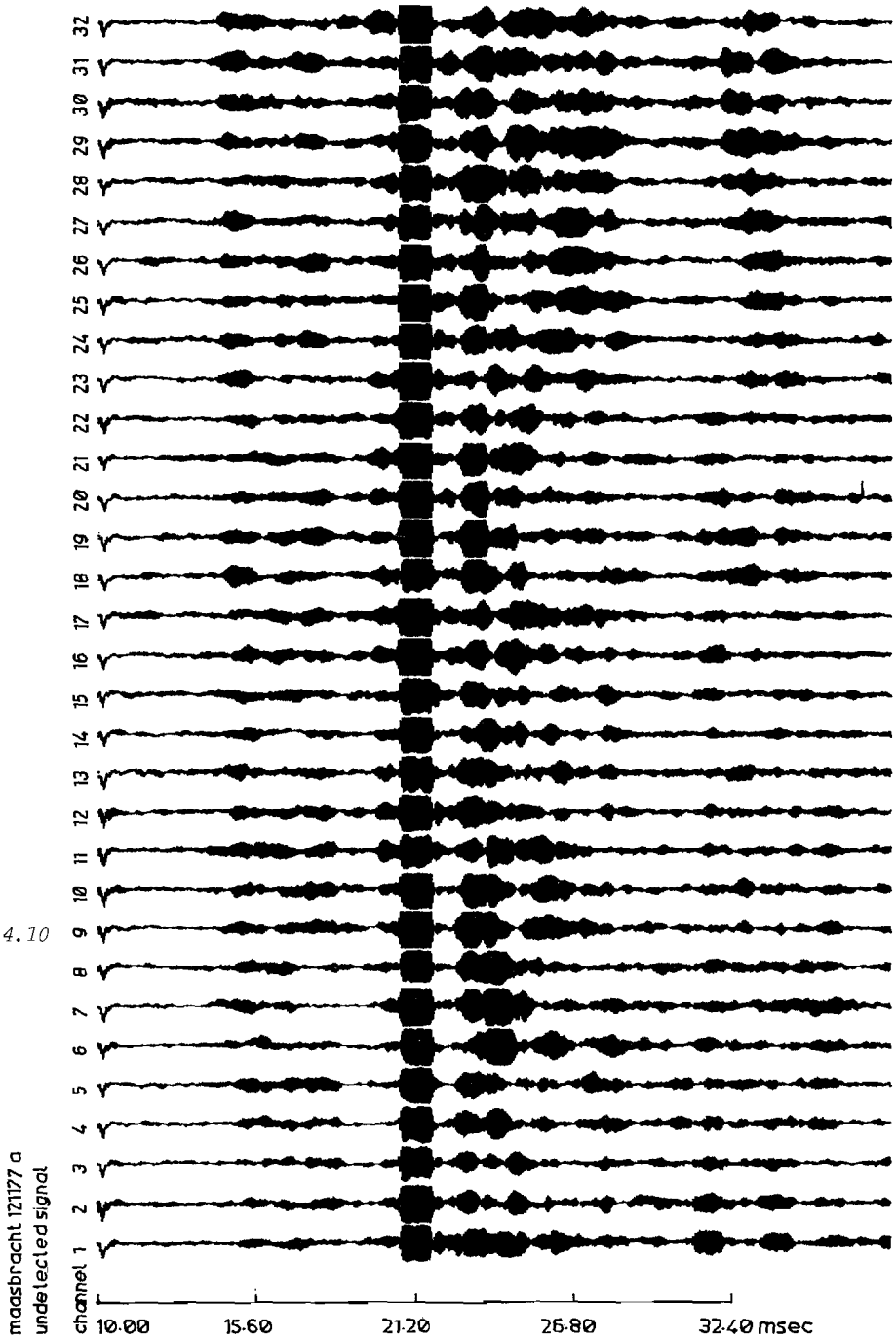
maasbracht 121177 a
undelected signal
channel 1
2
3
4
5
6
7
8
9
10
11
12
13
14
15
16
17
18
19
20
21
22
23
24
25
26
27
28
29
30
31
32
10.00
15.60
21.20
26.80
32.40 msec

Figure 4.10

The measured signals

Figure (4.10) shows an example of a set of signals collected (i.e. file A). The computational procedure applied to all files is slightly different from that described in the previous chapter. No digital filtering was done because the signals were already filtered when in analog form. This analog filtering was needed because of the limited dynamic range of the A-D converter. Quadrature detection was done according to equations (2.70) and (2.71) with the time weighting function (3.6a). The resulting in-phase and quadrature signals from file A are shown in figures (4.11) and (4.12), whereas figure (4.13) displays the modulus of the detected signal. The detected signal was transformed using a simple Taylor weighting function with $F_1 = 0.33$ (equation 2.65). The general beam pattern for this weighting function is shown in figure (4.14). It has a maximum sidelobe level of -30 dB and a beamspread factor (the ratio between beamwidths with and without shading) of 1.30. The beam patterns for the experiment in Maasbracht (16 and 32 element arrays with their respective array lengths, receivers with reflector, the appropriate sound velocity) are given in figure (4.15) for 32 elements, and figure (4.16) for 16 elements. The sound velocity was calculated using a simplified formula (Medwin, 1975), derived from the NRL II formula (Del Grosso, 1974), using measured values for the salinity (less than 500 mg l^{-1} for the river Meuse, Zuurdeeg, 1980) and the temperature (12°C, Rijkswaterstaat, 1978). In this manner a sound velocity of 1450 m s^{-1} was calculated.

The actual transformation was done with the FFT (equations 2.60 and 4.3), generating 32 beams and 16 beams from 32 and 16 elements respectively. The beam amplitude was calculated according to formula (3.7) with $M = 80$ (20 wavelengths). This amplitude is displayed as a time series in figure (4.17). In this figure channel 1 represents the beam with "look" direction $\ell = 0$, pointing downward in this experiment. Most of the signal energy is transformed to channels 32 and 31, adjacent to channel 1 (see also figure 4.18). This is explained by the position of the transmitter relative to the receiver array, which was for this file 169 cm, causing the specular reflection against the flat floor of the chamber to be received at an angle corresponding to the beam angle of beam 31 and 32.

These transformed signals can be displayed better by projecting them on a

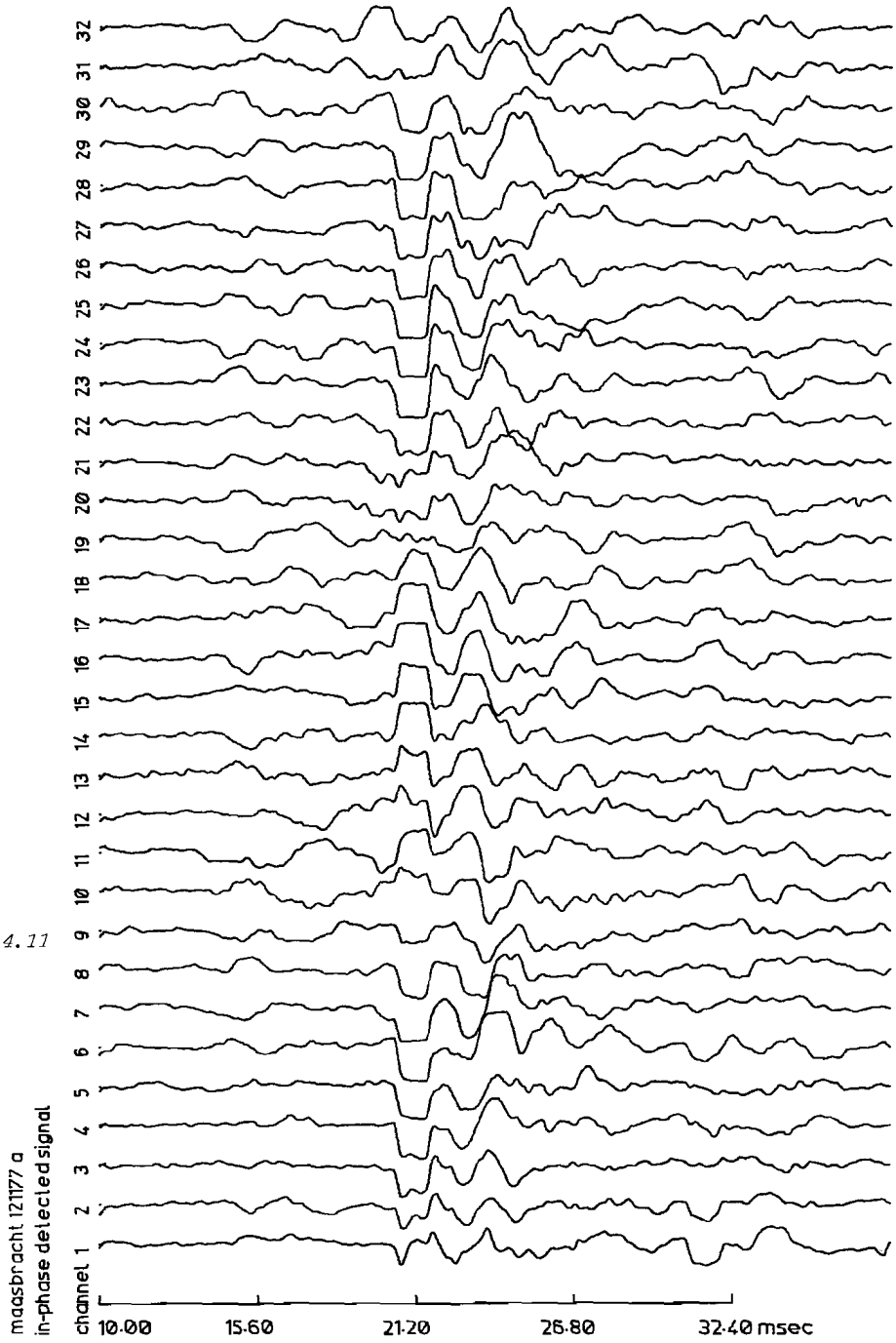
maasbracht 121177 a
in-phase detected signal
channel 1 2 3 4 5 6 7 8 9 10 11 12 13 14 15 16 17 18 19 20 21 22 23 24 25 26 27 28 29 30 31 32
10.00
15.60
21.20
26.80
32.40 msec

Figure 4.11

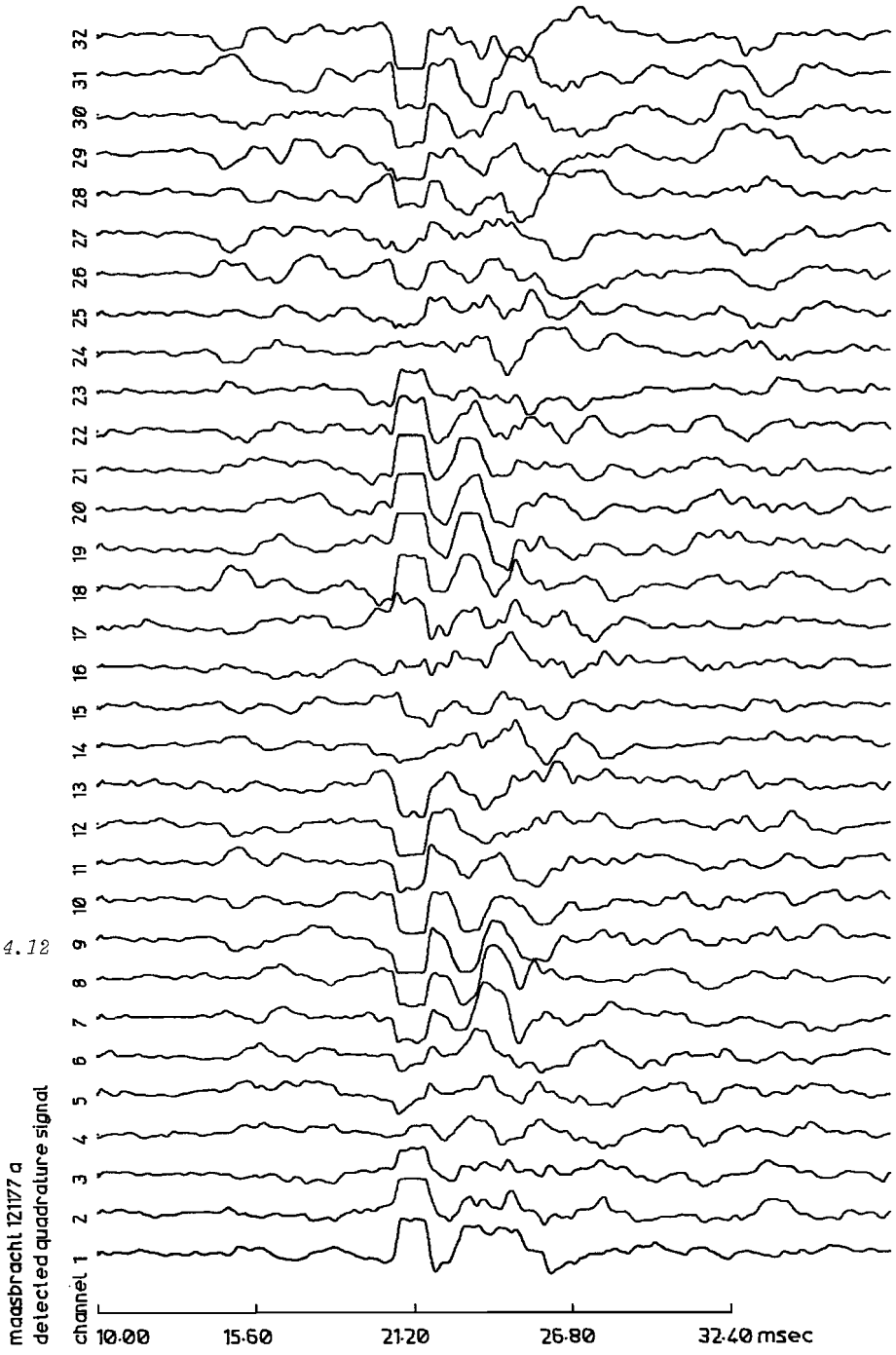
maasbracht 121177 a
detected quadrature signal
channel 1
2
3
4
5
6
7
8
9
10
11
12
13
14
15
16
17
18
19
20
21
22
23
24
25
26
27
28
29
30
31
32
10.00
15.60
21.20
26.80
32.40 msec

Figure 4.12

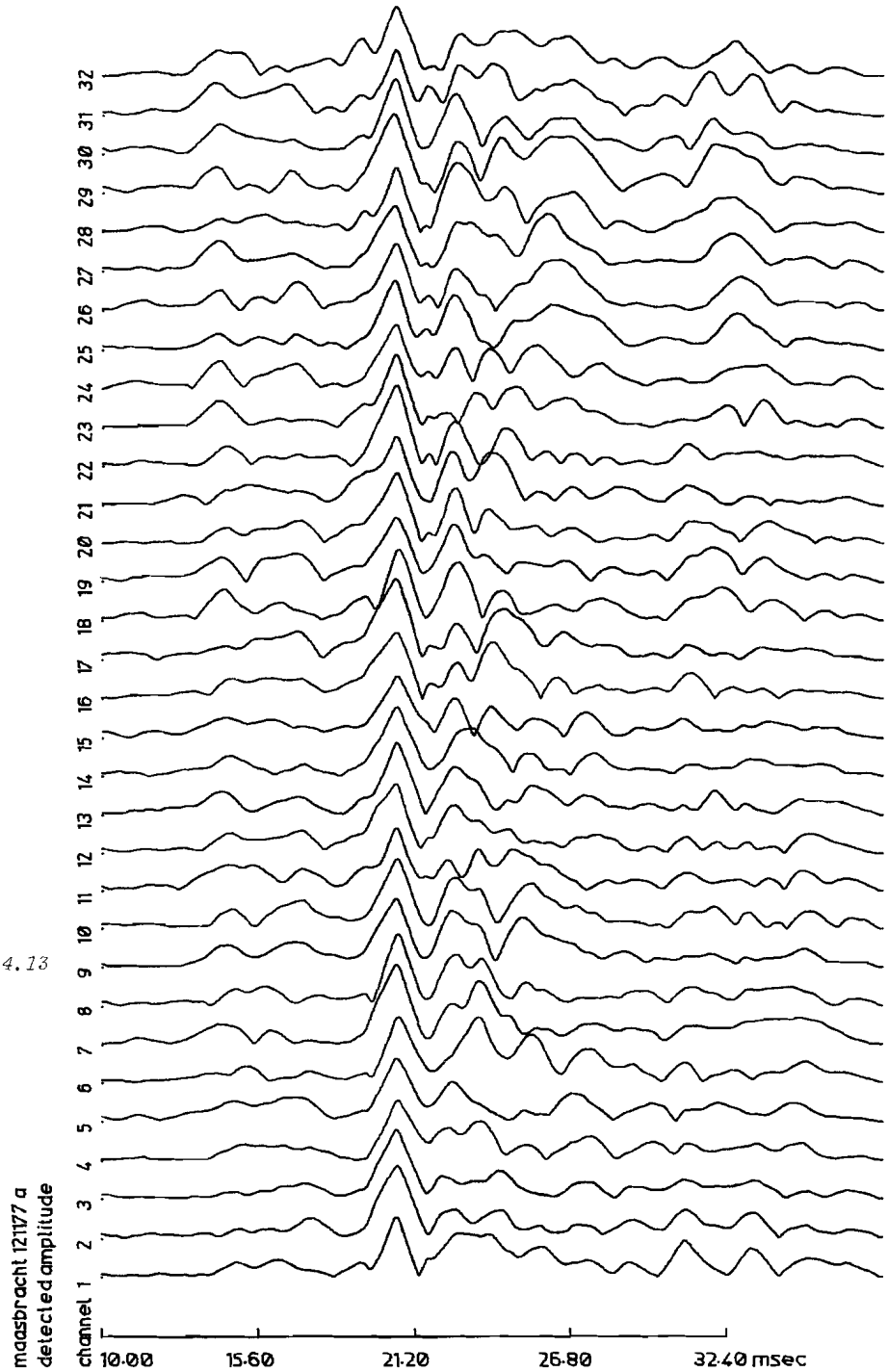
maasbracht 121177 a
detected amplitude
channel 1 2 3 4 5 6 7 8 9 10 11 12 13 14 15 16 17 18 19 20 21 22 23 24 25 26 27 28 29 30 31 32
10.00
15.60
21.20
26.80
32.40 msec

Figure 4.13

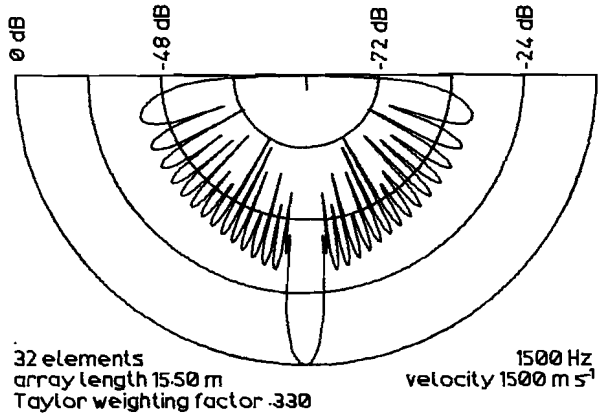

Figure 4.14 One-dimensional beam pattern with simple Taylor shading: $F_1 = 0.33$

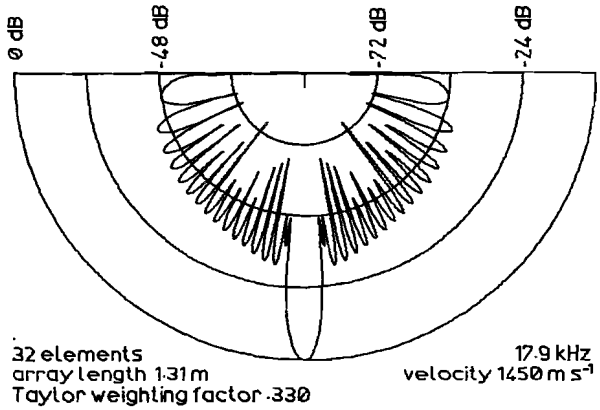

Figure 4.15 The pattern of the synthetic aperture from Maasbracht(32 elements)

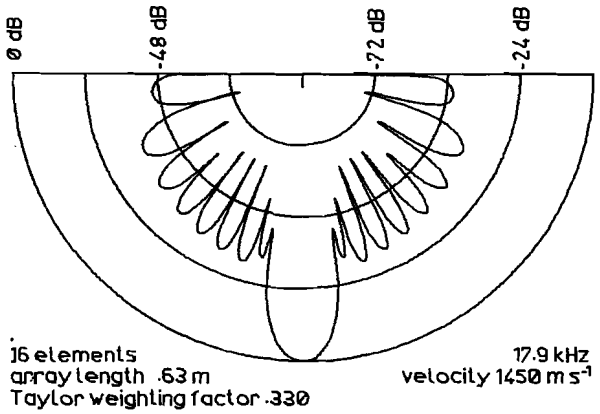

Figure 4.16 The pattern of the synthetic aperture from Maasbracht(16 elements)

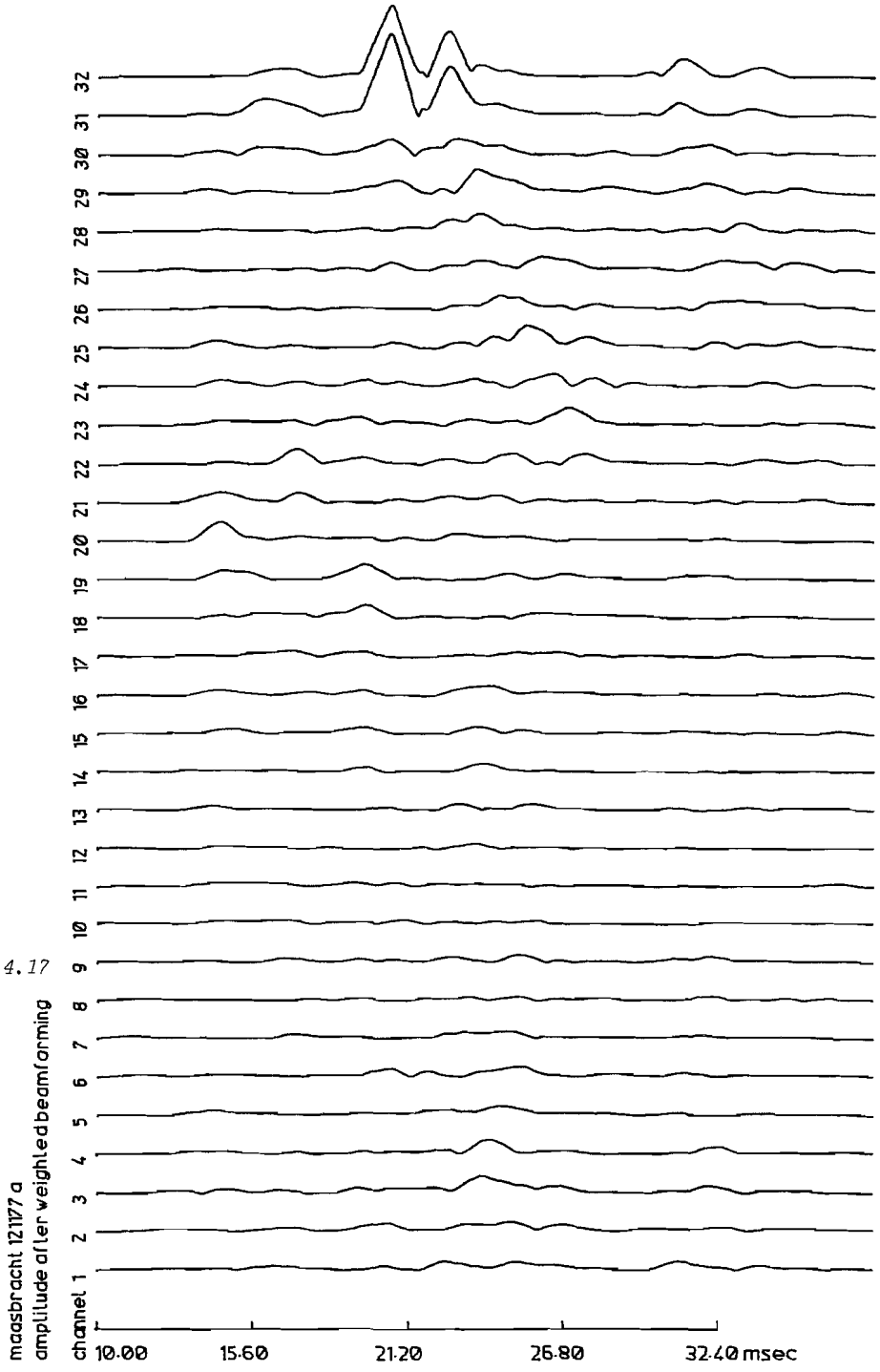
maasbracht 121177 a
amplitude after weighted beamforming
channel 1
2
3
4
5
6
7
8
9
10
11
12
13
14
15
16
17
18
19
20
21
22
23
24
25
26
27
28
29
30
31
32
10.00
15.60
21.20
26.80
32.40 msec

Figure 4.17

vertical plane through the axis of the lock chamber, taking into account the beam direction and the sound velocity. Figures (4.18) through (4.22) give the projected images for the files A through E respectively. In the 32 beam files beam 17 on the left side is repeated on the right side for completeness. As it has a major lobe in both these directions, it is worthless for measurement purposes. This lobe is caused by the difference between the half-wavelength and the element spacing.

Echo detection

Figures (4.18) through (4.22) are still difficult to interpret. However, comparison with figure (4.4) shows that in some beams maximums appear at places where they are to be expected. But other maximums occur too. To sort out these echoes a detection program was constructed operating in the following way on the beam amplitude of each file.
All beams were scanned to determine a noise threshold. For this the mean beam amplitude was calculated and all amplitudes below this mean beam amplitude were considered to be noise. Per beam the mean noise level $\bar{v}_n$ was calculated and the noise threshold was defined by

$$\bar{v}_T = 4\ N^{-1} \sum_{n=1}^{N} \bar{v}_n$$

All echoes having a beam amplitude less than $\bar{v}_T$ were discarded. The value of 4 was chosen empirically.

Relative noise levels are given in the next table:

file	A	B	C	D	E	
mean noise level	-1	-1	-7	-3	4	dB

It can be seen that difference in stacking between D and E is not fully reflected in the noise levels. If this noise was non-coherent the noise-level differences between E and A, B, C, or D would have been 10, 10, 13 and 13 dB. So at least part of the noise in this experiment is coherent.

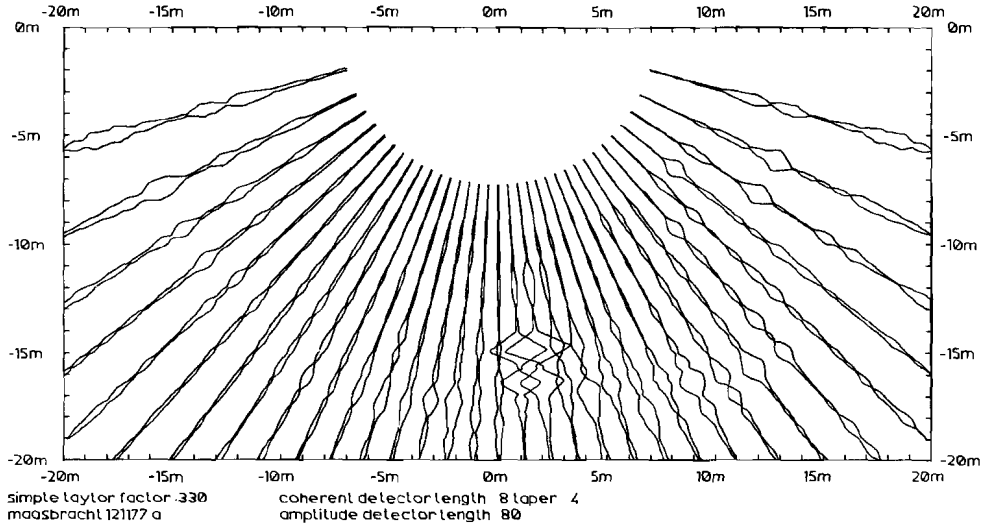

Figure 4.18 Beam amplitude from file A (with lock-gate closed).

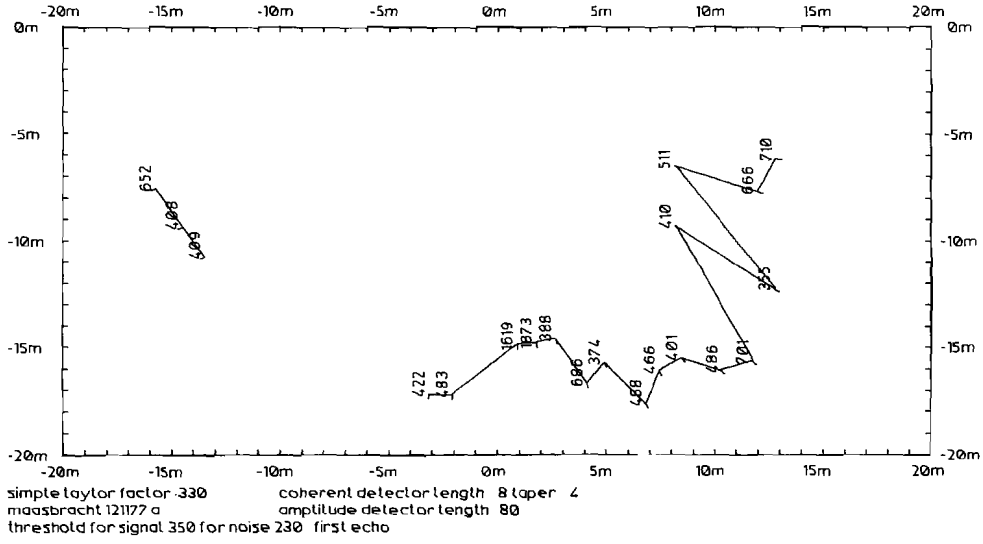

Figure 4.23 Detected depths from file A (with lock closed).

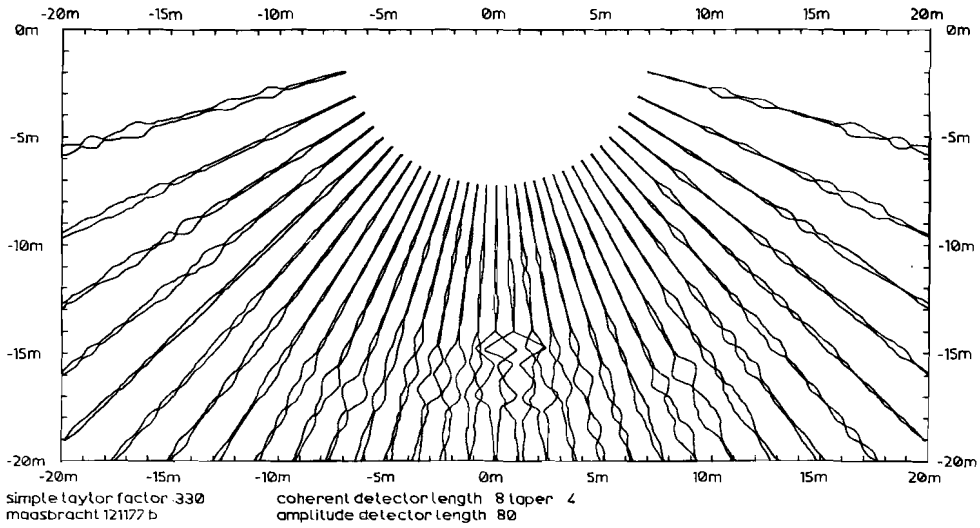

Figure 4.19 Beam amplitudes from file B (with lock-gate open but same array as A).

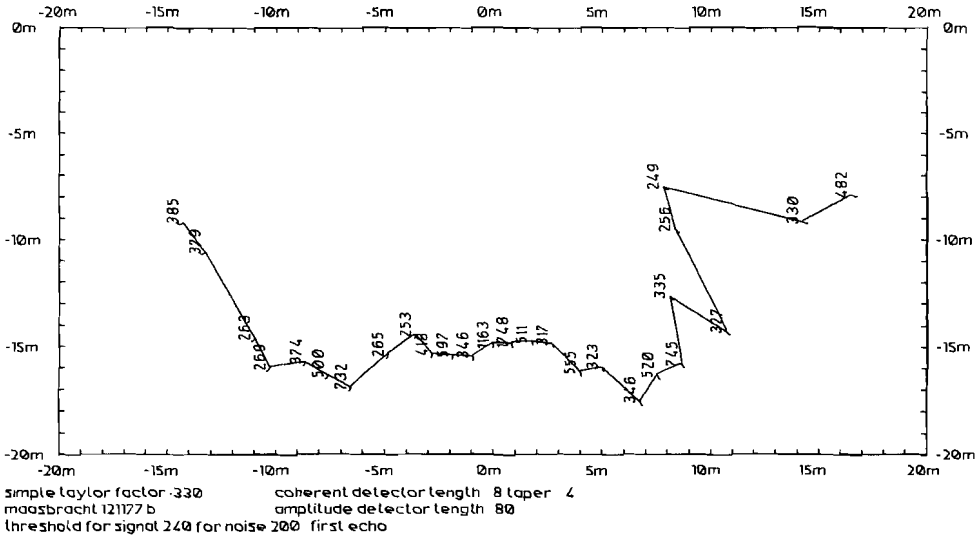

Figure 4.24 Detected depths from file B (with lock-gate open but the same array).

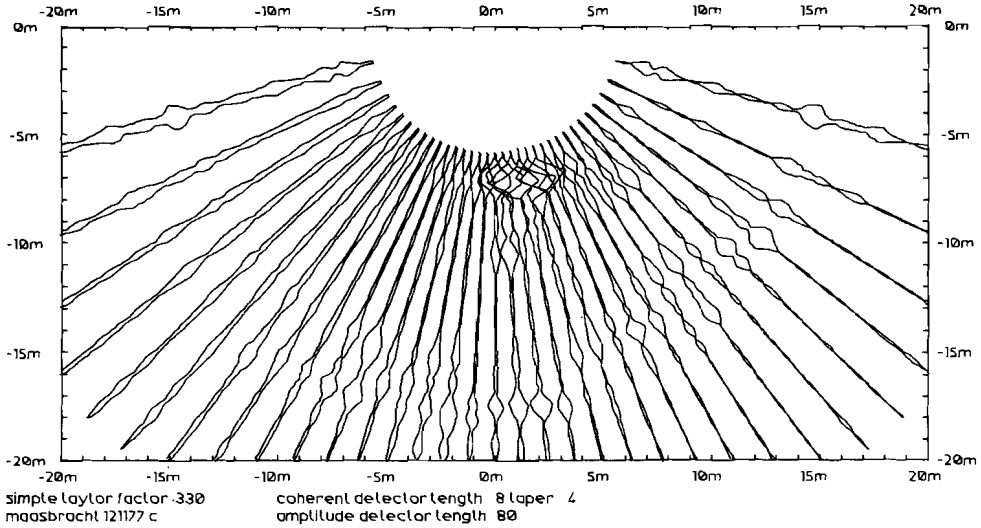

Figure 4.20 Beam amplitudes from file C (over the sill).

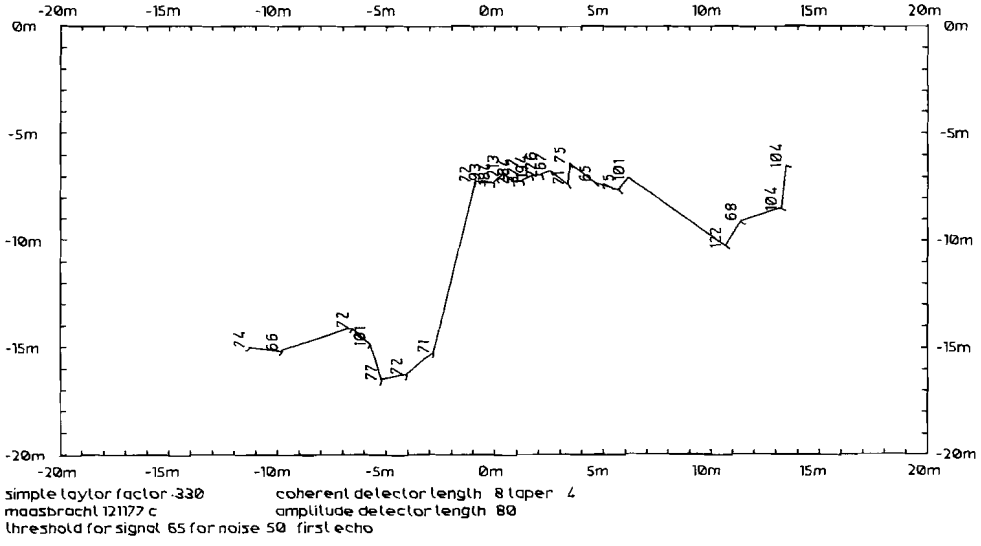

Figure 4.25 Detected depths from file C (over the sill).

Further an echo threshold was determined. For this determination the beam amplitude was corrected for spherical spread (equation 2.41 with $\beta = 0$) and for the influence of the reflector (equation 4.2, approximated for simplicity by cos θ). After this correction the maximum echo amplitude $\overline{C}_M$ of all beams was determined and the echo threshold set at

$$\overline{C}_T = 0.15\ \overline{C}_M$$

If this threshold came below $1.2\ \overline{v}_T$ it was set at $1.2.\ \overline{v}_T$. Now the first echo with an amplitude exceeding $\overline{C}_T$ was considered to be the return from a part of the chamber.

Results of echo detection

Figure (4.23) displays the first echoes for each beam in file A with detected echo amplitudes and with a line drawn between them if no more than two adjacent beams missed the echo. The figure shows a good resemblance to the cross-section of the chamber, especially in the right part, where even the lower part of the lock gate is recognizable. Of course, the finite beamwidth (4° in the 32 beam case) does not permit pinpoint location of echoes, but their range is correct. For the remainder it can be said that, apparently, flat concrete constitutes a bad backscattering boundary, especially at scattering angles larger than 5°. For beams, where the reflection coefficient for backward scattered sound is such, that the threshold $\overline{C}_T$ is not reached no echoes may be detected, or, worse, interfering echoes caused by reflection against the sides of the lock chamber may be detected as bottom. If figure (4.23) is compared with figure (4.4) it is evident that 8 beams have wrong echoes, 12 beams have correct echoes and 11 beams have no echoes.

The next tables summarize the results for all 5 files. In the preparation of these tables three horizontal flat surfaces with known depth were chosen. The depth measurement accuracy is listed for each file separately and for each surface separately.

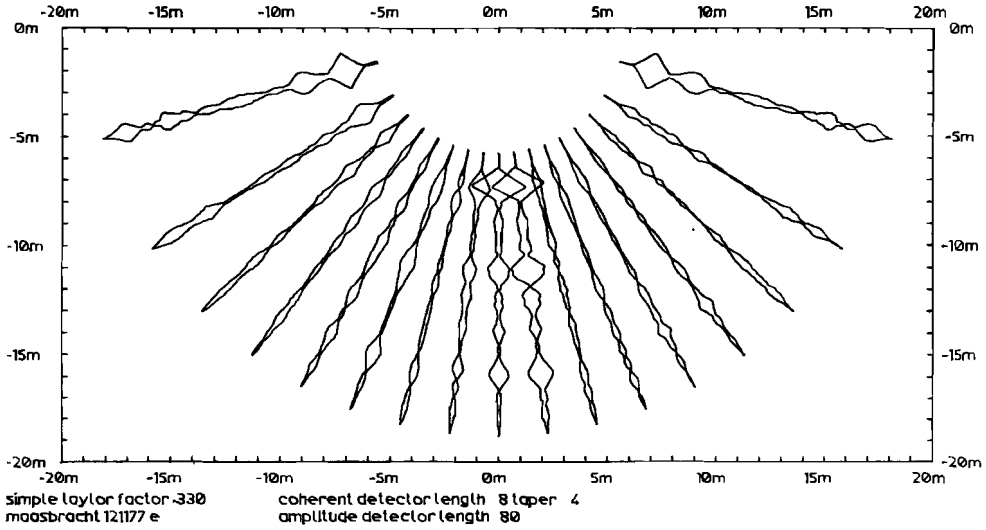

Figure 4.22 Beam amplitudes from file E (in the shallow part; without stack).

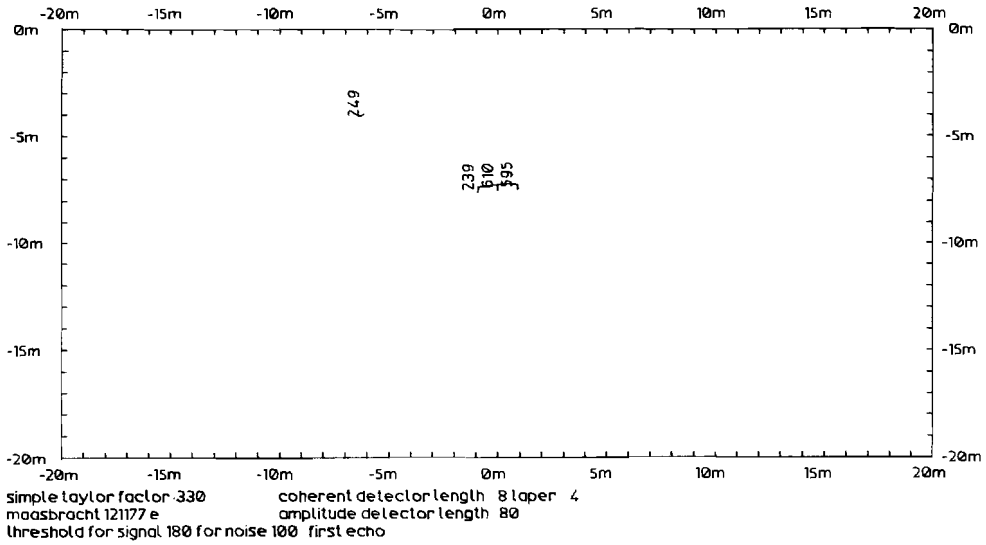

Figure 4.27 Detected depths from file E (in the shallow part; without stack).

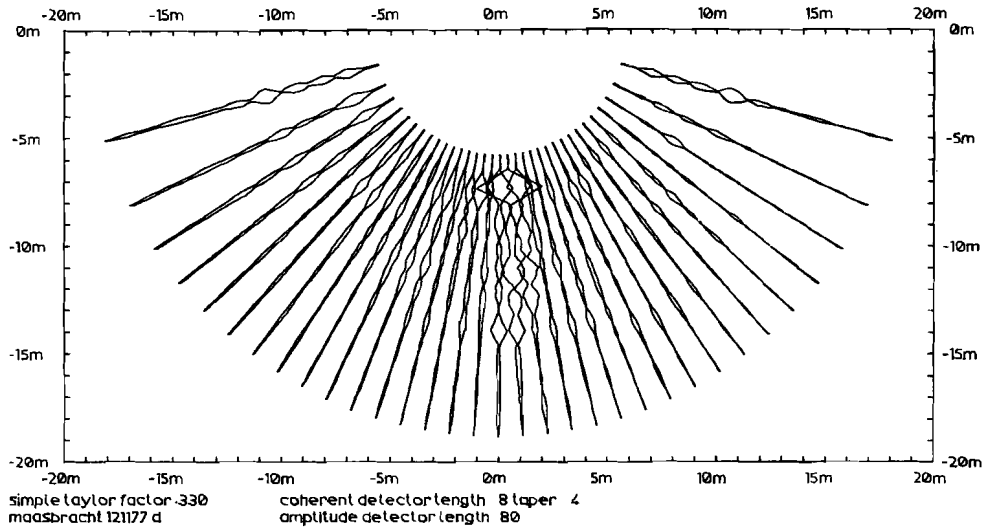

Figure 4.21 Beam amplitudes from file D (in the shallow part; with 20-fold stack).

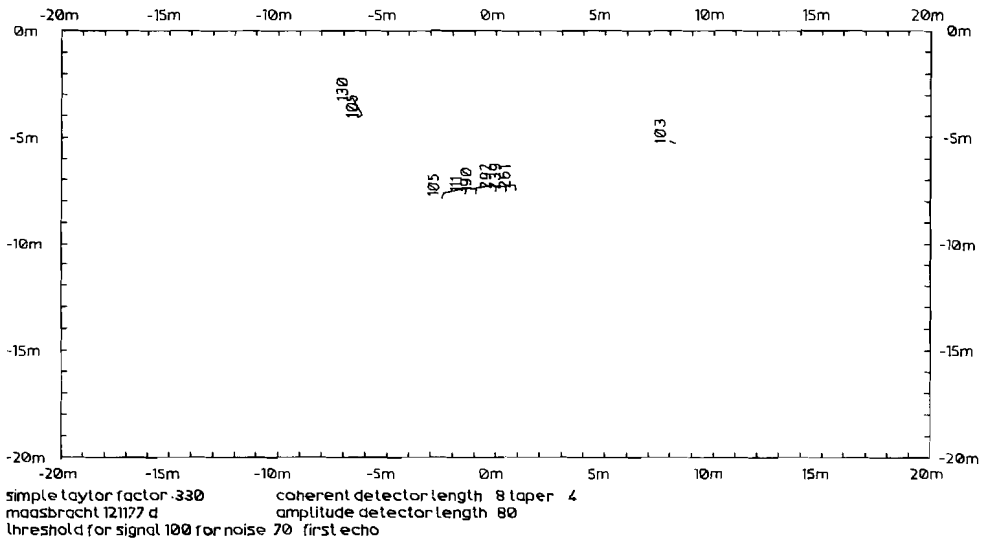

Figure 4.26 Detected depths from file D (in the shallow part; with 20-fold stack).

For each file:

file	number of elements in array	detected echoes			depth measurement accuracy	
		total	correct	used in accuracy measure-ment	systematic error	standard deviation
A	32	20	12	8	-20	25
B	32	27	17	8	- 3	16
C	32	25	18	10	- 1	44
D	32	9	6	5	2	9
E	16	4	3	3	0	9
					cm	cm

For each reflector:

reflector number	known height above NAL	depth below reference level	number of echoes used	depth measurement accuracy	
				systematic error	deviation
1	24.25+	728	11	1 1.3	15 21
2	16.80+	1473	11	- 2 1.4	27 18
3	15.50+	1603	12	-15 10	37 23
total			34	- 5 -	28 -
	m	cm		cm ‰	cm ‰

In the evaluation of these results it is important to notice that the wavelength of the measuring signal is 8.1 cm and the length of the pulse is 162 cm.
Furthermore the relative inaccuracy of the depth determination in a beam depends on beamwidth $\hat{\ell}$ and on look direction θ :

$$\frac{\Delta d}{d} = \tfrac{1}{2} \hat{\ell} \tan \theta$$

For the beam parameters used in this experiment and in the direction of 45° this relative inaccuracy amounts to 4 percent (viz. the sill echoes in file A and B). This uncertainty applies especially to isolated scattering objects. If an area is evenly covered with scattering objects the length of the beam amplitude detector (M in equation 3.7) can be adapted thus, that the mean depth of these scatterers is detected, which results in a higher accuracy.

To conclude, figure (4.28) displays a composite picture in which all detected echoes are superimposed on the longitudinal cross-section of the lock chamber.

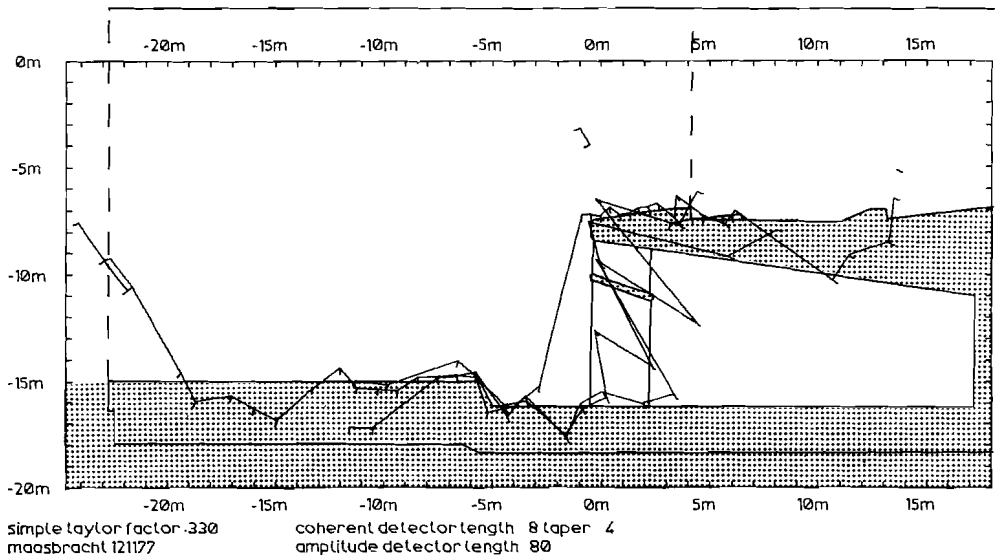

Figure 4.28 Longitudinal cross-section of chamber with all detections superimposed.

C. Proposal for a multi-beam echosounder

General overview

The basic principle of the multi-beam system proposed here is that all signal processing on which the operator of the system might wish to have influence is performed in a digital computer. This computer also controls all equipment involved in the multi-beam echosounder and collects other data relevant to the operation of the multi-beam system. Thus the program in this computer has two tasks:

1. High speed collection, processing, display and storage of received acoustic signals, and
2. Peripheral control, including control of the projector signal (the ping), interface with the operator and the updating of relevant variables.

The final result of this program can be a contourstripchart of the surveyed area. Processed data must be stored for subsequent merging and area contourchart production. The other elements of the proposed multi-beam system are grouped around this computer. They consists of:

1. The projector system: power amplifiers and projectors,
2. The receiver system: hydrophones, preamplifiers and anti-alias filters,
3. Platform parameter indicators: speed, heading, pitch, roll, yaw, heave.

Projector and receiver hardware

The experiment in the previous section proved that it is possible to generate simultaneously multiple beams in one direction with the outputs of a line array of equally spaced elements using a digital computer. In two directions this generation can be done with a two-dimensional array located on a flat surface. However, the number of array elements and signal lines involved then grows quadratically with the number of beams that can be generated. In addition, since the platform on which a multi-beam system is installed is moving, there is no need to generate simultaneous beams in the

direction parallel to the track. The only beamforming that has to be performed in this direction should serve to assure a narrow beamwidth along-track. This can be done by using a line projector array along the ship's axis that forms a fan-shaped beam with a small beamwidth along-track and a large athwartship beamwidth. It is then sufficient to use a line receiver array across the ship's axis to form simultaneous beams with small beamwidth across-track. The combination will generate simultaneous multiple beams with a small beamwidth in two directions. The technique described above is called crossed-fan beamforming. It is used in Seabeam and Bo'sun multi-beam echosounders. The proposed projector as well as the receiver thus each consist of a line array of elements, with the projector mounted alongship and the receiver mounted athwartship.

Attitude correction

A major problem with multi-beam and narrow-beam echosounders is the influence of the platform's attitude (pitch, roll, yaw). Correction for attitude can be done in real time, by actively altering beam directions to eliminate this influence and off-line, by recording the platform's attitude together with the measured signals, performing corrections afterward.

Real-time projector attitude correction can be done by steering the projector beam in the correct direction. Elac's narrow-beam sounder VM11 has a gyro-stabilized servo-controlled transducer. Seabeam uses an electronic pitch-resolver to introduce phase shifts in the signals for the projector array, in this way steering the projector beam in the vertically downward direction. In the proposed system the signals for the projector array elements would be generated within the computer under program control. The ability to steer the projector beam can be used with advantage to obtain a contour chart of a part of the ocean floor while the platform is on station by "fanning" the floor from fore to aft with this steered beam. Off-line correction for projector attitude is done by relocation of detected echoes in the processing program. Here the projector element signals are not phase-shifted with respect to each other and the projector beam always has the same direction with respect to the platform. Off-line correction implies a simpler interface between projector and computer and less time-consuming,

phase-shifting software, but no possibility to "fan" the bottom while on station.

Real-time receiver attitude correction can also be done by steering all receiving beams in the correct directions. This is a particularly time consuming solution as it inhibits the use of the FFT for beamforming. Therefore it is recommended to use off-line correction by relocation of echoes after depth detection. Generally, a true vertical beam is not obtained in this manner but the beam nearest to vertical can be used as such without much deviation if the angular distance between adjacent beams is not too large.

Computer hardware

The performance of quadrature detection and simultaneous beamforming in the computer requires special hardware. These signal processing tasks can easily interfere with the controlling task of the computer. The solution can be found in the use of a guest-computer that, controlled by the host-computer, performs all digital signal processing. The only type of guest-computer fast enough to perform this task is a so-called array processor (Savit, 1978). An array processor is a special purpose computer that operates fast on data sequences (Wittmayer, 1978). It uses a pipeline structure with high-speed hardware and it is comparatively easily controlled by the host-computer. The host-computer should be easily programmable in a high-level computer language to facilitate the implementation of the control functions.

Hardware parameter choice

The major hardware parameters are: receiver length and number of elements, useful frequency band, computer memory size, projector length and number of elements and the emitted projector power.

The receiver array length depends on the space available under the ship's keel and on the beamwidth to be attained at the frequencies utilized. The number of elements depends on the arithmetic capability of the processor

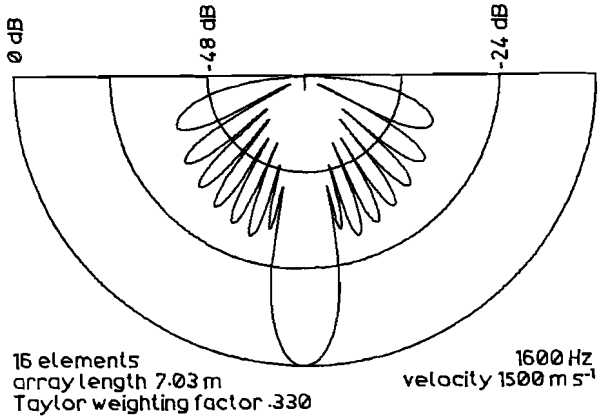

Figure 4.29 Pattern of proposed central beam at 1.6 kHz.

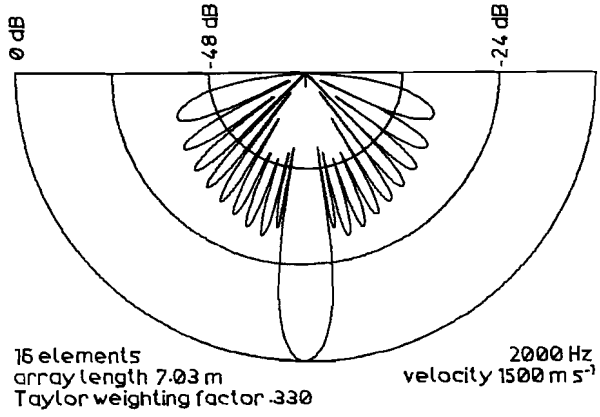

Figure 4.30 Pattern of proposed central beam at 2.0 kHz.

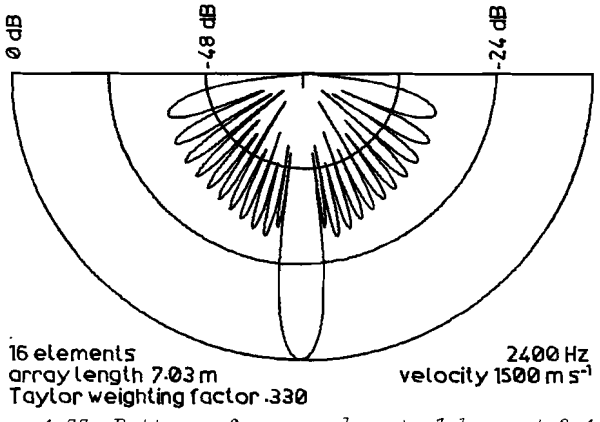

Figure 4.33 Pattern of proposed central beam at 2.4 kHz.

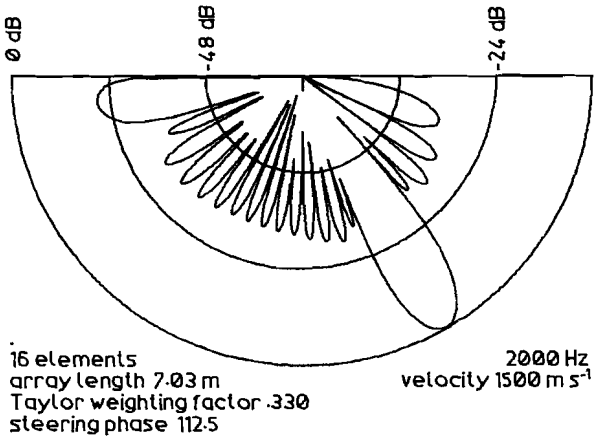

Figure 4.31 Side beam pattern at 2.0 kHz without secondary major lobe.

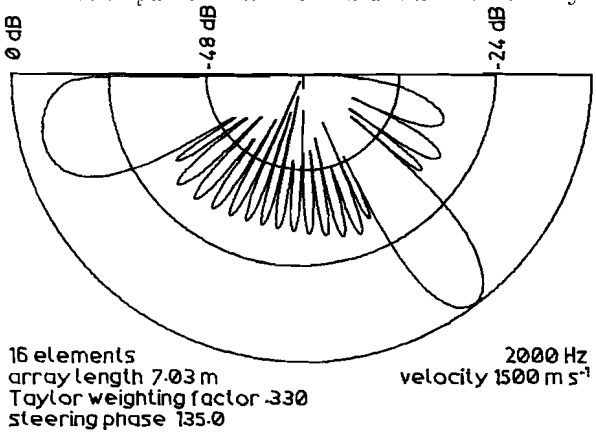

Figure 4.32 Side beam pattern at 2.0 kHz showing a harmless secondary lobe.

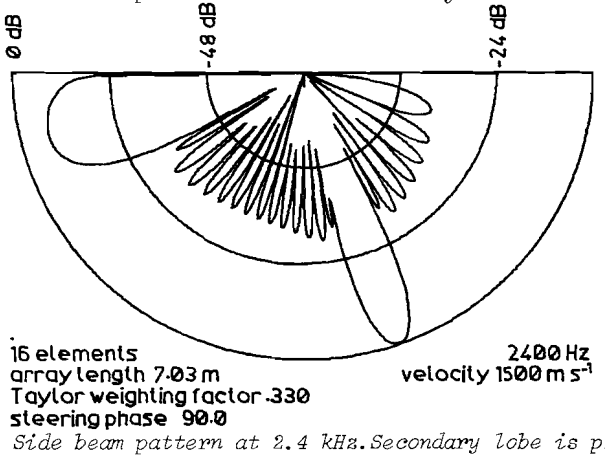

Figure 4.34 Side beam pattern at 2.4 kHz. Secondary lobe is present at low beam angle

system. Here a number of 16 elements is suggested with an aperture of 703 cm. If the signal frequency is 1.6 kHz, giving a wavelength of 94 cm at 1500 m s^{-1} sound velocity, the unshaded central beam is 7.2° wide. This corresponds to an element distance of 0.5 λ_0. The shaded array pattern is shown in figure (4.29). These parameters yield 11 processable beams with a total athwartship coverage of 78°. If the frequency is allowed to be 2 kHz 13 processable beams are formed with a total coverage of 74° and an unshaded central beamwidth of 5.7° (figure 4.30). Here, because the wavelength (75 cm at 1500 m s^{-1}) is smaller than the inter-element distance, non-zero order maximums occur in the outer side beams (figures 4.31 and 4.32). As these lobes point at directions no signals are expected from, they can be allowed. If the signal frequency is set at 2.4 kHz only 9 processable beams are formed with a total coverage of 40° and an unshaded central beamwidth of 4.8° (figure 4.33). The properties of the beam collections pertaining to these frequencies are summarized in the following table.

beam number	FFT phase-shift	beam direction		
		at 1.6 kHz	at 2.0 kHz	at 2.4 kHz
1	0°	0° (fig. 4.29)	0° (fig. 4.30)	0° (fig. 4.33)
2 and 16	22.5°	7°	6°	5°
3 and 15	45°	15°	12°	10°
4 and 14	67.5°	22°	18°	15°
5 and 13	90°	30°	24°	20° (fig. 4.3)*
6 and 12	112.5°	39°	30° (fig. 4.31)	25° * (useless)
7 and 11	135°	49° (useless)	37° (fig. 4.32)*	30° * (useless)

* a non-zero maximum occurs in these beams.

The beams not listed are useless because the beamwidth is too wide or secondary major lobes point in directions from which interfering signals can be expected. Beams 7 and 11 at 1.6 kHz are useless because the beamwidth is too large. It is seen that by varying the transmission frequency, the receiver beam parameters can be adjusted. The transformation procedure is not influenced by the frequency change.

The proposed output power for the projector can be calculated by considering the ambient noise level (+62 dB re 1 μPa), the detection threshold (+14 dB), the attenuation of sound by spherical spread (+120 to +154 dB) and absorption (+1 dB), the matched filter gain for the receiver array (-12 dB), the matched filter gain for amplitude detection (-13 dB) and the reflection or backscatter coefficient at moderate angles (+21 dB). The ambient noise level holds for distant shipping and wind-induced noise up to 8 Beaufort, at frequencies between 1.6 and 2.4 kHz (Perrone and King, 1975). The detection threshold follows from the experimental results in the previous section. The spherical spread loss is calculated from equation (2.39) assuming $\beta = 0$ and an operating depth from 1000 to 5000 m and a maximum beam direction angle of 45° across a flat bottom. The absorption loss is estimated from Albers (1965) for frequencies up to 2.5 kHz over the same range. Also adapted from Albers (1965) is the backscattering coefficient for rock, mud and coarse sand at scatter angles up to 45° The necessary sound level at 1m from the projector is thus 227 dB re 1 μPa. This level has yet to be corrected for the projector pattern. If 20 projector elements are used at $0.5\ \lambda_0$ separation, the pattern correction for the projector is 13 dB and the total projected energy will be 20 kW (Rijnja, 1971). As projecting transducers nowadays have efficiencies of 50% or higher (catalog ITC, undated), 40 kW of electrical power is needed. This power is distributed over the twenty projector elements, each with an input power of 2 kW. To avoid insonifications of unwanted areas the projector elements should be spaced at the half-wavelength of the highest frequency used (31.3 cm). The proposed projector aperture is then 594 cm. The resulting unshaded beamwidth for 1.6, 2.0 and 2.4 kHz operation is 8.6°, 6.9° and 5.7° respectively.

Proposed software

The proposed software will follow closely that described for the model experiment. First, the controlling program orders the array processor to put out a signal to the projector array amplifier. The form and frequency of this signal has been specified by the operator. The controlling program simultaneously takes a reading of the pitch angle. If projector beam steering is done, this value is used to compute projector phaseshifts and to apply them to the output signals. Then, based on previous detections, or set by the

operator, a time window is set up to include the relevant information in all beams. Due to memory economy considerations this window is limited to 3.33 sec. for the highest frequency. This length suffices if the depth of an otherwise flat area in a 45° beam does not exceed 6000 m.

The array processor puts in 16 channels of A-D converted data at a rate, depending on the output frequency , of 6.4 through 9.6 kHz per channel. Maximum data input rate thus is 154 kHz. To accept these inputs 512k of fast data memory is required in the array processor. Simultaneously the host-computer takes readings of roll and yaw. Thereupon a digital filter is applied to the 16 channels, performing narrow-band filtering, quadrature detection and application of the transform weighting function. The parameters used in this process can be controlled by the operator. Then the distance-to-direction transform is performed and the useful channels are selected for echo detection. Detected echoes, together with quality indicators (e.g. channel and beam signal-to-noise ratios) are passed to the host-computer for further processing, display and storage.

The host-computer performs beam relocation, ray tracing to correct for refraction effects (applying equation 2.37 and, if instructed by the operator to do so, equation 2.40). The parameters for ray tracing must be measured or inferred and fed into the program. A graphic recording of the modulated beam signal (equation 3.8) of the most vertical beam can be used as the system's primary registration. The array processor will provide the output for this recording. The relocated and ray-traced echoes can be used to produce on-line a contourstripchart of the area swept by the system. To eliminate the disturbing influence of the unevenly spaced measured points (along-track density is greater than across-track density) and of heave (McPhee, 1977), it is recommended to contour with a digital filter (Slootweg, 1978) to get a realistic contourchart.
All calculated echoes and the parameters used in relocation and ray tracing should be stored for after-mission evaluation and merging. For the keeping of original date (one ping generates 512k words of data), if wanted, mass storage is needed. A modern high-density magnetic tape e.g. stores up to 40 minutes of unprocessed data.

Timing of the array processor

The ping repetition rate can be determined by the host-computer if the program knows when the array processor is ready to collect the next signal set. Anticipating this moment the host-computer can order the array processor to emit a ping at such a time, that the start of the time window coincides with the end of the processing of the previous ping. Thus array processor time can be optimized.
An estimate for the processing time can be calculated if one assumes the array processor to be a Floating Point System AP-120B (FPS, 1979).

1. time window		3.33 - 5 s
2. 16 times FFT on 32 k elements		2.1 s
3. 16 × 32 k complex multiplication	}filter	0.5 s
4. 16k complex FFT on 16 elements		0.5 s
5. beam gating is done to minimize computer time		0.2 s
6. 11-13 times inverse FFT on 8 k elements		0.2 s
7. amplitude detection on 11-13 times 8 k complex elements		0.4 s
	total	7.3 - 8.9 s

This demonstrates the usefulness of a computer-array processor system for data collection and processing.

Recapitulation of hardware

The proposed system consists of:

1. Interface between the array processor and the projector amplifiers. The multibeam echosounding waveform (ping) having a frequency from 1.6 kHz to 2.4 kHz is passed via this interface to the amplifiers.
2. Projector amplifiers (20 pieces). The amplifiers (2 kW each) feed the ping with minimal distortion into the
3. Projectors (20 pieces). Mounted equidistant along the ship's axis under the keel. 2kW (electrical) each. Minimal 50% efficiency. Array length 594 cm.

4. Receivers (16 pieces). Mounted equidistant athwartship in reflectors of rubber bonded cork. Should be omnidirectional and have high mechanical resonance frequency. Array length 703 cm.
5. Preamplifiers. 16 pieces, including anti-alias filters. Should have digitally programmable gain for dynamic range correction.
6. Interface to array processor. 16 channel parallel Analog to Digital conversion. Conversion rate 154 kHz.
7. Array processor as guest in a fast general purpose computer, preferably a Floating Point Systems AP-120B, with 512 k words of data memory, 1 k of FFT table memory and 1 k of program memory.
8. Fast general purpose computer with a controlling program that directs the array processor and allows operator intervention for parameter change. It also relocates and ray-traces detected echoes and stores and displays them.
9. Storage and display devices, e.g. a graphic recorder and a digital plotter for contourstripchart.

References

Ahluwalia, D. S. and J. B. Keller, Exact and asymptotic representations of the sound field in a stratified ocean, in *Wave Propagation and Underwater Acoustics* editors J. B. Keller and J. S. Papadakis, Springer, Berlin, 1977.

Albers, V. M., *Underwater Acoustics Handbook - II*, Pennsylvania State University Press, 1965.

Allmendinger, R. W. and F. Riis, The Galapagos Rift at 86° W, 1. Regional morphological and structural analysis, *J. Geophys. Res.*, *84*, 5379-5389, 1979.

Anton, J. J. and A. J. Rockmore, A unified approach to array-factor synthesis for line arrays with nonuniformly positioned elements, *IEEE J. of Oceanic Engin.*, *1*, 14-21, 1976.

Ballard, R. D. and T. H. van Andel, Project FAMOUS: Operational techniques and American submersible operations, *Geol. Soc. America Bull.*, *88*, 495-506, 1977.

Bannister, R. W., R. N. Denham, K. M. Guthrie, D. G. Browning and A. J. Perrone, Variability of low-frequency ambient sea noise, *J. Acoust. Soc. Am.*, *65*, 1156-1163, 1979.

Bedenbender, J. W., R. C. Johnston and E. B. Neitzel, Electroacoustic characteristics of marine seismic streamers, *Geophysics*, *35*, 1054-1072, 1970.

Belderson, R. H., N. H. Kenyon, A. H. Stride and A. R. Stubbs, *Sonographs of the Sea Floor*, Elsevier, Amsterdam, 1972.

Berkhout, A. J. and D. W. van Wulfften Palthe, Migration in the presence of noise, paper presented at the *41th Meeting of the EAEG*, Hamburg, 1979.

Bracewell, R. N., *The Fourier Transform and its application*, 2nd edition, McGraw-Hill, New York, 1978.

Bryn, F., Optimum signal processing of three-dimensional arrays operating on Gaussian signals and noise, *J. Acoust. Soc. Am.*, *34*, 289-297, 1962.

Burke, R. and J. Robson, An evaluation of the Bo'sun multi-beam sonar system, *Int. Hydrogr. Rev.*, *52*, 53-69, 1975.

Catalog of Underwater Sound Transducers, International Tranducer Corp., Goleta, Ca., undated.

Choy, G. L. and P. G. Richards, Pulse distortion and Hilbert transformation in multiply reflected and refracted body waves, *Bull. Seism. Soc. Am.*, *65*, 55-70, 1975.

Cooley, J. W. and J. W. Tukey, An algorithm for the machine calculation of complex Fourier series, *Math. Computation*, *19*, 297-301, 1965.

Del Grosso, V. A., New equation for the speed of sound in natural waters (with

comparison to other equations), *J. Acoust. Soc. Am., 56,* 1084-1091, 1974.

Dolph, C. L., A current distribution of broadside arrays which optimizes the relationship between beamwidth and side-lobe level, *Proc. IRE, 34,* 335-356, 1946.

Ewing, J. and R. Zaunere, Seismic profiling with a pneumatic sound source, *J. Geophys. Res., 69,* 4913-4915, 1969.

FPS, *AP math library manual, vol. 2,* Floating Point Systems, Beaverton, 1979.

G - AE Subcommittee on Measurement Concepts, What is the Fast Fourier Transform?, *IEEE Trans. A-E, AU-15,* 45-55, 1967.

Giles, B. F., Pneumatic acoustic energy source, *Geophys. Prospect., 16,* 21-53, 1968.

Glenn, M. F., Introducing an operational multi-beam array sonar, *Int. Hydrogr. Rev., 47,* 34-39, 1970.

Goldstein, H., *Classical Mechanics,* Addison-Wesley, Reading, 1950.

Harris, F. J., On the use of windows for harmonic analysis with the discrete Fourier transform, *Proc. IEEE, 66,* 51-83, 1978.

HP 1000 computers, Hardware data, Hewlett-Packard, Cupertino, 1978.

Horton, C. W., Sr., *Signal Processing of Underwater Acoustic Waves,* Government Printing Office, Washington, 1969.

Huang, K., *Statistical mechanics,* John Wiley and Sons, New York, 1963.

Hubbard, A. C., Preliminary notes on profiler eel directivity, *Internal report,* L-DGO, New York, 1965.

Hueter, T. F. and R. H. Bolt, *Sonics,* John Wiley and Sons, New York, 1955.

Jones, J. L., C. B. Leslie and L. E. Barton, Acoustic characteristics of underwater bottoms, *J. Acoust. Soc. Am., 36,* 154-157,1964.

Kays, J. L., M. J. Jacobson and W. L. Siegmann, Analysis of acoustical effects of receiver and source motion at short ranges in a deep ocean, *J. Acoust. Soc. Am., 66,* 1120-1130, 1979.

Knott, S. T. and R. T. Nowak, A continuous configuration hydrophone array for broadband continuous seismic profiling, and A comparison between the responses of a continuous line array and a discrete linear array, *WHOI Technical report 69-12,* 1969, unpublished manuscript.

Lewis, J. B. and P. M. Schultheiss, Optimum and conventional detection using a linear array, *J. Acoust. Soc. Am., 49,* 1083-1091, 1971.

Matthews, D. J., Tables of the velocity of sound in pure water and sea water for use in echo-sounding and sound-ranging, 2nd edition, *British Admiralty Hydrographic Department No. 282,* 1939.

Mazzola, C. J., J. D. Birdwell and M. Athans, On the application of modern control theory to improving the fidelity of an underwater projector, *J. Acoust. Soc. Am., 66,* 739-750, 1979.

McCord, H. L., Synthetic aperture radar systems, *ICS course 475*, 1978.

McPhee, S. B., An evaluation of the Sea Beam system, *J. of the Can. Hydrogr. Ass.*, Nov. 1977.

Medwin, H., Speed of sound in water: A simple equation for realistic parameters, *J. Acoust. Soc. Am.*, *58*, 1318-1319, 1975.

Medwin, H., J. Bailie, J. Bremhorst, B. J. Savage and I. Tolstoy, The scattered acoustic boundary wave generated by grazing incidence at a slightly rough rigid surface, *J. Acoust. Soc. Am.*, *66*, 1131-1134, 1979.

Metherell, A. F., H. M. A. El-Sum and L. Larmore, *Acoustical Holography, vol 1*, Plenum, New York, 1969.

Nahi, N. E., *Estimation theory and applications*, John Wiley and Sons, New York, 1969.

Newman, P., Analytic signal concept applied to seismic data analysis and interpretation, paper presented at *EAEG Silver Anniversary Meeting*, The Hague, 1976.

OCD, High resolution bathymetry workshop, *report*, Texas A&M University, 1979.

Officer, C. B., *Introduction to the theory of sound propagation with application to the ocean*, McGraw-Hill, New York, 1958.

Papoulis, A., *The Fourier integral and its applications*, McGraw-Hill, New York, 1962.

Perrone, A. J. and L. A. King, Analysis technique for classifying wind- and ship-generated noise characteristics, *J. Acoust. Soc. Am.*, *58*, 1186-1189, 1975.

Phillips, J. D. and H. S. Fleming (compilers), Multibeam sonar study of the Mid-Atlantic rift valley, 36° - 37° N, FAMOUS, *Geol. Soc. Am., Map Chart Sec.*, MC-19, 1978.

Pritchard, R. L., Optimum directivity patterns for linear point arrays, *J. Acoust. Soc. Am.*, *25*, 879-891, 1953.

Rayleigh, J. W. S., *The Theory of Sound*, Dover, New York, 1945.

Renard, V. et J.- P. Allenou, Le Sea-beam, sondeur à multi-faiscaux du n/o *Jean Charcot*, description,évaluation et premiers résultats, *Revue Hydrogr. Intern.*, *LVI*, 1979.

Riblet, H. J., Discussion of Dolph's paper, *Proc. IRE*, *35*, 489-492, 1947.

Rijkswaterstaat, RIVV, RIVD, *Kwaliteitsonderzoek in de rijkswateren*, 4e kwartaal 1977, Lelystad, 1978.

Rijnja, H. A. J., Transducers for active sonar, *De Ingenieur*, *83 ET*, 183-188, 1971.

Rusby, J. S. M., A long range side-scan sonar for use in the deep sea (GLORIA project), *Int. Hydrogr. Rev.*, *47*, 25-39, 1970.

Rutten, K. W., Verslag air-gun signaal, *internal report*, VML, Utrecht, 1969.

Savit, C. H., Geophysical DP requirements could exceed the world's GP capacity by 1985, paper presented at the *National Computer Conference*, 1978.

Schultheiss, P. M., Some lesson from array processing theory, in *Aspects of Signal Processing, Part 1*, editor G, Tacconi, Reidel, Dordrecht, 1977.

Skolnik, M. I., *Radar Handbook*, McGraw-Hill, New York, 1970.

Slootweg, A. P., Computer contouring with a digital filter, *Mar. Geophys. Res., 3*, 401-405, 1978.

Smith, S. G. and E. D. van Riessen, The Meriadzek terrace: a marginal plateau, *Mar. Geophys. Res., 2*, 83-94, 1973.

Sommerfeld, A., *Vorlesungen über theoretische Physik, Band II: Mechanik der deformierbaren Medien*, Geest u. Portig, Leipzig, 1964.

Taylor, T. T., Design of line-source antennas for narrow beamwidth and low sidelobes, *IRE Trans. on Ant. and Prop., AP-3*, 16-28, 1955.

Tolstoy, I. and C. S. Clay, *Ocean Acoustics*, McGraw-Hill, New York, 1966.

Tucker, D. G., Directional echosounding, *Int. Hydrogr. Rev., 37*, 43-53, 1960.

Ulrich, J., Possibilities of application of modern echo-sounding systems in oceanographic research, *Scientific and technical application of echo-sounding and sonar installations*, Report '76/3A, 1-19, Electroacustic, Kiel.

Van der Burgt, C. M., PXE high intensity transducers, in *Piezoelectric Ceramics*, 69-87, Philips, Eindhoven, 1968.

Van der Steen, A. J., Test of some Fast Fourier Transform routines in FORTRAN and ALGOL 60, *Technical report TR-8*, Accu-reeks 25, Utrecht, 1978.

Wang, H. S. C., Amplitude shading of sonar transducer arrays, *J. Acoust. Soc. Am., 57*, 1076-1084, 1975.

Wijmans, W., An experimental study of the reflection of underwater sound from the sea surface, *Saclantcen memorandum SM-51*, La Spezia, 1974.

Willey, R. E., Space tapering of linear and planar arrays, *IRE Trans. on Ant. and Prop., AP-10*, 369-377, 1962.

Wittmayer, W. R., Array processor provides high throughput rates, *Computer Design*, 93-100, 1978.

Wolff, C. J. M., A parallel analog Fourier transformer for acoustic underwater holography and sector scanning sonar, paper presented at the *Conference on Recent Developments in Underwater Acoustics*, Portland (GB), 1976.

Ziolkowski, A., A method for calculating the output pressure waveform from an air gun, *Geophys. J. R. astr. Soc., 21*, 137-161, 1970.

Zuurdeeg, B. W., The natural chemical composition of river Meuse water, *H_2O, 13*, 2-7, 1980.

Curriculum Vitae

De schrijver van dit proefschrift behaalde in 1962 het einddiploma HBS-B aan het Hervormd Lyceum te Amsterdam, waarop hij begon met de studie natuurkunde aan de Universiteit van Amsterdam. Na het kandidaatsexamen d_n (natuurkunde "met nadruk" en wiskunde met scheikunde) in 1966 en een assistentschap bij de afdeling Hoge Energie Fysica van het Zeeman Laboratorium te Amsterdam van 1967 tot 1971 sloot hij de studie experimentele natuurkunde met bijvakken wiskunde en prehistorie af met het doctoraal examen in 1971.
Na het militair intermezzo van de eerste oefening trad de auteur in januari 1973 in dienst van de afdeling Mariene Geofysica aan de Rijksuniversiteit te Utrecht, waar hij van januari 1974 tot februari 1980 werkzaam geweest is in de rang van wetenschappelijk medewerker op een promotieplaats van de Nederlandse organisatie voor zuiver-wetenschappelijk onderzoek.
Sinds 1 februari 1980 is de auteur aangesteld als wetenschappelijk ambtenaar bij de Koninklijke Nederlandse Akademie van Wetenschappen, gedetacheerd bij de afdeling Mariene Geofysica.

Errata

page 6 line 18: threee → three

page 7 line 10: fabrik → fabric

page 8 line 19: aterture → aperture

page 12 line 8: add (2.7) at the end of the line.

page 15 line 7: indes → index

page 20 line 14: equation (2.27) → equation (2.28)

page 23 fig. 2.1: interchange θ_{01} and θ_{02}.

page 27 line 3: $\beta(\alpha^1, \beta^1, \omega)$ → $B(\alpha^1, \beta^1, \omega)$

page 27 line 10: add (2.43) at the end of the line.

page 28 line 12: $B(\alpha, \beta, \omega)$ → $B(\alpha^1, \beta^1, \omega)$

page 43 line 8: $(\ell x+my)\ d\ell\ dm$ → $(\ell x+my))\ d\ell\ dm$

page 47 line 11: shoud → should

page 47 line 21: propellor → propeller

page 48 line 10: array again → array gain

page 51 line 14: bubble pule → bubble pulse

page 57 line 6: side-lokking → side-looking

page 74 table 3.1: add Depths in column (b) are in uncorrected meters based on a sound velocity of 1500 m s^{-1}. Depths in column (a) are in corrected meters.

page 86 line 5: delete state.

page 108 lower table: deviation → standard deviation

page 115 line 25: non-zero maximum → non-zero order maximum

A. P. Slootweg, *Multiple beam generation with a digital computer for echosounding at low and high frequencies.*